HIGH TEMPERATURE PHASE RELATIONS IN THE TiO_X-FeO_Y-VO_Z SYSTEM

by

Theresa Coetsee

Submitted in partial fulfillment of the requirements for the degree

Master of Engineering

in the Department of Materials Science and Metallurgical Engineering, Faculty of Engineering, University of Pretoria, Pretoria, Republic of South Africa

Supervisor: Professor P.C. Pistorius

July, 1998

ACKNOWLEDGEMENTS

I thank the following people and institutions for contributions made to this work. This project would not have been completed sucessfully without them.

- Dr. Andrie Garbers-Craig for technical advice and guidance on this project.
- Prof. Chris Pistorius for leadership and advice in completing this project.
- Prof. Rian Dippenaar who gave me the opportunity to do this project.
- Dr. Willem van Niekerk for supporting this project.
- Iscor Ltd. for financial support.
- Department of Metallurgical Engineering, Pretoria University, for facilities.
- Nico Botha and Quintin Prinsloo for preparing samples.
- Corelie Visser for assistance in XRD analyses.
- Dr. Jacques Smuts, Villie Viljoen and Andrè Botha for electron microscopy analyses and photographs.
- Helmut Oltmann who taught me to use a pyrometallurgical laboratory.
- My mother for never giving up.

S.D.G.

Summary

The minerals rutile (TiO_2) and ilmenite ($FeTiO_3$) are used as raw materials in the production of titanium oxide pigments. The two main processing routes are the sulphate and the chloride processes. Over the last four decades the trend has been to produce more titanium dioxide pigment via the chlorination process. TiO_2-rich slag, produced by carbothermic reduction of ilmenite, is used as feed material to the chlorination process. One of the quality specifications on the slag is that the vanadium content, expressed as $\%V_2O_5$, be less than 0.6% V_2O_5. Approximately 10% FeO is retained in the slag for fluxing purposes. From the standard free energies of formation of vanadium and iron oxides all of the FeO would first have to be reduced before vanadium oxide will be reduced into the metal if all species are present at unit activity. However, when mixtures of elements in the metal, and oxides in the slag are considered some vanadium may be recovered to the metal. The activity-composition behaviour of vanadium oxide in high TiO_2 slags is not known. Before the activity of vanadium oxide can be determined phase relations within the TiO_X-FeO_Y-VO_Z system, at the high TiO_X side, should be known. In this study phase relations within the two pseudo-binary systems FeO-V_2O_3 and TiO_2-V_2O_3 at 1400 °C, 1500 °C and 1600 °C at partial oxygen pressures of 3.02×10^{-10} atm, 2.99×10^{-9} atm and 2.31×10^{-8} atm respectively were determined with the quench technique. Analysis techniques used in determining the phase relations within the reacted samples were X-ray diffraction, Electronprobe microanalysis (Energy dispersive spectrometry and Wavelength dispersive spectrometry), and optical microscopy. The V_2O_3-TiO_2 pseudo-binary phase diagram contains the solid solution phases M_2O_3, M_3O_5 and higher Magneli phases (M_nO_{2n-1}) with M=(V, Ti). In these solid solution phases V^{4+} substitute for Ti^{4+}, and V^{3+} substitute for Ti^{3+}. The V_2O_3-FeO pseudo-binary phase diagram consists of the solid solution phases M_2O_3 and M_3O_4, as well as liquid, M=(V, Fe). In the M_2O_3 and M_3O_4 solid solution phases V^{3+}, Fe^{3+} and Fe^{2+} can substitute for each other. This work is a first step in determining the activity-composition behaviour of vanadium oxide in high TiO_2 slag.

Opsomming

Die minerale rutiel (TiO_2) en ilmeniet ($FeTiO_3$) word as roumateriaal in die produksie van titaandioksiedpigment gebruik. Hoofsaaklik twee prosesse, die sulfaatproses en die chlorineringsproses, word gebruik. Die neiging oor die afgelope vier dekades was om meer titaandioksiedpigment via die chlorineringsproses te produseer. TiO_2-ryke slak, geproduseer

titaandioksiedpigment via die chlorineringsproses te produseer. TiO_2-ryke slak, geproduseer deur die karbotermiese reduksie van ilmeniet, word gebruik as toevoermateriaal tot die chlorineringsproses. Een van die gehaltespesifikasies vir die slak is dat die vanadiuminhoud, uitgedruk as $\%V_2O_5$, minder as 0.6% V_2O_5 moet wees. Ongeveer 10% FeO word oorgehou in die slak ten einde die slak vloeibaar te maak. Die standaard vrye energie van vorming vir vanadium- en ysteroksiede toon aan dat al die FeO eers gereduseer moet word na die metaal alvorens vanadiumoksied gereduseer sal word, as alle spesies by eenheidsaktiwiteit is. Indien egter mengsels van elemente in die metaal, en oksiede in die slak beskou word, mag vanadium tog na die metaal herwinbaar wees. Die aktiwiteit-samestellingsgedrag van vanadiumoksied in TiO_2-ryke slak is nie bekend nie. Alvorens die aktiwiteit van vanadiumoksied bepaal kan word, moet die faseverwantskappe in die TiO_X-FeO_Y-VO_Z sisteem, aan die TiO_X kant, eers bekend wees. In hierdie werk is die faseverwantskappe in die pseudo-binêre sisteme FeO-V_2O_3 en TiO_2-V_2O_3 by 1400 °C, 1500 °C en 1600 °C by parsiële suurstofdrukke van 3.02 x 10^{-10} atm, 2.99 x 10^{-9} atm en 2.31 x 10^{-8} atm onderskeidelik bepaal deur van die afblustegniek gebruik te maak. Analisetegnieke gebruik om die faseverwantskappe in die gereageerde monsters te bepaal, was X-straal diffraksie, mikrosonde-analises (Energie gedisperseerde spektrometrie and Golflengte gedisperseerde spektrometrie), and optiese mikroskopie. Die V_2O_3-TiO_2 pseudo binêre fasediagram bevat die vaste oplossingsfases M_2O_3, M_3O_5 and hoër Magneli fases (M_nO_{2n-1}) met M=(V, Ti). In die kristalstruktuur van die vaste oplossingsfase word Ti^{4+} deur V^{4+} vervang, en Ti^{3+} word deur V^{3+} vervang. Die V_2O_3-FeO pseudo binêre fasediagram bevat die vaste oplossingsfases M_2O_3 en M_3O_4, asook vloeistof, M=(V, Fe). In die M_2O_3 en M_3O_4 vaste oplossingsfases kan V^{3+}, Fe^{3+} en Fe^{2+} mekaar onderling in die kristalstruktuur vervang. Hierdie werk is die eerste stap in die bepaling van die aktiwiteit-samestellingsgedrag van vanadiumoksied in TiO_2-ryke slak.

Key words

ilmenite, chloride process, vanadium oxide, phase relations, high TiO_2-slag, partial oxygen pressure, quench technique, equilibrium, pseudo-binary system, V_2O_3, FeO, TiO_2

Sleutelwoorde

ilmeniet, chloriedproses, vanadiumoksied, faseverwantskappe, TiO_2-ryke slak, parsiële suurstofdruk, afblustegniek, ewewig, pseudo binêre sisteem, V_2O_3, FeO, TiO_2

TABLE OF CONTENTS

1. INTRODUCTION[1,2,3]

The minerals rutile (TiO_2) and ilmenite ($FeTiO_3$) are used as raw materials in the production of titanium dioxide pigments. The two main processing routes for the production of pigment are the sulphate and the chloride processes, with ilmenite being used as feed material to the sulphate process and rutile as feed material to the chloride process.

The world production of ilmenite is approximately eight times the quantity of rutile beneficiated from natural mineral deposits. Because of the decrease in rutile mineral availability as feedstock to the chloride process, rutile substitutes are used. One of the substitutes is a titanium slag (85% TiO_2), as produced by Richards Bay Minerals (Tisand PTY) in South Africa, by carbothermic reduction of ilmenite at temperatures in excess of 1600°C. A similar process is used by Namakwa Sands on the west coast of South Africa, and is to be used in Iscor's planned smelter at Empangeni, South Africa. Titanium slag is also used as feedstock in the sulphate process. This slag has a TiO_2 content ranging from 71-74% in slags produced by QIT in Canada, to 90% in slags produced in Japan.[1]

In the chloride process rutile is chlorinated under reducing conditions, at 800-1000°C, in a fluidized bed to form titanium tetrachloride ($TiCl_4$). Coke is used as reductant and chloride gas as the reacting gas. TiO_2 pigment is subsequently formed by burning the $TiCl_4$ with oxygen in a specially designed burner at temperatures above 600°C. The TiO_2 produced requires the same final processing, milling etc., as used in the sulphate process. The $TiCl_4$ formed as intermediate product in the process can be purified by distillation to remove impurities in the form of chlorides.

In the sulphate route ilmenite (or certain other titanium-bearing phases: see below) is digested with strong sulphuric acid to render the titanium in solution as titanyl sulphate, $TiOSO_4$. The ferric iron (Fe^{3+}), which is also in solution, is reduced with scrap iron to ferrous iron (Fe^{2+}), and the solution is then cooled down to crystallize the iron out as copperas ($FeSO_4.7H_2O$). The solution is adjusted with respect to pH and TiO_2 content and then boiled to precipitate the titanium dioxide in very fine colloidal form. The TiO_2 is washed to remove impurities and the TiO_2 pulp is then calcined to remove absorbed water and to establish the optimum crystal size. The TiO_2 is subsequently wet milled, hydroclassified, dried and shipped. Only natural ilmenite and titanium slag can be used as feedstock for the sulphate process because rutile is

not digested by sulphuric acid. The most suitable phase for the sulphate process is pseudo-brookite because it is easily digested by sulphuric acid.

Rutile is a much better feedstock for pigment production by chlorination than ilmenite because it contains more titanium and therefore less waste is produced. The sulphate process generates 3.5 tonnes of waste per tonne of TiO_2 product and the chloride process generates only 0.2 tonnes of waste per tonne of TiO_2 product.[1] Over the last four decades the trend has been to produce more titanium dioxide pigment via the chlorination process.

Iscor's Rooiwater ilmenite deposit contains vanadium within the magnetite which is associated with ilmenite in the ore.[13] The vanadium substitutes for the iron within the spinel structure of magnetite. Vanadium chlorides and oxychlorides formed in the chlorination process have boiling points close to the boiling point of $TiCl_4$ and are therefore not easily separated from $TiCl_4$ through a distillation process. Thus one of the quality specifications for TiO_2-rich slag produced for chlorination processing is that the vanadium content, expressed as $\%V_2O_5$, be less than 0.6 $\%V_2O_5$[4].

In the carbothermic reduction of ilmenite pig iron is produced in addition to the TiO_2-rich slag. Because of the specification on the maximum amount of V_2O_5 allowed in the slag one would wish to transfer as much as possible vanadium from the slag into the metallic phase. However approximately 10% FeO should be maintained within the slag for fluxing purposes. Consideration of the standard free energies of formation of vanadium and iron oxides from the elements indicates that vanadium oxides are more stable than FeO. Therefore all of the FeO would first have to be reduced into the metallic phase before vanadium oxides can be carbothermically reduced. However, this is the situation when the pure components, for which the activities are equal to unity, are considered. Of importance are the activities of the metallic components within the multicomponent metallic phase, and the activities of the oxide components within the complex slag. For all practical purposes the activity of iron is equal to unity since it constitutes almost the entire metallic phase. The activity coefficient (γ_V°) of vanadium in iron, with solid vanadium as the reference phase, is 0.1 at 1600 °C and 0.11 at 1750 °C[33] so that the transfer of vanadium from the slag to the metal through reduction is enhanced. Carbon is the major solute in the iron with 2% carbon in the iron and the first order interaction coefficient (e_V^C) of carbon on vanadium in liquid iron is –0.34[33] so that the activity

coefficient of vanadium in the liquid iron will be further reduced. The activity coefficient of vanadium within the metallic phase will not be substantially lowered further without the addition of large quantities of alloying elements to the metallic iron phase. The study of activity-composition relations of iron oxides and vanadium oxides in TiO_2-rich slags are therefore of importance. The activity behaviour of the vanadium and iron oxides in the TiO_2-rich slag may render the carbothermic reduction of vanadium from the slag possible, whilst still maintaining FeO as flux.

Furthermore the activities of the iron and vanadium oxides in the liquid phase of the TiO_2-rich slag are of great significance, because reduction of the oxides predominantly occurs from the liquid portion of the slag due to kinetic considerations. Determination of phase relations is necessary groundwork that has to be done before activity-composition relations within the oxide system can be measured. Furthermore, from crystal chemical considerations the phase relation data indicates the activity behaviour to be expected in the oxide mixtures e.g. the ionic radii of vanadium and iron cations indicates that solid solution formation between Fe^{2+}, Fe^{3+} and V^{3+} is possible because the ionic radii of the cations differ by less than 15%.[25] The ionic radii of titanium and vanadium cations indicates that V^{5+}, V^{4+} and V^{3+} may substitute for Ti^{4+}, and V^{3+} and V^{2+} may substitute for Ti^{3+} to form vanadium containing titanium-rich solid solutions. Consequently, it is imperative that phase constitution of slags within the TiO_2-FeO_Y-VO_Z pseudo-ternary oxide system be known so that the liquid phase areas can be fully defined. Neither this phase diagram, nor the two pseudo-binary phase diagrams, VO_X-FeO_Y and VO_Z-TiO_2, are known. This study therefore focused on the determination of phase relations within these binary oxide systems at 1400°C, 1500°C and 1600°C and P_{CO}/P_{CO_2} = 3. This gas mixture represents oxygen partial pressures of 3.02×10^{-10} atm, 2.99×10^{-9} atm and 2.31×10^{-8} atm at 1400°C, 1500°C and 1600°C respectively. All of these partial oxygen pressures were chosen to be slightly above the Fe/FeO equilibrium oxygen partial pressure as is summarised in Table 1.1. The reason for using these partial oxygen pressures is that the phase constitution of the respective oxide systems, in the presence of FeO, is of interest.

Table 1.1: Fe/FeO Equilibrium Oxygen Partial Pressures at 1400, 1500 and 1600 °C[32]

Temperature (°C)	Equilibrium Partial Oxygen Pressure (atm.)	Experimental Partial Oxygen Pressure (atm.)
1400	4.84×10^{-11}	3.02×10^{-10}
1500	3.45×10^{-10}	2.99×10^{-9}
1600	2.12×10^{-9}	2.31×10^{-8}

The equilibrium partial oxygen pressures for the VO/V_2O_3 and V_2O_3/VO_2 equilibria are indicated in Table 1.2. Comparison of the partial oxygen pressures for the vanadium oxides in Table 1.2 with the experimental partial oxygen pressures in Table 1.1 indicates V_2O_3 to be the stable vanadium oxide under experimental conditions used in this work.

Table 1.2: Equilibrium Oxygen Partial Pressures for Vanadium Oxides at 1400, 1500 and 1600 °C[34]

Reaction	Reaction Temperature (°C)		
	1400	1500	1600
$2VO+1/2O_2 \leftrightarrow V_2O_3$	1.50×10^{-14} atm	2.65×10^{-13} atm	3.45×10^{-12} atm
$V_2O_3 + 1/2O_2 \leftrightarrow 2VO_2$	1.42×10^{-6} atm	2.88×10^{-6} atm	5.29×10^{-6} atm

The information determined in this study will be the basis for the complete determination of phase relations within the TiO_2-FeO_Y-VO_Z pseudo-ternary oxide system, as required for activity measurements. Such activity data will provide clarity on the criteria for the optimum transfer of vanadium from the slag into the metallic phase under the constraints outlined above. This project therefore makes a first but essential contribution towards an answer to this problem.

2. PREVIOUS WORK

2.1. TiO_2 - FeO System

Phase relations in the TiO_2-FeO system, at liquidus temperatures and under reducing conditions, were studied by Grieve and White[6], MacChesney and Muan[5] and Grau[8]. Grieve and White[6] used the differential thermal analysis (DTA) technique for the examination of the FeO-TiO_2 system. Tungsten-molybdenum thermocouples were used. Samples were contained in molybdenum crucibles, while the standard for the differential thermocouple was also molybdenum. Three heating and two cooling curves were measured for each composition studied. The samples were made up from powdered ferrous oxide and titania and were heated in a "Pythagoras"* furnace tube situated within a molybdenum-wound furnace. Heating of the samples was done either in vacuo or in a nitrogen atmosphere. The molybdenum equipment used in the experiments would have limited the partial oxygen pressures to a maximum which is indicated by the equilibrium partial oxygen pressure between molybdenum and molybdenum oxide. These partial oxygen pressures were calculated as 2.25×10^{-11} atm at 1305°C and 1.60×10^{-8} atm at 1600°C. The samples were examined microscopically under reflected light, and X-ray diffraction analyses were done. The FeO-TiO_2 phase diagram as determined by Grieve and White[6] is shown in Fig. 2.1. This diagram shows four different compounds: FeO, TiO_2, $2FeO.TiO_2$ and $FeO.TiO_2$. The eutectic points are found in the system at 5, 42 and 68 mass% TiO_2 respectively. The maximum liquidus temperature within the system, that is the liquidus temperature of TiO_2, could not be determined with certainty and was therefore indicated to be in excess of 1650°C.

MacChesney and Muan[5] conducted phase studies in the FeO-TiO_2 system employing the quench technique. Starting materials were Fe_2O_3 and TiO_2. The Fe_2O_3-TiO_2 mixtures were brought close to equilibrium with the partial oxygen pressure for which iron and wüstite coexist in equilibrium. This was accomplished by pre-reacting the mixtures in iron crucibles under a nitrogen atmosphere at 1300°C. In the actual experiments the pre-reacted oxide sample was contained in an iron crucible and sealed, together with an iron-wüstite buffer, in a vitreous silica tube. The iron-wüstite buffer was maintained at a temperature ±20°C below the sample temperature so that the partial oxygen pressure of the gas phase, as defined by the metallic iron-wüstite equilibrium, was slightly lower than that defined by the iron-wüstite buffer at the sample temperature. The partial oxygen pressure of the gas phase, calculated

* Chemical composition: SiO_2 - Al_2O_3 (approximately 67 %) Can be used at temperatures up to 1600°C

from the iron-wüstite equilibrium is approximately $10^{-10.7}$ atm at 1312°C and $10^{-9.1}$ atm at 1494°C. Some experimental runs were also made with the oxide sample contained in an iron crucible under a nitrogen atmosphere. The samples were rapidly quenched to room temperature after being held at the selected temperature until equilibrium was attained. Experimental temperatures employed were between 1250°C and 1500°C. The phases were identified by microscopic examination under reflected light, as well as X-ray diffraction analysis. The compositions of the reacted samples were determined by chemical analyses. Metallic iron was present in the quenched samples. MacChesney and Muan[5] indicated that, according to the phase rule, iron should not be present as an equilibrium phase in their experiments. They attributed the presence of iron in the melts to the conversion of Fe_2O_3 to FeO by reaction with the iron crucible:

$$Fe_2O_3 + Fe \rightarrow 3FeO$$

The FeO formed in this reaction may be reduced partially to metallic iron by the atmosphere before the FeO reacts with TiO_2 to form phases in which Fe^{2+} is stabilised. The FeO-TiO_2 phase diagram determined by MacChesney and Muan[5] is shown in Fig. 2.2. This phase diagram has four eutectic points at 10, 47, 58 and 83 mass% TiO_2 respectively, and contains five phases: FeO, TiO_2, 2FeO.TiO_2, FeO.TiO_2 and FeO.2TiO_2.

Smith and Bell[7] determined the solubility limit of TiO_2 in FeO at 1475°C under an argon atmosphere, using iron crucibles, to be 64.5 mass% TiO_2.

Grau[8] determined liquidus temperatures in the 'FeO'-TiO_2 system in the composition range of 52,7 mass% TiO_2*-82 mass% TiO_2. The cooling curve technique was used to determine liquidus temperatures. The melts were contained in molybdenum crucibles and a thermocouple with a molybdenum sheath was immersed in the melt. The method consisted of recording the melt temperature during cooling. The beginning of crystallisation, and therefore the liquidus temperature, is indicated by an arrest in the time-temperature curve. Experiments were conducted under argon which was deoxidised by copper turnings at 400°C. Grau[8] maintains that the oxygen partial pressure in this argon gas was low enough to prevent oxidation of the molybdenum in the experimental apparatus. Slag analyses were determined by chemical analysis. Samples were prepared from synthetic ilmenite to which TiO_2 in the

* Ilmenite composition

form of anatase was added in order to adjust the sample composition. The synthetic ilmenite was prepared by mixing stoichiometric amounts of pure iron, Fe_2O_3 and TiO_2 for the reaction

$$Fe + Fe_2O_3 + 3TiO_2 \rightarrow 3(FeO.TiO_2)$$

to occur after the mixture was pressed into pellets and reacted under argon at 1200-1300°C for ±12 hours. X-ray diffraction confirmed the formation of ilmenite. Metallic molybdenum was found in the slags, varying between 0.6 mass% Mo for the slag containing 52.4 mass% TiO_2 and 2.2 mass% Mo for slag containing 79.5 mass% TiO_2. Grau[8] explains the presence of molybdenum in the slag by erosion of the molybdenum crucible by the slag and also by the solubility of molybdenum metal in the melts. The metallic molybdenum appeared as fine particles, forming a separate phase in the liquid slag melts. Therefore the chemical analysis of the melts was reported only in terms of FeO and TiO_2 after a correction was made for the molybdenum contamination.

Grau's[8] FeO-TiO_2 phase diagram is shown in Fig. 2.3. This diagram differs from the one proposed by MacChesney and Muan[5] for the composition range above 70 mass% TiO_2. Grau[8] subsequently proposed modifications to the phase diagram of MacChesney and Muan.[5] These modifications are shown in Fig. 2.4 and include: (a) the congruent melting of pseudobrookite ($FeO.2TiO_2$) at 1475°C during which rutile and a liquid phase which contains ± 68 mass% TiO_2 are produced, and (b) eliminating the eutectic point at 83 mass% TiO_2.

Pseudobrookite becomes unstable below 1140 ±10°C[9], decomposing to rutile and ilmenite according to the reaction:

$$FeO.2TiO_2 \rightarrow FeO.TiO_2 + TiO_2$$

In a recent study of Eriksson et al.[35] the decomposition point was determined as 1135 ±5°C. Therefore, the minimum temperature in the FeO-TiO_2 phase diagram was restricted to 1200°C. According to this transformation FeO-TiO_2 slags with an overall composition between those of ilmenite and pseudobrookite will on slow cooling contain rutile in addition to ilmenite. Similarly, an ilmenite phase should be found in slowly cooled slags with a composition richer in TiO_2 than pseudobrookite. The degree to which pseudobrookite decomposes to ilmenite and rutile will be dictated by the cooling rate of the oxide mixture.

The FeO-TiO_2 phase diagram as determined by Grieve and White[6] does not contain the $FeO.2TiO_2$ phase, as reported by MacChesney and Muan[5]. The reason for this discrepancy is

not clear. One of the photomicrographs shown in the work of Grieve and White[6] is for 30 mass% FeO and 70 mass% TiO_2. According to MacChesney and Muan's[5] phase diagram one would expect the sample to consist of 100% $FeO.2TiO_2$ at temperatures up to 1433°C and predominantly consist of $FeO.2TiO_2$ with a small quantity of liquid phase at temperatures from 1433°C to the liquidus temperature. Instead Grieve and White[6] identified ilmenite and rutile. However, they did not indicate the thermal history of their samples, and therefore one assumes that the photomicrographs were produced from the samples used in the DTA studies. This explanation agrees with Lindsley's[9] finding, as discussed by Grau[8], that pseudobrookite is unstable below ±1140°C, and decomposes into ilmenite and rutile, the phases identified by Grieve and White[6].

The origin of the difference between the FeO-TiO_2 phase diagrams (especially the liquidus temperatures) proposed by Grau[8] and by MacChesney and Muan[5] above 70 mass% TiO_2 might be that MacChesney and Muan[5] fixed the partial oxygen pressure in their experiments, while Grau[8] did not. Grau[8] also states that no attempt was made to equilibrate the slags with the oxygen in the gas phase in order to avoid compositional changes in the slag and also because of the "dynamic" nature of the DTA technique. It is therefore incorrect to compare the liquidus temperatures as determined by Grau[8] with that of MacChesney and Muan[5] because the partial oxygen pressure in the work of MacChesney and Muan[5] was fixed for most of their experiments whilst the partial oxygen pressure in Grau's[8] work is uncertain and clearly higher than that of MacChesney and Muan[5]. The presence of molybdenum in the slags from Grau's[8] work indicates a partial oxygen pressure reducing with respect to the Mo/MoO equilibrium partial oxygen pressure. Because of the similar partial oxygen pressures imposed by the Fe/FeO and Mo/MoO equilibria it is possible that significant amounts of molybdenum oxide was present in the slag. On cooling the molybdenum oxide could have decomposed to form metallic molybdenum which was found in the slags. It should be borne in mind that metallic molybdenum was also present in the slags produced by Grieve and White[6].

Eriksson and Pelton[12] used all the available thermodynamic and phase equilibrium data to obtain a set of model equations for the Gibbs energies of all the phases, as a function of temperature and composition. A modified quasichemical model was used to represent the thermodynamic properties. Coefficients within the model were obtained by optimisation of the available data. The calculated FeO-TiO_2 diagram is shown in Fig. 2.5. The diagram agrees well with the data of Grau[8] at high TiO_2 contents and with the diagram of MacChesney and

Muan[5] for TiO_2 constents below 50 mol% TiO_2. Eriksson and Pelton[12] estimated the probable maximum inaccuracy in the assessed diagram to be ±20°C.

2.2. FeO - VO_X System

Wakihara and Katsura[10] determined phase equilibria in the FeO-Fe_2O_3-V_2O_3 system at 1227°C under various oxygen partial pressures ranging from 1.15 x 10^{-3} to 1.40 x 10^{-14} atm. This was done by using quench and thermogravimetric techniques. The quench technique consisted of equilibrating the samples in gas mixtures, of specific oxygen partial pressure, followed by quenching in cold water. The oxygen partial pressure was regulated by either a CO_2/H_2 or a CO_2/O_2 gas mixture. X-ray diffraction was used to identify the phases present in the quenched samples. The thermogravimetric method consisted of continuously weighing an oxide pellet, which was suspended from a thin platinum wire, in a vertical tube furnace. The mass changes were recorded at constant temperature as a function of time at different oxygen partial pressures. The applicable oxygen partial pressure within the furnace was measured by the use of a solid electrolyte cell with partially stabilised zirconia as the solid electrolyte. The 1227°C isothermal section of the FeO-Fe_2O_3-V_2O_3 system as determined by Wakihara and Katsura[10] is shown in Fig. 2.6. Three solid solution phases can be distinguished in this system, namely a sesquioxide solid solution, a spinel solid solution and the wüstite solid solution.

Phase equilibria within the Fe-Fe_2O_3-V_2O_3 system were determined by Katsura et al.[11] at 1227°C under partial oxygen pressures between 1.05 x 10^{-9} and 3.55 x 10^{-14} atm. The oxide samples were contained in alumina crucibles and the experimental procedure employed was similar to that used by Wakihara and Katsura.[10] Katsura et al.[11] did not report any contamination of samples due to the use of alumina crucibles. Fig. 2.7. shows the phase diagram determined by Katsura et al[11]. The diagram indicates that the M_3O_4 solid solution, with composition ranging from that of Fe_3O_4 to the composition point B, is in equilibrium with vanadowüstite on line (C)-(E). However, the M_3O_4 solid solution phase from composition point B to FeV_2O_4 is in equilibrium with metallic iron. This phase diagram corresponds with the phase diagram of Wakihara and Katsura[10] in that both contain the spinel solid solution phase between FeV_2O_4 and Fe_3O_4, the wüstite phase field and the corresponding two phase and three phase fields between the spinel solid solution, wüstite and iron.

Schmahl and Dillenburg[14] equilibrated condensed phase mixtures with CO/CO_2 gas mixtures at 900°C. The gas mixture was pumped in a closed loop over the condensed phase until

equilibrium was attained. The CO/CO_2 ratio was analysed in situ and a ternary phase diagram was constructed from the data as shown in Fig. 2.8. The phases Fe_2O_3, V_2O_3, Fe, $FeO_{1.04}$ and FeV_2O_4 were identified.

General agreement exists between Wakihara and Katsura[10], Katsura e.a.[11] and Schmahl and Dillenburg[14] on phase relations in the iron-rich corner of the Fe-V-O system. These phase relations cover the temperature range of 850°C to 1227°C and indicates that the spinel and sesquioxide solid solutions are to be expected above 1227°C because these are phases of high melting temperatures and spinels are stable up to high temperatures.

2.3. TiO_2 - VO_X System

The only TiO_2-VO_X phase diagram which could be obtained from the literature is the TiO_2-VO_2 phase diagram[15] in the temperature range of 27-107°C. This diagram is however of little value to the present study.

2.4. TiO_2 - VO_X - FeO_Y System

The ternary phase diagram TiO_2-V_2O_5-Fe_2O_3 is known at temperatures below 700°C, as is shown in Fig. 2.9.[16] Although V_2O_5 and Fe_2O_3 are not stable at the oxygen potentials employed in the present study, the ternary diagram serves as a reference point as to the type of phases to be expected. These are phases similar to $FeVO_4$, $Fe_2V_4O_{13}$ in the FeO-VO_X system and Fe_2TiO_5 in the TiO_2-FeO system. No other phase studies within the TiO_2-VO_X-FeO_Y ternary system could be found in the literature.

2.5. TiO_2 - Ti_2O_3 System

Eriksson and Pelton[12] constructed an optimised phase diagram of the TiO_2-Ti_2O_3 system as is shown in Fig. 2.10. As for the FeO-TiO_2 diagram discussed in 2.1, a modified quasichemical model was used to represent the thermodynamic properties and the coefficients within the model were obtained by optimisation of the available data. The system contains the compound Ti_3O_5 with a pseudobrookite structure, and a series of defect compounds known as Magneli phases.

Magneli phases are crystallographic shear structures represented by the general formula Ti_nO_{2n-1} for Ti-O mixtures.[21] The phases with $4 \leq n \leq 10$ have crystal structures derived from the rutile structure.[12] Phases with $n > 10$ have structures based on other shear planes and so

form different families of phases.[21] For Magneli phases consisting of Ti and O the largest value for n has been estimated to be as high as 99. However, according to Murray and Wriedt[21] the lower estimates for the value of n are more realistic because these estimates are based on structural data.

Eriksson and Pelton[12] relied heavily on the work of Zador and Alcock[20] in constructing the phase diagram in Fig. 2.10. For the higher Magneli phases n was arbitrarily set equal to 20, and all of the higher Magneli phases are represented by $Ti_{20}O_{39}$ on the diagram. The probable maximum inaccuracy in the optimised Ti_2O_3-TiO_2 diagram of Eriksson and Pelton[12] is estimated by them as ± 20 °C for mole fraction TiO_2 in excess of 0.4.

2.6. Conclusion

From the literature reviewed in 2.1 to 2.5 it is evident that only a small amount of data is available on phase relations in the TiO_2-FeO_Y-VO_Z pseudo-ternary system. Although the TiO_2-FeO binary system has been studied in detail by a number of researchers, considerable disagreement exists between their reported results. These differences in reported phase relation data can be explained by differences in experimental procedures employed in the different studies. The only recent study on the high TiO_2 side of the TiO_2-FeO pseudo binary system is the study made by Du Plooy[36] employing a thermal analysis technique, similar to that of Grau.[8] The maximum temperature at which phase relations in the FeO-V_2O_3-Fe_2O_3 ternary system is known is 1227°C[10]. Phase relations in the FeO-V_2O_3 binary system are available from the FeO-V_2O_3-Fe_2O_3 system. Therefore considerable room exists for phase relation determinations in the FeO-V_2O_3 system at temperatures above 1227°C. No data could be found on the TiO_2-VO_X binary system, or the TiO_2-FeO_Y-VO_Z pseudo-ternary system at relevant oxygen partial pressures. Therefore there is great need for data on phase relations in the pseudo-binary phase diagrams which constitute the TiO_2-FeO_Y-VO_Z pseudo-ternary system, as well as in the TiO_2-rich side of this pseudo-ternary system.

Fig. 2.1: FeO-TiO_2 Phase Diagram: Grieve and White[6]

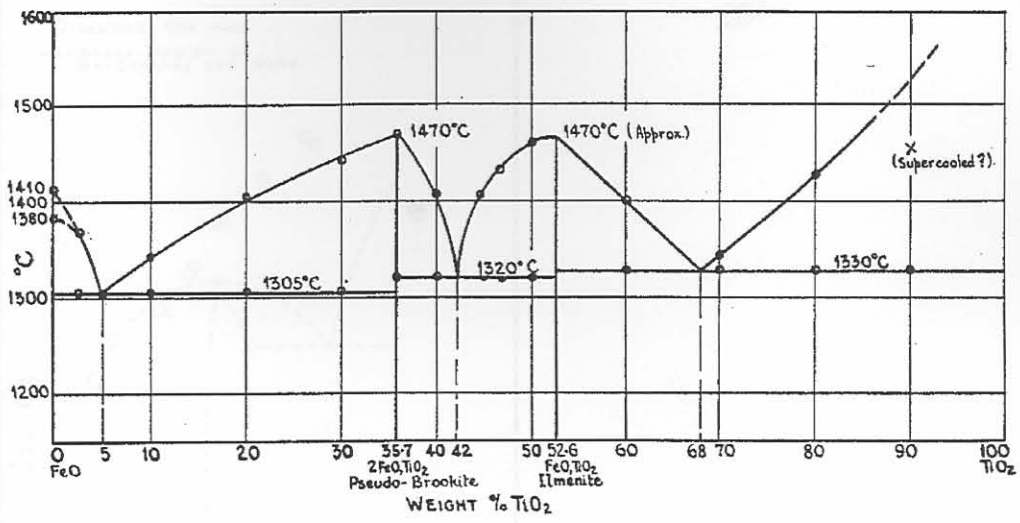

Fig. 2.2: FeO-TiO_2 Phase Diagram: MacChesney and Muan[5]

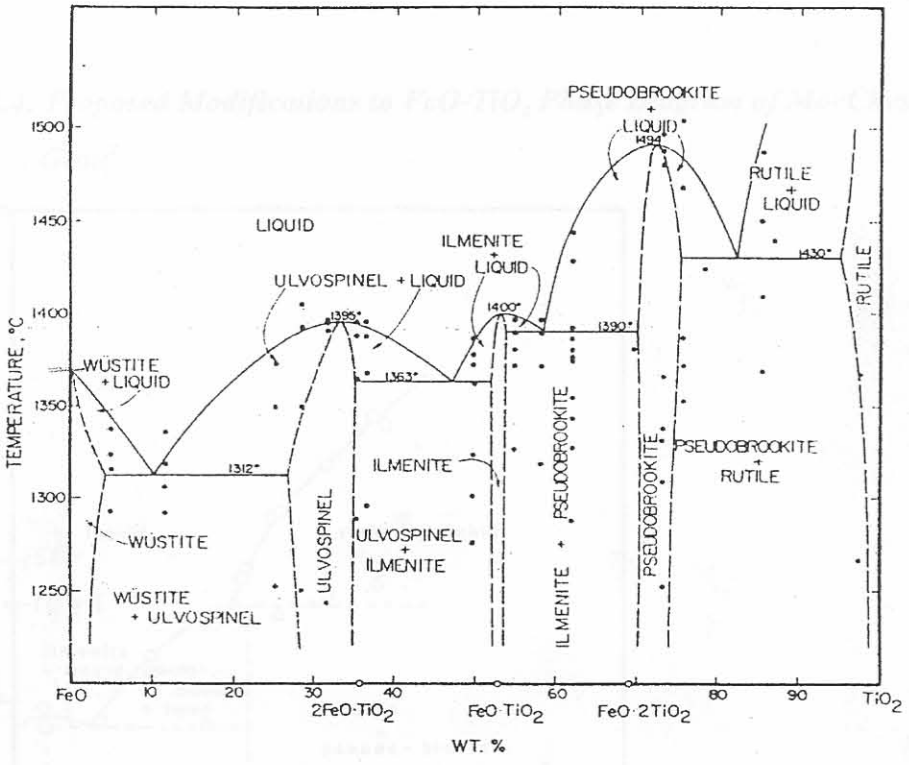

Fig. 2.3: Liquidus Temperature Measurements in $FeO-TiO_2$ System: Grau[8]

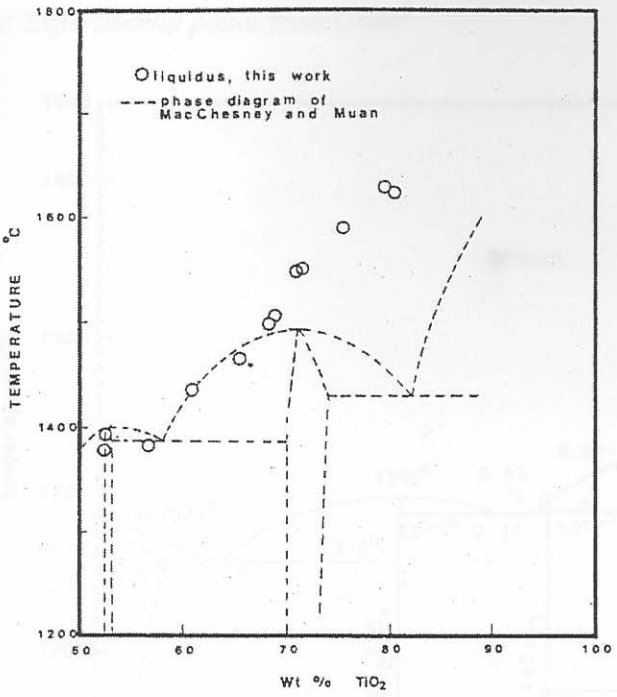

Fig. 2.4: Proposed Modifications to $FeO-TiO_2$ Phase Diagram of MacChesney and Muan[5] *: Grau*[8]

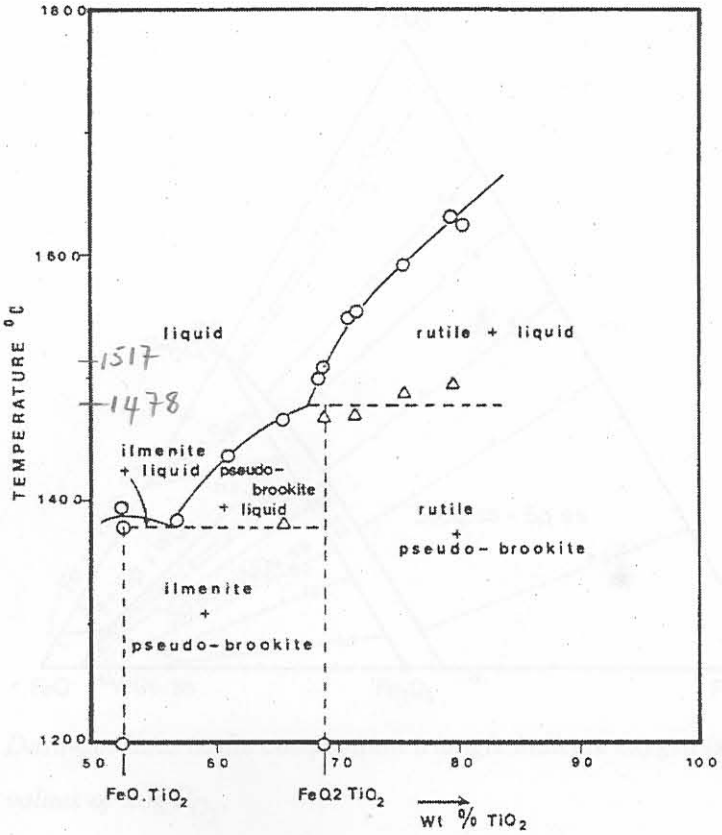

Fig. 2.5: Optimised FeO-TiO_2 Phase Diagram: Eriksson and Pelton[12]

o: *Experimental points from Grau[8]*

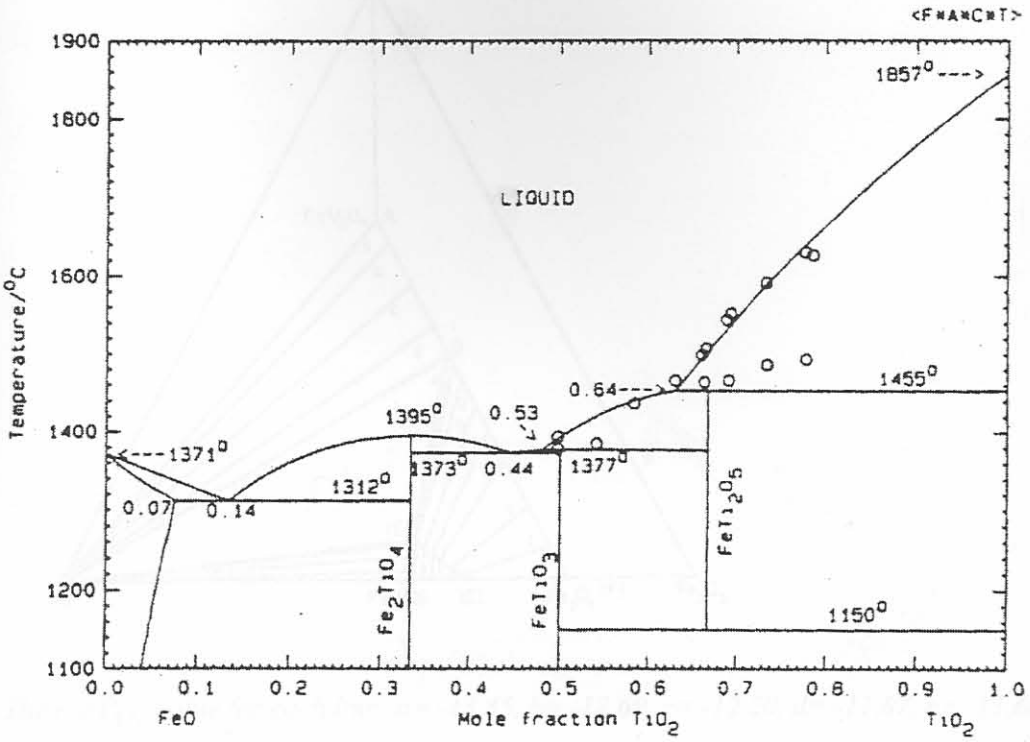

Fig. 2.6: FeO-Fe_2O_3-V_2O_3 Phase Diagram (mole %) at 1227°C: Wakhihara and Katsura[10]

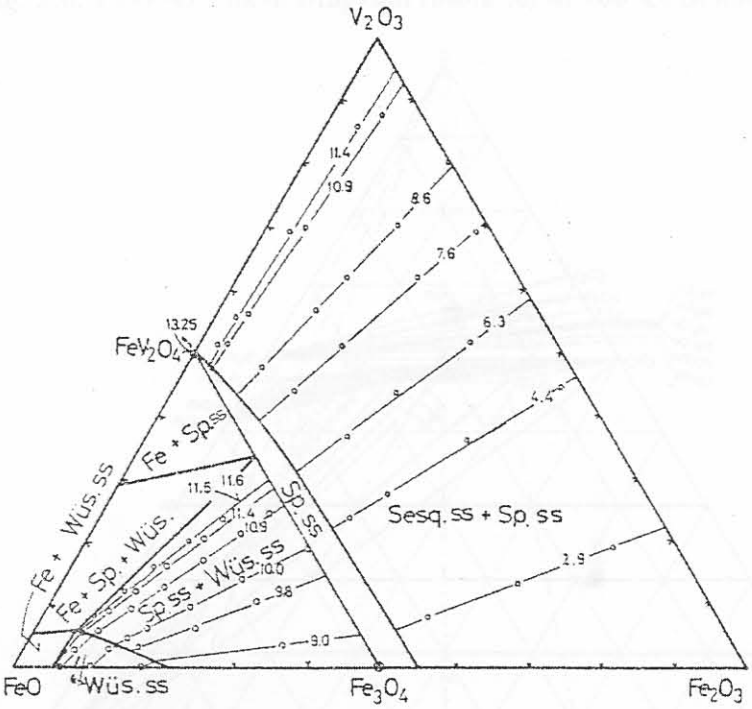

Dash-dot lines in the composition triangle indicate oxygen isobar and numbers on the lines are values of $-\log P_{O_2}$.

Fig. 2.7: Fe-Fe_2O_3-V_2O_3 Phase Diagram (mole %) at 1227°C: Katsura et al[11]

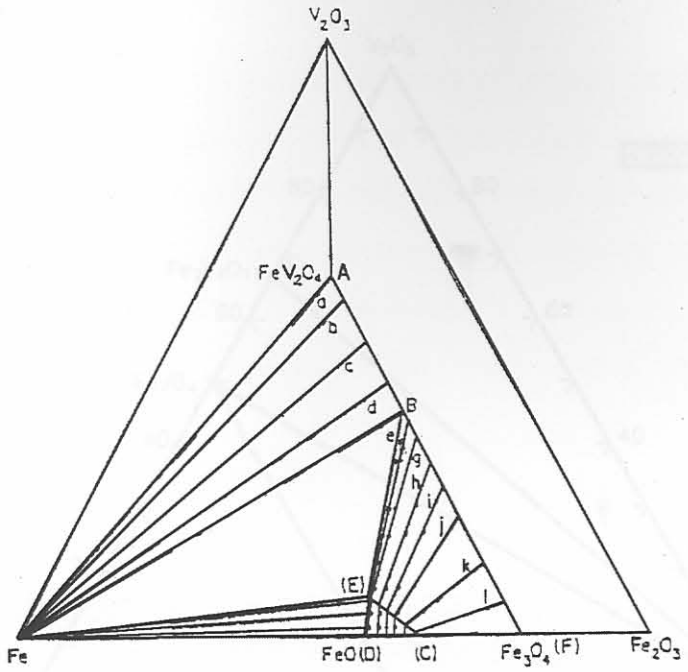

The log P_{O_2} value for each line: a= -13.45, b= -12.69, c= -12.20, d= -11.87, e= -11.68, f= -11.56, g= -11.37, h= -10.83, i= -10.45, j= -10.03, k= -9.39, l= -8.98.

B: 42.80% Fe_2O_3, 20.00% Fe, 37.20% V_2O_3; E: 51.60% Fe_2O_3, 41.70% Fe, 6.70% V_2O_3.

Fig. 2.8: Fe-V-O Phase Diagram (mole %) at 900°C: Schmahl and Dillenburgh[14]

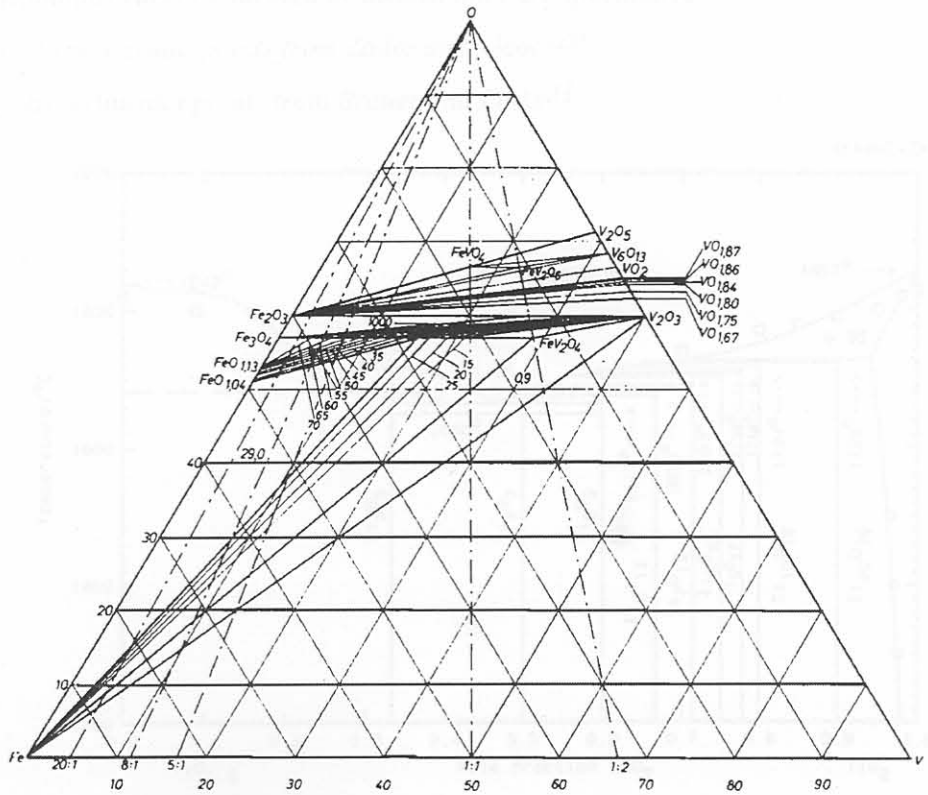

Fig. 2.9: TiO_2-V_2O_5-Fe_2O_3 Phase Diagram: Fotiev et al[16]

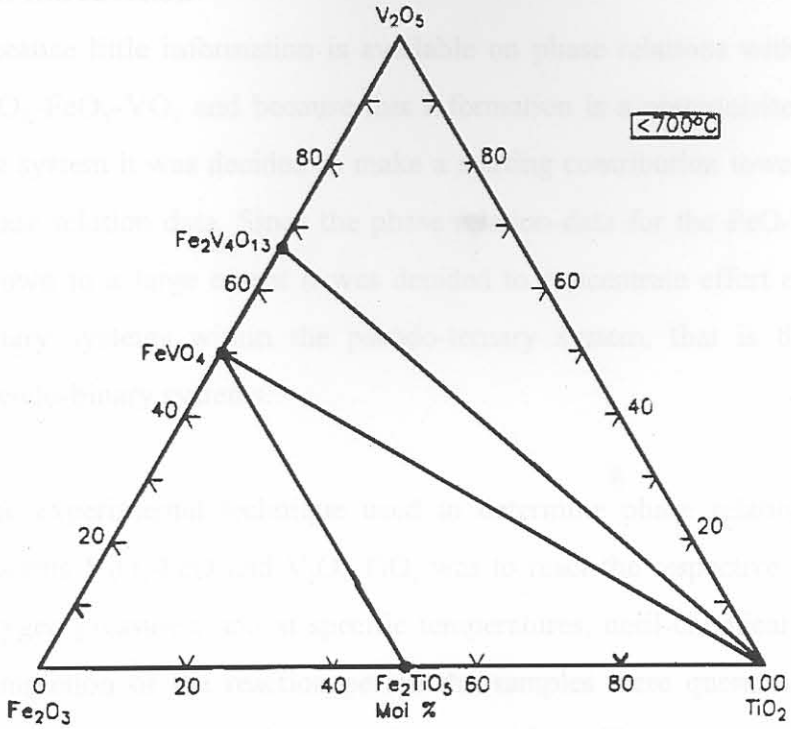

Fig. 2.10: Ti_2O_3 - TiO_2 Phase Diagram: Eriksson and Pelton[12]

(Liquidus curves indicated by dashed lines are speculative)

o: *Experimental points from Zador and Alcock*[20]

□: *Experimental points from Brauer and Littke*[31]

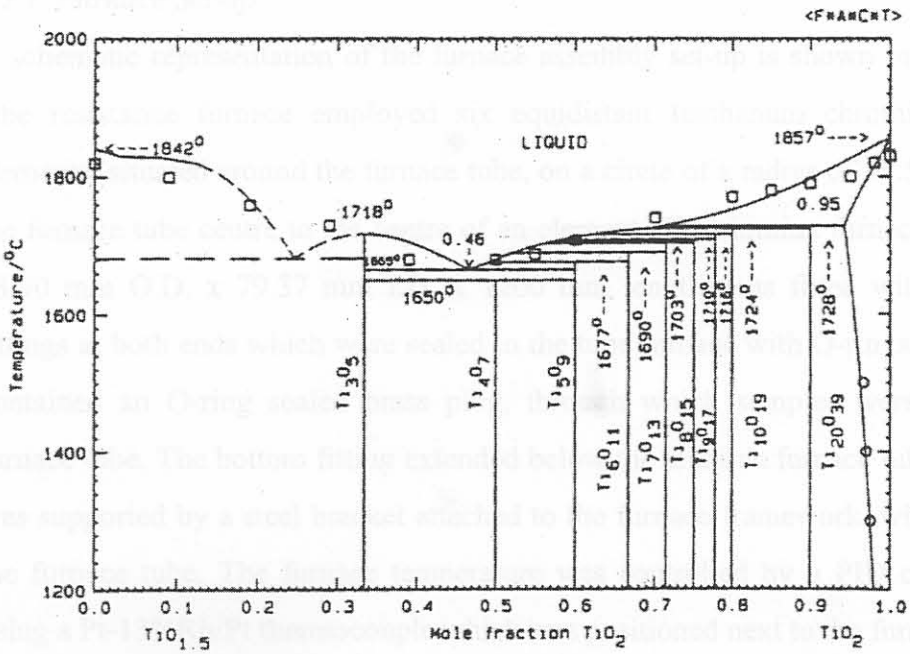

3. EXPERIMENTAL

3.1. Introduction

Because little information is available on phase relations within the pseudo-ternary system TiO_X-FeO_Y-VO_Z and because this information is a prerequisite for activity measurements in the system it was decided to make a starting contribution towards determining the necessary phase relation data. Since the phase relation data for the FeO-TiO_2 pseudo-binary system is known to a large extent it was decided to concentrate effort on the remaining two pseudo-binary systems within the pseudo-ternary system, that is the V_2O_3-FeO and V_2O_3-TiO_2 pseudo-binary systems.

The experimental technique used to determine phase relations in the two pseudo-binary systems V_2O_3-FeO and V_2O_3-TiO_2 was to react the respective samples under specific partial oxygen pressures, and at specific temperatures, until chemical equilibrium was attained. On completion of the reaction period the samples were quenched in water, and subsequently analysed for phase and chemical compositions. The experiments were conducted at 1400°C, 1500°C and 1600°C. The maximum temperature of 1600°C was used because that was the maximum temperature that the furnace could reach comfortably. In order to determine trends in the phase boundaries on the pseudo-binary diagrams the temperatures of 1400°C and 1500°C were chosen as experimental temperatures, in addition to 1600°C.

3.2. Experimental Set-up

3.2.1. Furnace Set-up

A schematic representation of the furnace assembly set-up is shown in Fig.3.1. The vertical tube resistance furnace employed six equidistant lanthanum chromite ($LaCrO_3$) heating elements, situated around the furnace tube, on a circle of a radius of 57.5 mm, measured from the furnace tube centre to the centre of an element. The alumina furnace tube, 99.8% Purity, 88.90 mm O.D. x 79.37 mm I.D. x 1200 mm length, was fitted with water-cooled brass fittings at both ends which were sealed to the tube furnace with O-rings. The top brass fitting contained an O-ring sealed brass plug, through which samples were introduced into the furnace tube. The bottom fitting extended below the alumina furnace tube. The bottom fitting was supported by a steel bracket attached to the furnace framework, which in turn supported the furnace tube. The furnace temperature was controlled by a PID controller/programmer using a Pt-13%Rh/Pt thermocouple which was positioned next to the furnace tube, close to the

hot zone. The exact position of the hot zone in the furnace was established by placing a hand held Pt-13%Rh/Pt thermocouple at various depths into the furnace tube.

Fig.3.1: Furnace Assembly Set-up

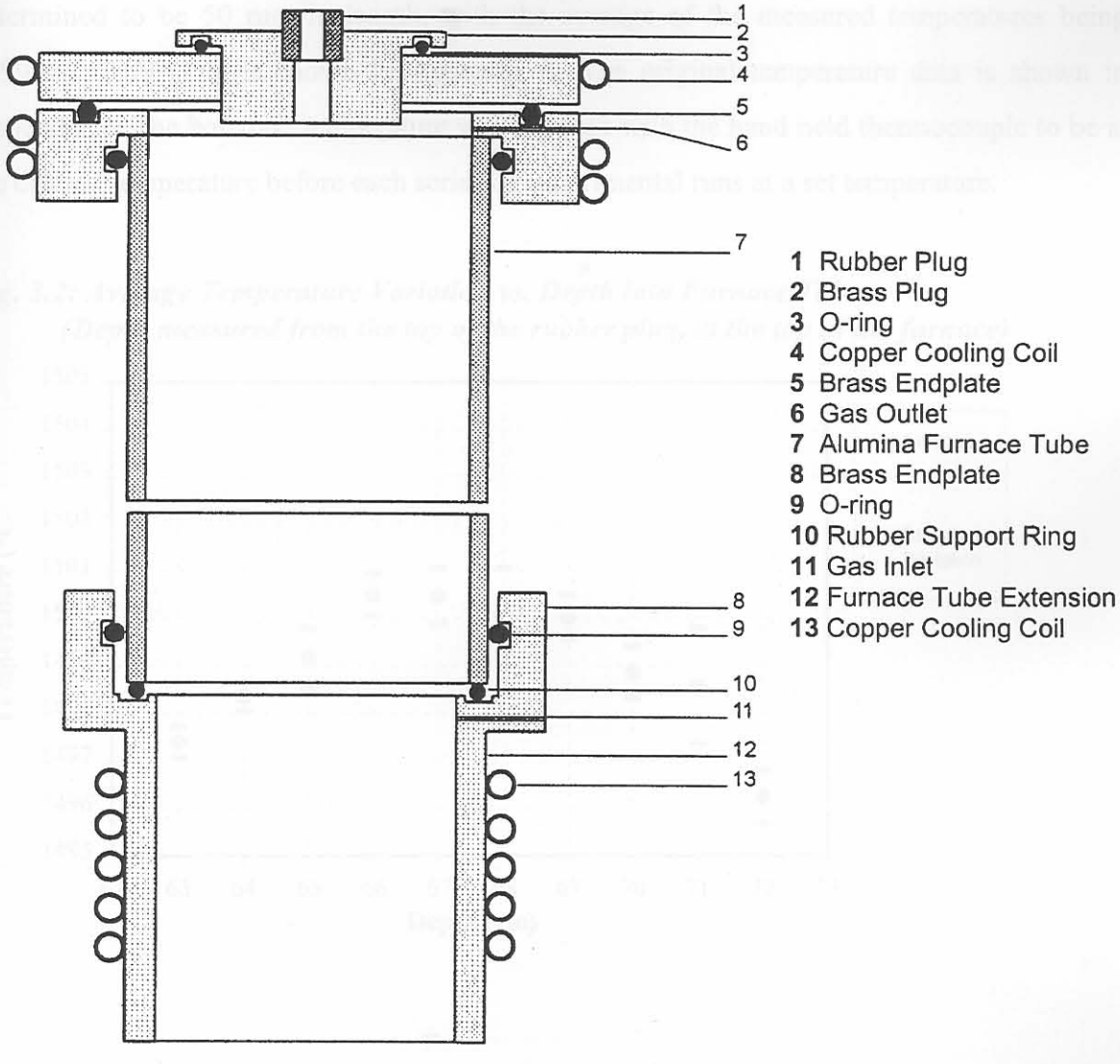

The hand held thermocouple was checked against a standard thermocouple which was certified to have a maximum deviation of ±1.003°C from the standard for 1100-1600°C. The hand held thermocouple measured 1500.21 ±0.27°C and the standard thermocouple measured 1499.86 ±0.26°C at the same temperature. The average temperature variation with increasing depth down the furnace tube is shown in Fig. 3.2, at 1500°C. The furnace hot zone was determined to be 50 mm in length, with the average of the measured temperatures being 1499.85 ±0.89°C as is shown in Appendix 1. The original temperature data is shown in Appendix 2. The hot zone temperature was checked with the hand held thermocouple to be at the desired temperature before each series of experimental runs at a set temperature.

Fig. 3.2: Average Temperature Variation vs. Depth into Furnace Tube
(Depth measured from the top of the rubber plug, at the top of the furnace)

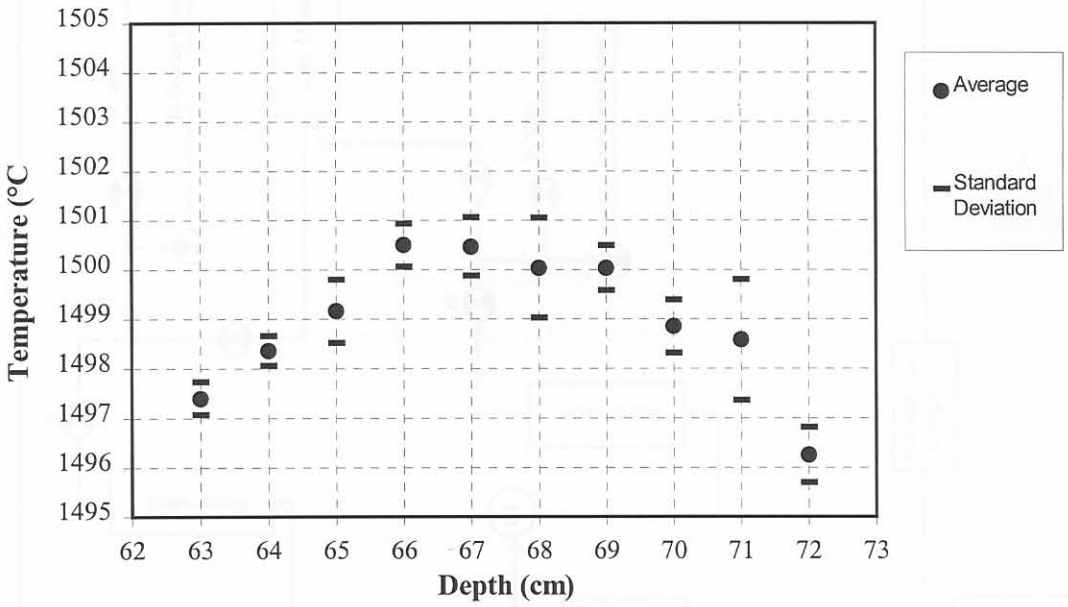

3.2.2. Gas System

A specific partial oxygen pressure was maintained within the furnace by mixing CO and CO_2 in specified volumetric proportions at a total flow rate of 600 cm^3/min at STP, that is a superficial velocity of 0.20 cm/s at STP, with the sectional area of the furnace tube being 50.3 cm^2. The volumetric proportions required to fix the oxygen partial pressure at a selected temperature were obtained from the tables compiled by Deines et. al.[17] In order to control gas flow rates and clean, mix and transport the gases a gas system was constructed from PVC tubing, ball valves and ring clamps. Fig. 3.3 shows a schematic representation of the gas system.

Fig. 3.3: Gas System

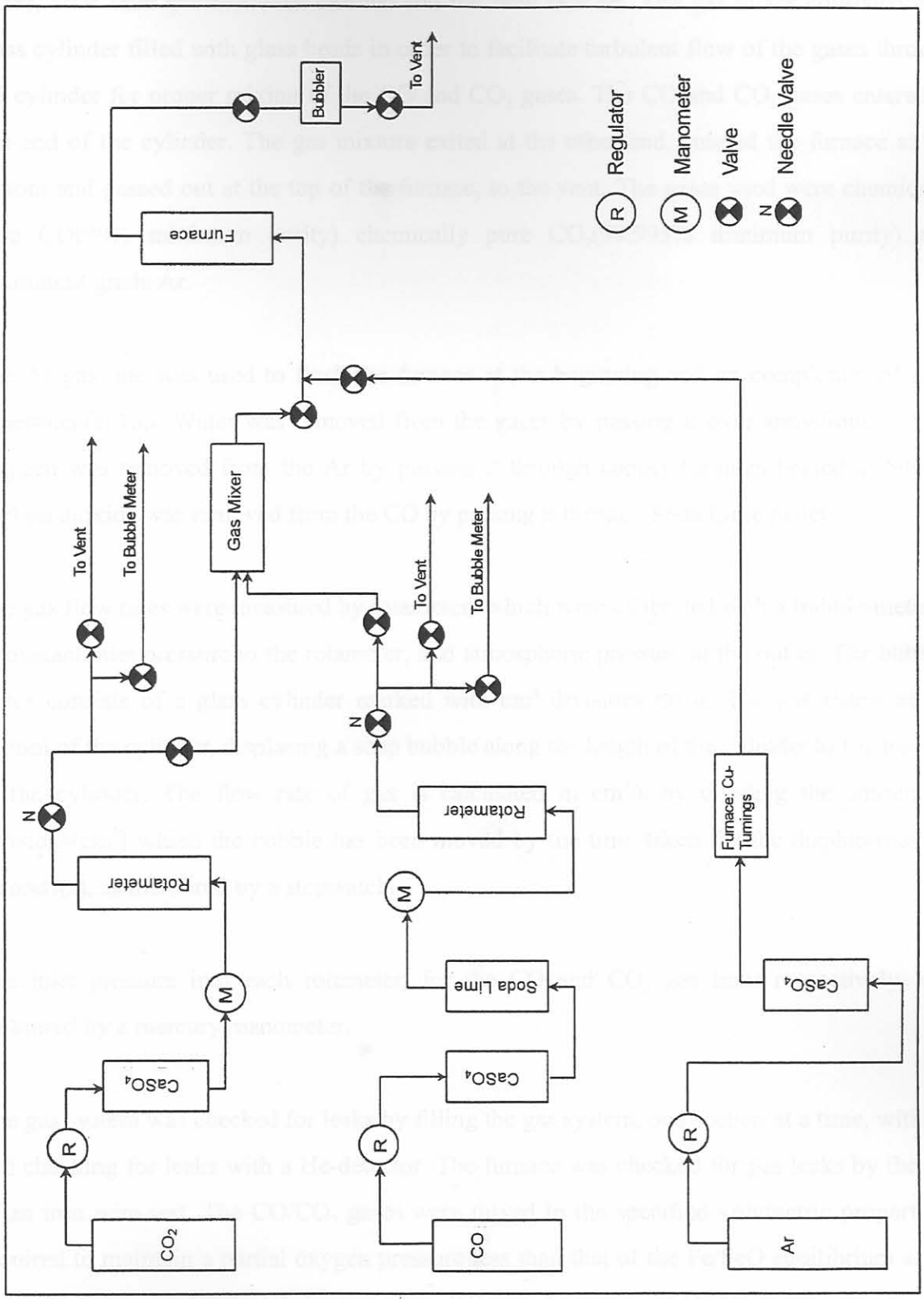

The gas system contained two separate gas lines for CO and CO_2, which joined at the gas mixer, after each gas had been cleaned and the flow rate set. The gas mixer consisted of a glass cylinder filled with glass beads in order to facilitate turbulent flow of the gases through the cylinder for proper mixing of the CO and CO_2 gases. The CO and CO_2 gases entered at one end of the cylinder. The gas mixture exited at the other end, entered the furnace at the bottom and passed out at the top of the furnace, to the vent. The gases used were chemically pure CO(99% minimum purity) chemically pure CO_2(99.995% minimum purity) and instrument grade Ar.

The Ar gas line was used to flush the furnace at the beginning and on completion of each experimental run. Water was removed from the gases by passing it over anhydrous $CaSO_4$. Oxygen was removed from the Ar by passing it through copper turnings heated at 500°C. Carbon dioxide was removed from the CO by passing it through Soda Lime pellets.

The gas flow rates were measured by rotameters which were calibrated with a bubble-meter at a constant inlet pressure to the rotameter, and atmospheric pressure at the outlet. The bubble-meter consists of a glass cylinder marked with cm^3 divisions on it. The gas enters at the bottom of the cylinder, displacing a soap bubble along the length of the cylinder to the top end of the cylinder. The flow rate of gas is calculated in cm^3/s by dividing the amount of divisions(cm^3) which the bubble has been moved by the time taken for the displacement in seconds(s), as measured by a stopwatch.

The inlet pressure into each rotameter, for the CO and CO_2 gas lines respectively, was measured by a mercury manometer.

The gas system was checked for leaks by filling the gas system, one section at a time, with He and checking for leaks with a He-detector. The furnace was checked for gas leaks by the use of an iron wire test. The CO/CO_2 gases were mixed in the specified volumetric proportions required to maintain a partial oxygen pressure less than that of the Fe/FeO equilibrium at the test temperature of 1303°C.[18] An iron wire, 0.9 mm diameter and 99.5% purity, was pushed through an alumina tube with at least 50 mm of iron wire protruding from one end of the tube, and the piece of iron wire protruding from the other end bent through 180°. The tube was sealed with silicone sealant at this end as shown in Fig. 3.4. This iron wire and alumina rod assembly was subjected to the above conditions for 1 hour. The iron wire was pulled up the

alumina rod, leaving the bottom 70 mm in the tube section protruding from the furnace in order for the iron wire to cool down, after which it was removed from the alumina rod. The absence of oxidation products on the iron wire indicated the absence of leaks in the furnace.

The variation in the set partial oxygen pressure was estimated by employing the procedure used in checking the furnace tube for leaks, that is the iron wire test described above. The CO/CO_2 gases were mixed in the specified volumetric proportions required to maintain a partial oxygen pressure $0.5\log_{10}$ units above and below that of the Fe/FeO equilibrium at the test temperature of 1303°C. The equilibrium partial oxygen pressure (P_{O2}) for the Fe/FeO equilibrium is 1.91×10^{-11} atm ($\log P_{O2} = -10.72$ atm) at 1303°C[18]. Therefore the partial oxygen pressure was set at 6.03×10^{-12} atm ($\log P_{O2} = -11.22$ atm) for checking the variation in the set partial oxygen pressure on the Fe side of the Fe/FeO equilibrium, and set at 6.03×10^{-11} atm ($\log P_{O2} = -10.22$ atm) to check the variation in the set partial oxygen pressure on the FeO side of the Fe/FeO equilibrium, at 1303°C. No oxidation product was observed on the iron wire for the test done at the partial oxygen pressure of 6.03×10^{-12} atm, and wüstite was observed on the iron wire for the test done at 6.03×10^{-11} atm indicating that the variation in the set partial oxygen pressure was within a factor of $10^{0.5}$ of the Fe/FeO equilibrium partial oxygen pressure at 1303°C.[18]

3.2.3. Quenching Set-up

The bottom end of the furnace tube was sealed by a PVC membrane, thickness = 50 μm, wrapped over the furnace tube opening, with a layer of vacuum grease as sealant between the brass tube and the PVC. The PVC was held in place by two rubber bands. The PVC-covered tube end was immersed in water, contained in a bucket through which water was pumped continuously in order to keep the PVC cool.

The quenching rod, shown schematically in Fig. 3.5, consisted of a double bore alumina tube. Molybdenum wire of 1 mm diameter was pushed through each bore and bent at the top. The holes were sealed at the top with silicone sealant. The molybdenum wires protruding from the bottom of the alumina rod were bent to form two hooks. The hooks were bridged by 0.3 mm diameter molybdenum wire. The sample hung from this bridge. To quench the sample, an electrical current was sent through the molybdenum wire circuit via the top connections, and the 0.3 mm diameter molybdenum wire melted whereby the sample was released to fall through the PVC cover and into the water at the bottom of the furnace.

Fig. 3.4: Iron Wire and Alumina Rod Assembly

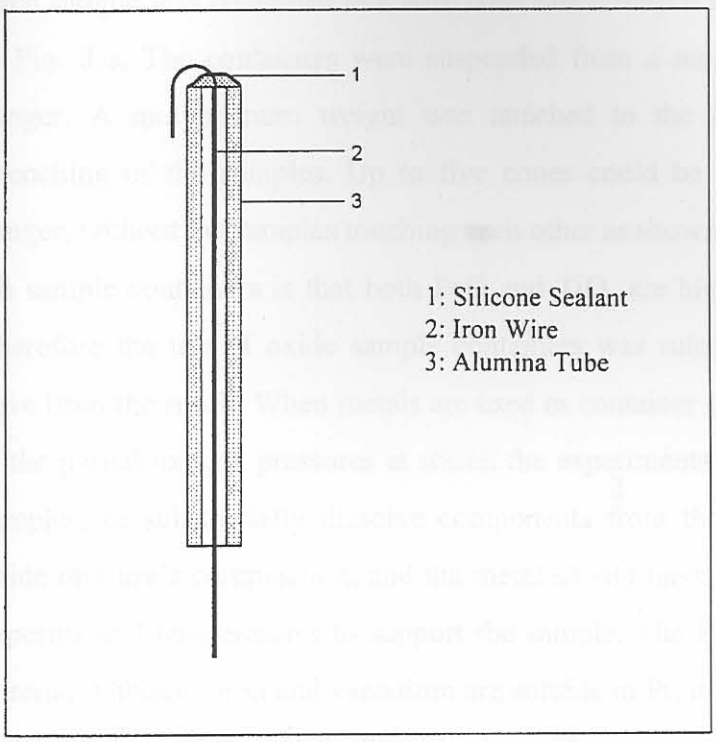

Fig. 3.5: Quenching Rod

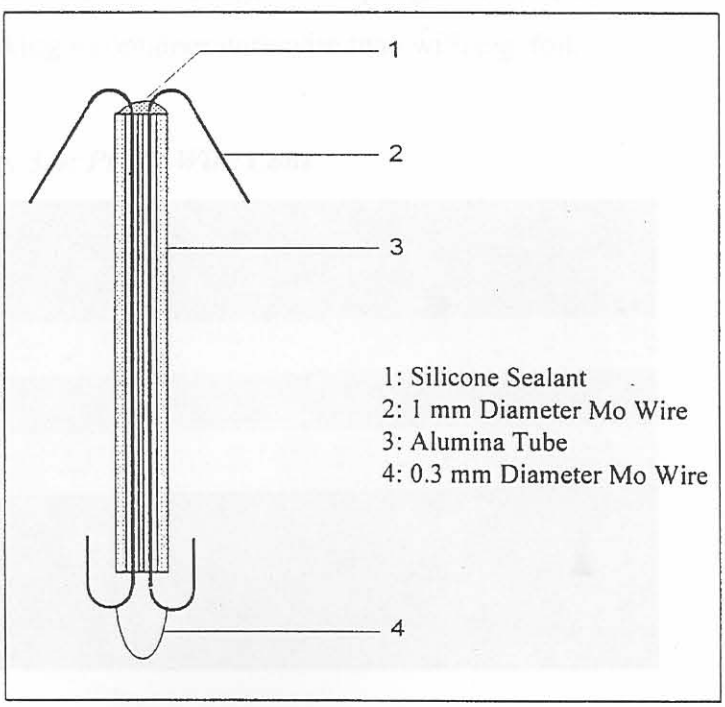

3.2.4. Crucibles

Each sample was contained in a wire cone made from 0.5 mm diameter Pt-Rh wire as shown in Fig. 3.6. The containers were suspended from a molybdenum wire bent into a circular hanger. A molybdenum weight was attached to the hanger in order to facilitate rapid quenching of the samples. Up to five cones could be suspended from each molybdenum hanger, without the samples touching each other as shown in Fig. 3.7. The reason for using Pt-Rh sample containers is that both FeO and TiO_2 are highly corrosive towards other oxides. Therefore the use of oxide sample containers was ruled out because contamination would have been the result. When metals are used as container material the metal should not oxidise at the partial oxygen pressures at which the experiments are done, or dissolve into the oxide samples, or substantially dissolve components from the oxide samples and so change the oxide mixture's composition, and the metal should have the required physical strength at the experimental temperatures to support the sample. The Pt and Pt-Rh mixtures satisfied these criteria. Although iron and vanadium are soluble in Pt, it was found that little or no vanadium and iron absorption into the Pt took place. This is most probably due to the partial oxygen pressures used in the experiments being oxidising relative to iron and vanadium. Furthermore, contact between the sample and sample container material was limited because the majority of the reacted samples remained solid throughout the experiments. Sample containers were made from wire to ensure good sample-gas contact, and because less Pt-Rh material is required in making a container with wire than with e.g. foil.

Fig. 3.6: Pt-Rh Wire Cone

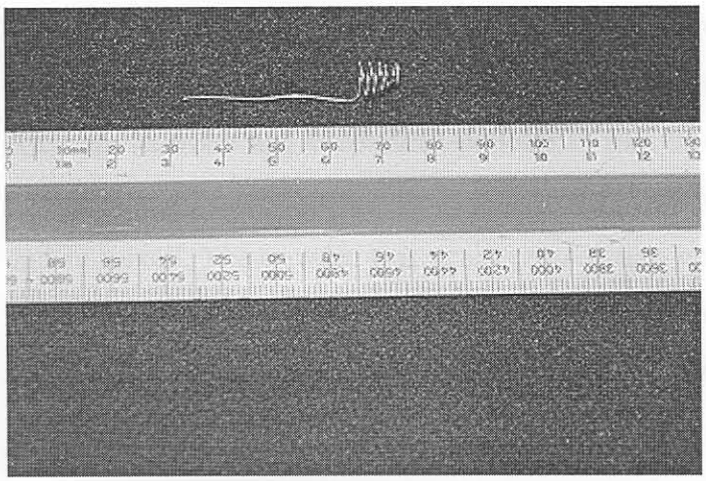

Fig. 3.7: Molybdenum Hanger and Pt-Rh Wire Cones

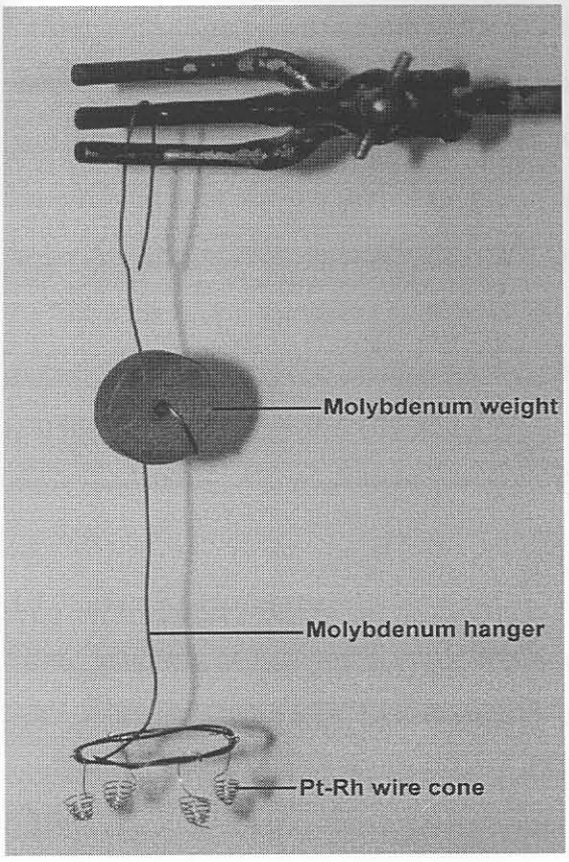

3.3. Experimental Procedure

3.3.1. Sample Preparation

The following chemicals were used: GP-grade V_2O_5 (Assay: >99%), Fe_2O_3 (Assay: minimum 99%) and extra pure TiO_2 (Assay: 99-100.5%). The powders were dried by heating at 400°C for 12 hours and stored in a desiccator. Samples were made up by determining the required mass of powders and mixing these thoroughly under acetone, with a spatula, on a watch-glass. After the acetone had evaporated pellets, 15 mm in diameter and 5-10 mm in height, were pressed from the mixture and these pellets were sintered for 48 hours at 550°C in air, crushed and re-mixed. The powder was again pressed into pellets and sintered for another 16 hours. The pellets were stored in a desiccator. The pellets were chipped down to pieces of 0.1-0.2 g which fitted easily into the sample containers to be used in the experiments.

3.3.2. Experimental Run

Before each experiment the furnace was flushed with purified Ar. The desired CO_2 flow rate was set by using the bubble-meter, after which it was bypassed to the vent. The CO flow rate was then fixed in a similar manner, after which it was combined with the CO_2 flow through the bubble-meter for the period of time taken to introduce the sample into the furnace tube, under Ar. The Ar was replaced with the CO/CO_2 gas mixture and the sample was lowered into the hot zone of the furnace. On completion of the reaction period of 24 hours, the sample was quenched in water. The sample was retrieved from the water and the CO/CO_2 gas flow replaced by Ar. After the CO and CO_2 gas was flushed from the furnace, the broken PVC cover was replaced with a new layer of PVC.

3.3.3. Sample Analyses

Phase analyses constituted X-ray diffraction (XRD), Electron probe microanalysis (EPMA)-EDS (Energy Dispersive Spectrometry) and optical microscopy. On completion of each experimental run, part of the sample was milled into powder for XRD analysis. XRD analysis was performed with a Siemens Kristalloflex 810 diffractometer, using Cu K_α radiation. Polished sections were also made from parts of the sample and these were studied under the optical microscope. With the XRD and optical microscopy information in hand, Electron probe microanalyses were done on the polished sections, using a JEOL JXA733 Electron probe microanalyser. Integration of the data from these analysis techniques made phase characterisation of each sample possible.

As an example of the process followed in phase characterisation, the 50 mass% V_2O_5-50 mass% Fe_2O_3 sample reacted for 2.67 hours at 1400°C, for equilibrium time determination purposes, is discussed in detail here. From the XRD pattern, shown in Fig. 3.10, the presence of a crystalline phase with metal and oxygen ions in the co-ordination M_3O_4 is identified. This is indicated by the match between the peaks in the diffraction pattern, and those for the magnetite (Fe_3O_4) standard. From the photomicrograph taken from the polished section, under reflected light, two phases are identified, the main phase which is beige in colour and a secondary phase which is yellow in colour(with an unfiltered tungsten light source). From the following observations it is concluded that one of the phases must be amorphous: only one crystalline phase is indicated on the XRD analysis and a quench structure is observed in the polished section. The EPMA analyses in Table 3.1 indicate that both phases contain iron and vanadium. The EPMA analyses are originally expressed in terms of FeO and V_2O_3 because

the cations expected to exist under the experimental conditions employed are Fe^{2+} and V^{3+}. This information indicates that the sample consists of two phases, a crystalline phase of M_3O_4 co-ordination consisting of 52.69 mass% FeO and 47.31 mass% V_2O_3, that is 0.73 mol Fe per 0.63 mol V, and a liquid phase consisting of 85.85 mass% FeO and 14.15 mass% V_2O_3, that is 1.19 mol Fe per 0.19 mol V.

3.3.4. Equilibrium Time Determination

In order to determine the minimum reaction time to establish chemical equilibrium within the samples, one of the initial sample compositions is reacted for increasing periods of time. Equilibrium is considered to have been reached when the number of phases in the sample, the volume fractions of the respective phases and the chemical composition of the respective phases cease to change with a further increase in reaction time. The minimum reaction time required to attain equilibrium throughout the sample is thus indicated by the period of reaction time that was needed for the onset of the stabilisation of the chemical composition of the phases, the particular phases present, as well as their volume fractions.

Samples containing 50 mass% V_2O_5 and 50 mass% Fe_2O_3 were reacted at 1400°C under a gas mixture of CO/CO_2=3 for increasing periods of time. The samples were contained in Pt-Rh wire cones as described in paragraph 3.2.4. The EPMA analyses are shown in Table 3.1. For the sample reacted at 2.67 hours a M_3O_4 phase and liquid were identified. In the 8, 16 and 24 hour samples the only phase present was the M_3O_4 phase, as is seen from the XRD patterns in Fig. 3.10. The liquid phase present in the 2.67 hour sample is not indicated on the XRD patterns since the liquid is not crystalline. The variations in chemical composition with reaction time for the VO_X-FeO_Y oxide phases are shown in Fig. 3.8. and Fig. 3.9. The above data, in combination, indicates reaction times of eight hours to be sufficient to reach equilibrium.

As a check on the homogeneity of the samples and the reliability of the chemical analyses, point counts were made on photomicrographs taken of the samples under reflected light. The samples used were the 10 mass% Fe_2O_3-90 mass% V_2O_5(initial composition) sample and the 30 mass% TiO_2-70 mass% V_2O_5(initial composition) sample, reacted for 24 hours at 1400°C. From the point counts the volume fractions of the phases present in the sample were calculated. The average sample composition calculated from the volume fraction of phases and the phase analyses was then compared to the composition of the sample mixture with

which the experiment was started. The results are summarised in Table 3.2. It is seen that the average volume fractions of the respective phases in the 10F14* sample are 0.808 ± 0.03 M_2O_3-phase and 0.192 ± 0.03 M_3O_4-phase. The 10F14 sample initially contained 0.151 mol V per 1.190 mol Fe, and the calculated mean sample composition corresponds to this initial composition with 0.142 mol V per 1.198 mol Fe. For the 30T14 sample the average volume fractions of the phases are 0.667 ± 0.038 M_3O_5-phase and 0.333 ± 0.038 M_2O_3-phase with the initial sample composition 0.428 mol Ti per 0.878 mol V and the calculated composition 0.375 mol Ti per 0.939 mol V. For the Fe_2O_5-V_2O_5 samples the correlation between the initial and calculated sample compositions is excellent within two decimal places for the composition expressed in mol. For the TiO_2-V_2O_5 samples the initial and calculated sample compositions correlate only within one decimal place when composition is expressed in mol. However, the correlation between the initial and calculated sample compositions does indicate that the chemical analyses are reliable.

*Code clarification: The first two numbers and the following letter together indicate the initial sample composition, the next two code digits indicate the temperature at which the sample was reacted. If more digits follow they indicate the reaction time in minutes. If no digits follow to indicate the reaction time the reaction time was 24 hours. Therefore the 30T14 code means that the sample with the initial composition of 30 mass% TiO_2-70 mass% V_2O_5 (the 70 mass% V_2O_5 is implied because only TiO_2-V_2O_5 and Fe_2O_3-V_2O_5 mixtures were reacted); was reacted at 1400°C for 24 hours. F indicates Fe_2O_3 in the Fe_2O_3-V_2O_5 samples.

Table 3.1: EPMA Analyses: 50 mass% Fe_2O_3 - 50 mass% V_2O_5 Samples used in Equilibrium Time Determination Experiments at 1400°C

Time Reacted (h) →	2.67		2.67		8		16		24	
Phase Identified →	M_3O_4		Liquid		M_3O_4		M_3O_4		M_3O_4	
Analyses, mol → Analysis No. ↓	Fe	V	Fe	V	Fe	V	Fe	V	Fe	V
1	0.66	0.70	1.20	0.19	0.72	0.65	0.71	0.65	0.69	0.67
2	0.72	0.65	1.20	0.18	0.71	0.65	0.63	0.73	0.69	0.67
3	0.78	0.59	1.18	0.20	0.71	0.66	0.68	0.68	0.68	0.69
4	0.78	0.59			0.68	0.68	0.66	0.70		
5	0.77	0.59			0.71	0.66				
6	0.69	0.67			0.64	0.72				
7					0.69	0.67				
Average mol Fe; mol V →	0.73	0.63	1.19	0.19	0.69	0.67	0.67	0.69	0.69	0.68
Standard Deviation on mol Fe; mol V→	0.05	0.05	0.01	0.01	0.03	0.03	0.03	0.03	0.01	0.01
95% Confidence Limit on mol Fe; mol V →	0.04	0.04	0.01	0.01	0.02	0.02	0.03	0.03	0.01	0.01

Table 3.2: Volume% Phases for 10F14 and 30T14 Samples

Sample →	10F14*		30T14#	
Phase in Sample	M_2O_3	M_3O_4	M_3O_5	M_2O_3
Average Volume Fraction of Phase	0.808	0.192	0.667	0.333
Standard Deviation	0.167	0.167	0.231	0.231
95% Confidence Limit	0.03	0.03	0.04	0.04
Number of fields◊ analysed	13		13	
	mol Fe	mol V	mol Ti	mol V
Initial Sample Composition →	0.151	1.190	0.428	0.878
Calculated Sample Composition →	0.142♦ ±0.008	1.198 ±0.03	0.375 ±0.011	0.939 ±0.029

*10F14 = 10 mass% Fe_2O_3-90 mass% V_2O_5 initial composition, reacted at 1400°C

#30T14 = 30 mass% TiO_2-70 mass% V_2O_5 initial composition, reacted at 1400°C

◊Each field consisted of a 13 by 10 grid, that is 130 points per field

---

♦Calculated sample composition:

$(X_{vol})_{M_2O_3}$ = Volume fraction of phase M_2O_3

$(V_{mol})_{M_2O_3}$ = Molar volume of phase M_2O_3

V_{Total} = Total sample volume

$X_{M_2O_3}$ = Mole fraction of phase M_2O_3

$(molV)_{M_2O_3}$ = mol V in M_2O_3 phase

$mm_{M_2O_3}$ = Molar mass of M_2O_3

$$X_{M_2O_3} = \frac{\left(\frac{(X_{vol})_{M_2O_3} \cdot V_{Total}}{(V_{mol})_{M_2O_3}}\right)}{\left(\frac{(X_{vol})_{M_2O_3} \cdot V_{Total}}{(V_{mol})_{M_2O_3}} + \frac{(X_{vol})_{M_3O_4} \cdot V_{Total}}{(V_{mol})_{M_3O_4}}\right)}$$

$$= \frac{(X_{vol})_{M_2O_3} \cdot (V_{mol})_{M_2O_3} \cdot (V_{mol})_{M_3O_4}}{(V_{mol})_{M_2O_3} \cdot (V_{mol})_{M_3O_4} \cdot (X_{vol})_{M_2O_3} + (V_{mol})^2_{M_2O_3} \cdot (X_{vol})_{M_3O_4}}$$

Similarly, $X_{M_3O_4}$ is calculated.

The average sample composition is calculated as follows:

$$(molV)_{sample} = (molV)_{M_2O_3} \cdot X_{M_2O_3} + (molV)_{M_3O_4} \cdot X_{M_3O_4}$$

$(V_{mol})_{M_2O_3}$ is calculated from the density of V_2O_3 as follows:

$$\rho_{V_2O_3} = 4.870\ g/cm^3$$ [38]

The M_2O_3 phase was analysed to consist of 1.248 mol V and 0.090 mol Fe. This equates to 1.866 mol V and 0.135 mol Fe for 3 mol O, that is $X_V = 0.933$ and $X_{Fe} = 0.067$. There is 0.065 mol V in 4.870 g V_2O_3. Therefore:

$$(molV)_{new} = (0.933)(0.065) = 0.061mol = 3.087g$$

$$(molFe)_{new} = (0.0673)(0.065) = 0.004mol = 0.246g$$

$$\Rightarrow (g/cm^3)_{new} = 3.330 + (4.870 - 3.311) = 4.889g/cm^3$$

$$mm_{M_2O_3} = 150.57g/mol$$

$$\Rightarrow (V_{mol})_{M_2O_3} = 150.57/4.889 = 30.80cm^3/mol$$; Similarly $(V_{mol})_{M_3O_4} = 45.45cm^3/mol$

$$\rho_{V_3O_4} = 4.762g/cm^3;\ \rho_{V_3O_5} = 4.724g/cm^3$$ [38]

The V_3O_5 density used to calculate the M_3O_5 phase density was adjusted with respect to volume because of a small shift in the X-ray diffraction analyses pattern with respect to the X-ray diffraction reference data for V_3O_5.

Fig. 3.8: Equilibrium Time Determination - M_3O_4 Phase

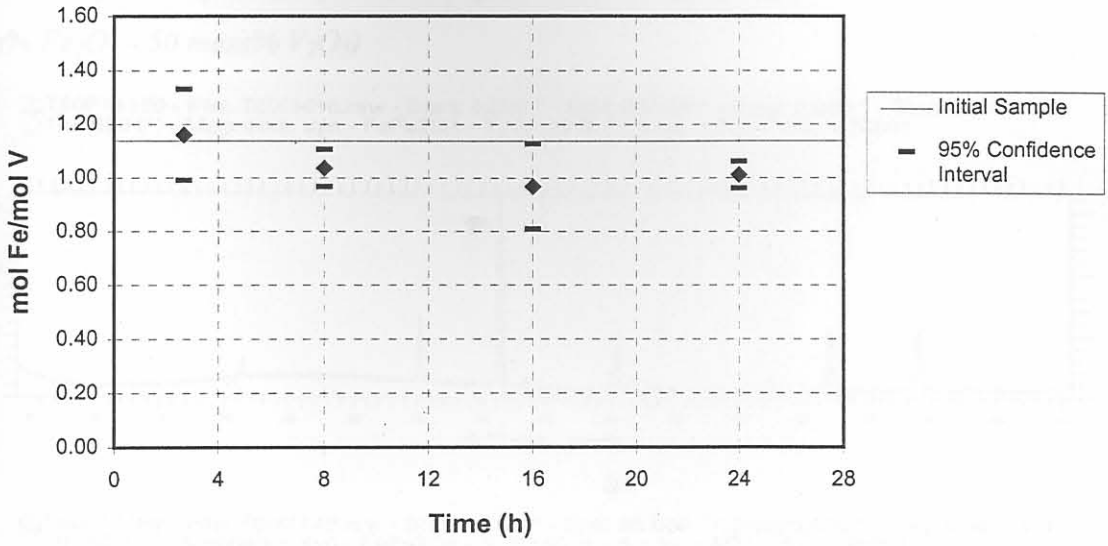

Fig. 3.9: Equilibrium Time Determination - Liquid Phase

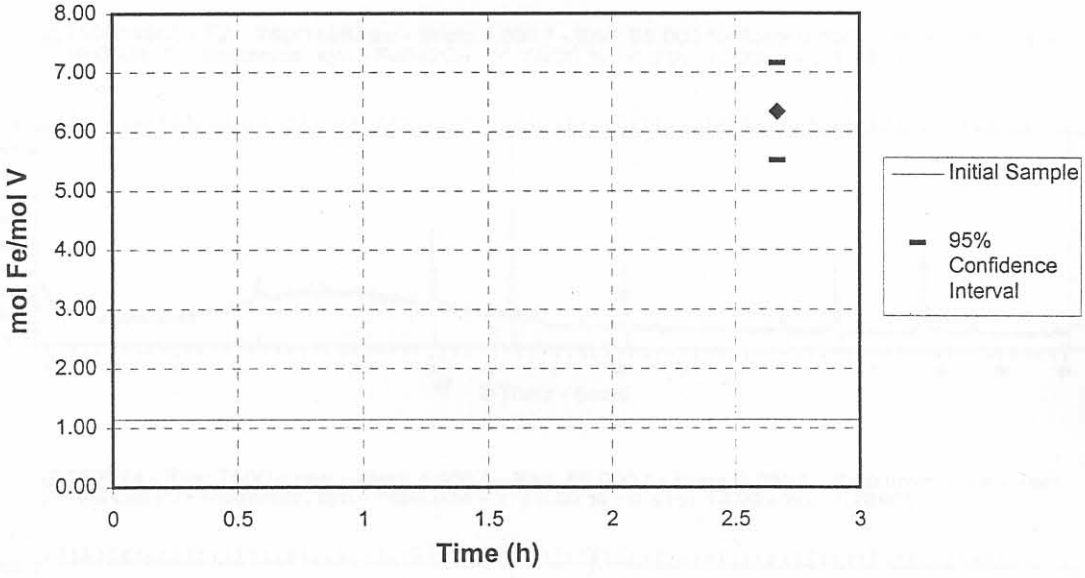

Fig. 3.10: XRD Patterns for Samples used in Equilibrium Time Determination

(Initial sample composition for all samples used in equilibrium time determination = 50 mass% Fe_2O_3 - 50 mass% V_2O_5)

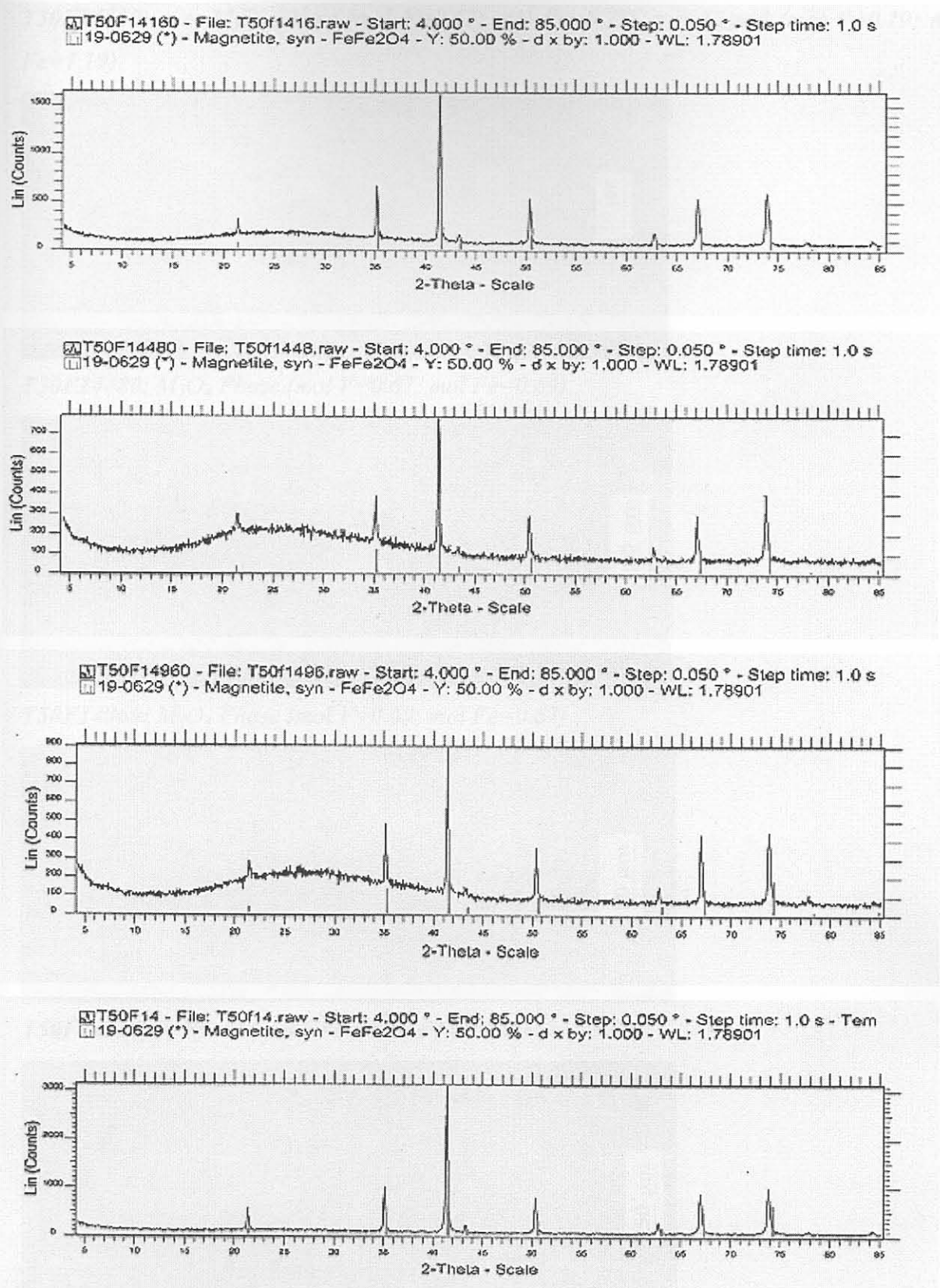

T50F14160 = 2.67 hours; T50F14480 = 8 hours; T50F14960 = 16 hours; T50F14 = 24 hours

Fig. 3.11: Photomicrographs for Samples used in Equilibrium Time Determination

(Initial sample composition for all samples used in equilibrium time determination = 50 mass% Fe_2O_3 - 50 mass% V_2O_5)

T50F14160: *a = M_3O_4 Phase (mol V=0.63; mol Fe=0.73), c = Liquid (mol V=0.19; mol Fe=1.19)*

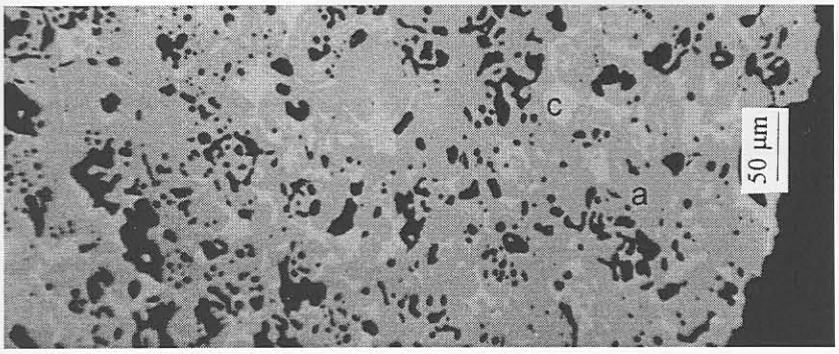

T50F14480: *M_3O_4 Phase (mol V=0.67; mol Fe=0.69)*

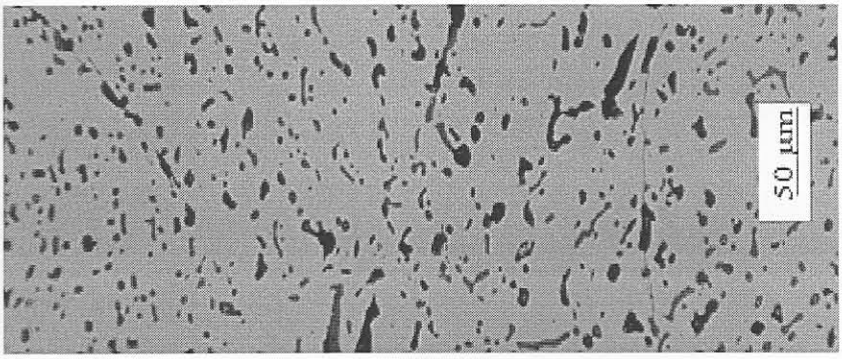

T50F14960: *M_3O_4 Phase (mol V=0.69; mol Fe=0.67)*

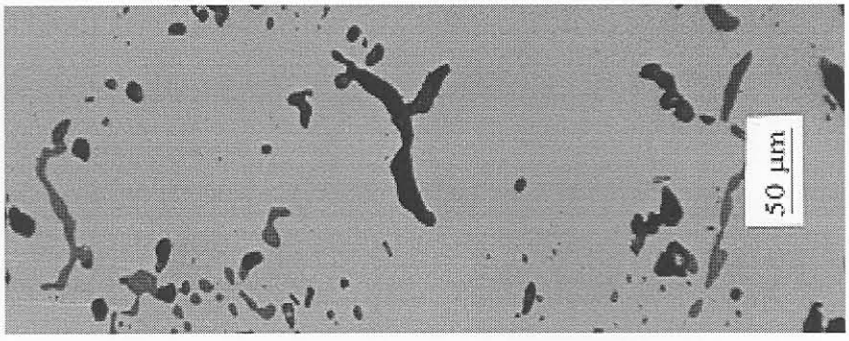

T50F14: *M_3O_4 Phase (mol V=0.68; mol Fe=0.69)*

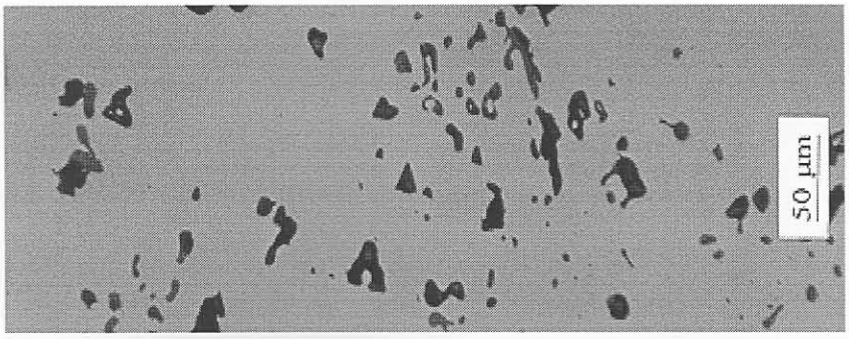

T50F14160 = 2.67 hours; T50F14480 = 8 hours; T50F14960 = 16 hours; T50F14 = 24 hours

3.4. Conclusion

The experimental apparatus and procedure described is suitable for studying phase relations in Fe_2O_3-V_2O_5 mixtures under partial oxygen pressures fixed by a CO/CO_2 gas mixture, with a reaction time of at least eight hours at 1400°C.

The sample holders facilitate good contact between the sample and the gas mixture so that the required reaction time for the attainment of chemical equilibrium is short. Employing the quench technique allows quenching of the reacted sample without reoxidation which would have occurred if the sample came into contact with oxygen in the air at experimental temperatures.

4. RESULTS AND DISCUSSION

4.1. V_2O_3 - TiO_2 System

Table 4.1. gives a summary of the sample compositions reacted, the reaction times used and phases identified in each sample. All of the samples were subjected to XRD analysis, optical microscopy under reflected light and EPMA, with WDS and EDS facilities respectively.

Table 4.1: Summary of Experiments

Reaction Temperature (°C)	Initial Composition (Mass %)		Reaction Time (Hours)	Phases Identified	mol Ti/ (mol Ti +mol V) in Phase
	TiO_2	V_2O_5			
1400	10	90	24	M_2O_3	$M_2O_3 = 0.08$
1400	30	70	24	$M_2O_3 + M_3O_5$	$M_2O_3 = 0.21$ $M_3O_5 = 0.35$
1400	50	50	24	$M_3O_5 + M_4O_7$	$M_3O_5 = 0.64$ M_4O_7 = N.A.
1400	70	30	24	Magneli	Magneli = 0.72
1400	90	10	24	Magneli	Magneli = 0.91
1500	10	90	24	M_2O_3	$M_2O_3 = 0.15$
1500	30	70	24	$M_2O_3 + M_3O_5$	$M_2O_3 = 0.17$ $M_3O_5 = 0.40$
1500	50	50	24	$M_3O_5 + M_4O_7$	$M_3O_5 = 0.42$ $M_4O_7 = 0.55$
1500	70	30	24	Magneli	Magneli = 0.73
1500	90	10	24	Magneli	Magneli = 0.91
1600	90	10	8	Magneli	Magneli = 0.91

The pseudo-binary V_2O_3-TiO_2 phase diagram constructed from the experimental data is shown in Fig. 4.1, and a summary of the EPMA analyses is given in Appendix 3 and Appendix 4. The phase fields identified are M_2O_3, $M_2O_3 + M_3O_5$ and Magneli phases, with M designating both vanadium and titanium ions existing within the particular crystal structure. As mentioned earlier, Magneli phases are crystallographic shear structures represented by the general formula Ti_nO_{2n-1} for Ti-O mixtures.[21] The phases with $4 \leq n \leq 10$ have crystal structures derived from the rutile structure.[12] Phases with $n > 10$ have structures based on other shear planes and so form different families of phases.[21] Both vanadium and titanium oxides form Magneli phases.[21,19]

The XRD patterns for the series of samples reacted at 1400°C are shown in Fig. 4.4. The corresponding photomicrographs for the samples are shown in Fig. 4.5. In Table 4.2 the

number of moles of Ti and V in the initial sample and in the reacted sample, for the single phase samples, are indicated. In the experiments only oxygen should have been removed from the sample because of reaction of the sample under reducing conditions with respect to the initial sample composition. Therefore the ratio of the number of moles of Ti to the number of moles of V in the initial sample should correspond with that of the reacted sample, as is the case in Table 4.2.

The 10 mass% TiO_2 sample consisted of the M_2O_3 phase only indicated by the composition points 0.08 mole fraction Ti at 1400°C and 0.15 mole fraction Ti at 1500°C in Fig. 4.1. The 30 mass% TiO_2 sample consisted of the M_2O_3 phase and M_3O_5 phase which are clearly identified by the XRD analyses shown in Fig. 4.4. The two respective phases could only be distinguished from each other under reflected light when large magnifications were employed, i.e. x400 and larger. The M_2O_3 phase appear pink, and the M_2O_5 phase yellow under reflected light. The M_2O_3 phase appeared as the lighter grey phase, and the M_3O_5 phase as the darker grey phase when viewed with the SEM-EDS facility.

The EPMA (EDS) analyses for the TiO_2-V_2O_3 samples were checked by performing analyses with an ARL-SEMQ (WDS)-Wave Dispersive Spectrometer, employing VO_2 and TiO_2 physical standards. Good agreement was obtained as is seen when the EPMA (EDS) analyses in Appendix 4 are compared to the EPMA (WDS) analyses in Appendix 3. For all of the single phase samples the agreement between the EPMA analyses done with the WDS facility and those done with the EDS facility is excellent. The WDS analyses were used to plot composition points on the phase diagram in Fig. 4.1 for the samples consisting of a single phase.

For the samples consisting of two phases, differences between the two sets of analyses do occur because one of the phases was not analysed with either one of the facilities. Due to the limited optical capability of the WDS facility phases could not be distinguished visually from each other. This resulted in different proportions of each phase being analysed, on each point chosen for analysis, resulting in a distribution of analyses. Therefore a frequency distribution was constructed for the analyses done on the samples as is shown in Fig. 4.2 and Fig. 4.3 for the 30T14 and 50T15 samples.

Subsequently the data were divided into two groups with the division point for the 30T14 sample being 26 mass% TiO_2 and that for the 50T15 sample 50 mass% TiO_2. The division

point for the 30T14 sample was decided with reference to the EDS analyses already in hand. For the 50T15 sample the division point was taken according to the obvious data grouping as shown in Fig. 4.3 because only one phase was analysed with the EDS facility. The respective groups of data were subjected to Chauvenet's criterion[26] in order to eliminate data points deviating significantly from the normal distribution. The remaining data points were used to plot Fig. 4.1.

For the 30T15* and 50T14 samples only one of the two phases present in the sample was analysed by the WDS facility. The WDS analysis data for these samples were also subjected to Chauvenet's criterion[26]. For the 50T14 sample the remaining data were then used to plot the composition point for only the M_4O_7 Magneli phase in Fig. 4.1. For the 30T15 sample the remaining data were combined with the EDS facility's data because it is evident from the EDS data and the XRD analysis that one of the two phases in the sample was not analysed with the WDS facility due to the operator not being able to distinguish between the two phases whilst with the EDS facility one could clearly distinguish between the phases.

*Code clarification: The first two numbers and the following letter together indicate the initial sample composition, the next two code digits indicate the temperature at which the sample was reacted. If more digits follow they indicate the reaction time in minutes. If no digits follow to indicate the reaction time the reaction time was 24 hours. Therefore the 30T14 code means that the sample with the initial composition of 30 mass% TiO_2-70 mass% V_2O_5 (the 70 mass% V_2O_5 is implied because only TiO_2-V_2O_5 and Fe_2O_3-V_2O_5 mixtures were reacted); was reacted at 1400°C for 24 hours. F indicates Fe_2O_3 in the Fe_2O_3-V_2O_5 samples.

Fig. 4.1: V_2O_3 - TiO_2 Phase Diagram

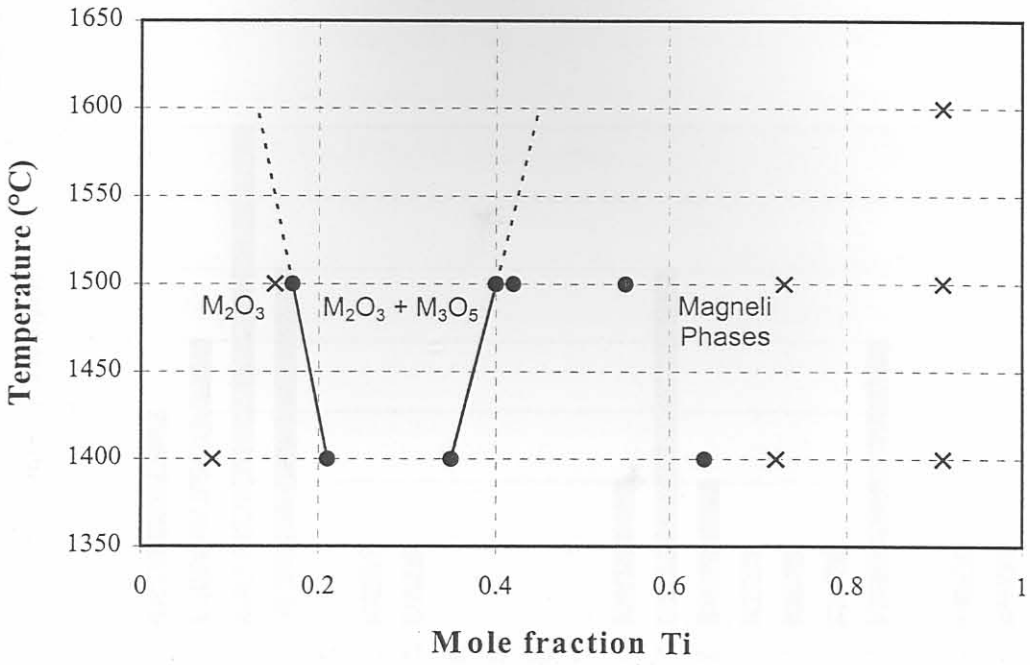

× : Composition points of samples consisting of one phase

• : Composition points of respective phases in two phase samples

Fig. 4.2: Analyses Frequency Distribution for 30T14 Sample (WDS analyses)

(XRD data indicate the presence of M_2O_3 and M_3O_5 phases-see Table 4.1)

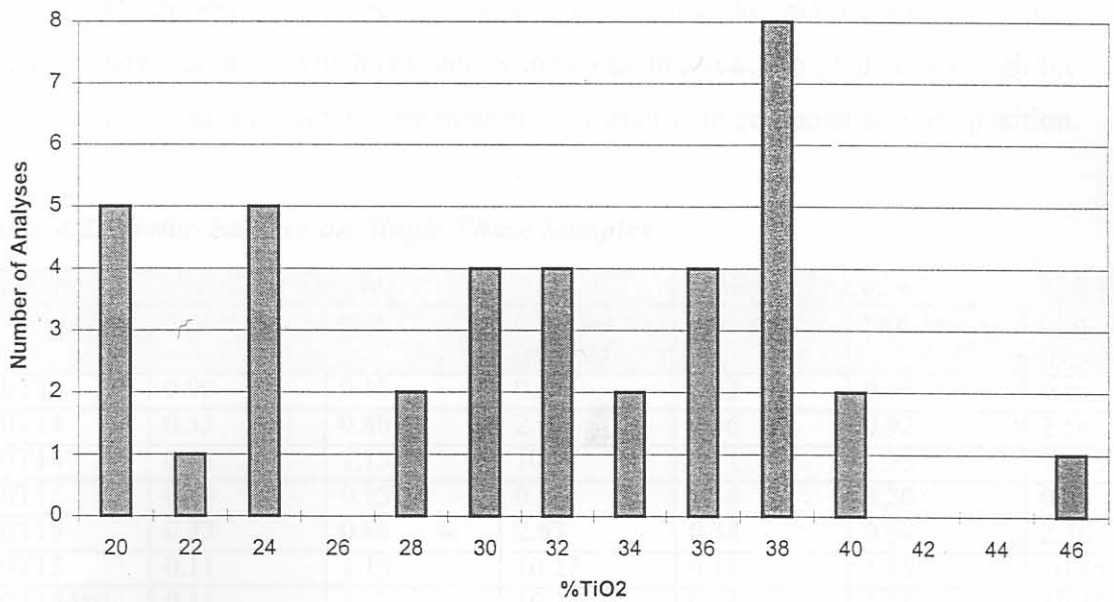

Fig. 4.3: Analyses Frequency Distribution for 50T15 Sample (WDS analyses)

(XRD data indicate the presence of M_3O_5 and M_4O_7 phases-see Table 4.1)

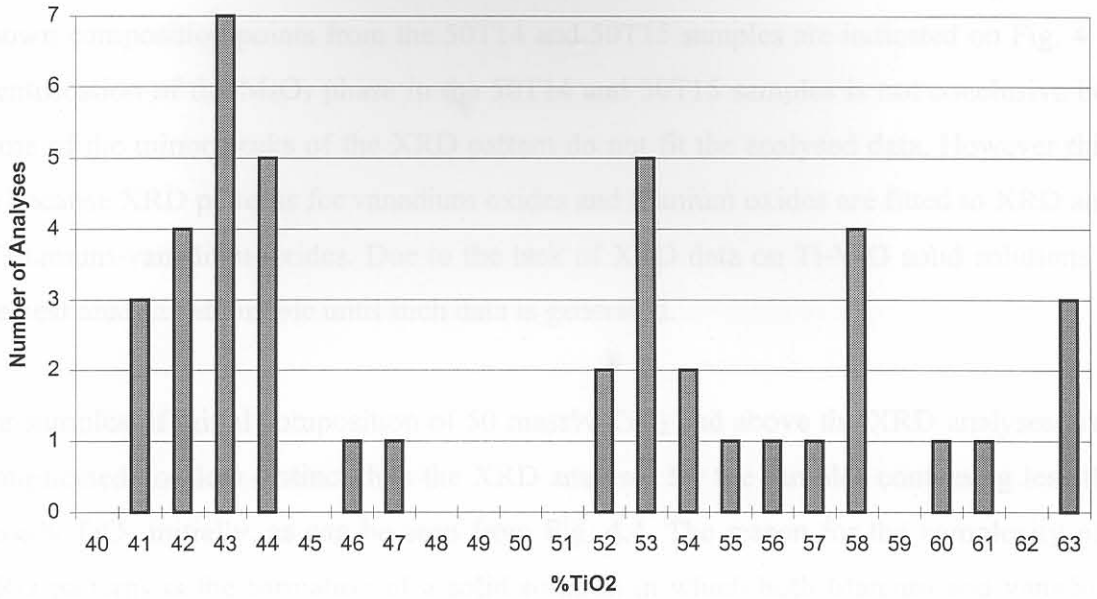

The 30T14, 30T15, 50T14 and 50T15 samples each contains two phases as indicated by the XRD analyses. In the 30T14 and 30T15 samples the respective phases could also be seen under reflected light and under the SEM(EDS). However, for the 50T14 and 50T15 samples the respective phases in each sample could only be identified with XRD analysis. The presence of two different phases in the 50T15 sample is supported by the EPMA(WDS) point analyses which were performed along a line crossing the sample surface, Fig. 4.7. The analyses show variation which is unlikely to be due to a reaction gradient through the sample, for which one would expect a more monotonic variation in composition with position.

Table 4.2: Molar-balance on Single Phase Samples

Sample	Initially in Sample			In Reacted Sample		
	mol V	mol Ti	(mol Ti)/ (mol V)	mol V	mol Ti	(mol Ti)/ (mol V)
10T14	0.99	0.13	0.13	1.22	0.11	0.09
70T14	0.33	0.88	2.67	0.36	0.92	2.56
90T14	0.11	1.13	10.27	0.11	1.15	10.45
10T15	0.99	0.13	0.13	1.14	0.20	0.18
70T15	0.33	0.88	2.67	0.34	0.94	2.76
90T15	0.11	1.13	10.27	0.11	1.15	10.45
90T16480	0.11	1.13	10.27	0.11	1.15	10.45

Due to the inability to distinguish the phases from each other when using the WDS facility only one of the phases was analysed in the 50T14 sample. The EDS analyses on the 50T14 and 50T15 samples were few and varied and not deemed conclusive. Therefore the phase boundary between the M_3O_5 and M_4O_7 phases could not be plotted onto Fig. 4.1, but the known composition points from the 50T14 and 50T15 samples are indicated on Fig. 4.1. The identification of the M_4O_7 phase in the 50T14 and 50T15 samples is not conclusive because some of the minor peaks of the XRD pattern do not fit the analysed data. However this may be because XRD patterns for vanadium oxides and titanium oxides are fitted to XRD analyses of titanium-vanadium-oxides. Due to the lack of XRD data on Ti-V-O solid solutions this is the best analysis attainable until such data is generated.

For samples of initial composition of 50 mass% TiO_2 and above the XRD analyses are more complicated and less distinct than the XRD analyses for the samples containing less than 50 mass% TiO_2 initially, as can be seen from Fig. 4.4. The reason for the complexity of these XRD patterns is the formation of a solid solution in which both titanium and vanadium are present. The XRD pattern will be further complicated by the presence of two solid solution phases in each sample. Although XRD data exist for the Ti_nO_{2n-1} ($4 \leq n \leq 10$) and V_nO_{2n-1} ($4 \leq n \leq 8$) Magneli phases, little XRD data could be found for the solid solution compositions of the type $(Ti, V)_nO_{2n-1}$. The available data are for the components $V_3Ti_6O_{17}$, $V_2Ti_7O_{17}$, $V_2Ti_3O_9$ and V_2TiO_5. For the 70T14 and 70T15 samples the XRD patterns of V_5O_9, V_7O_{13}, Ti_5O_9 and Ti_6O_{11} fitted the XRD analyses data the best. This is shown in Fig. 4.8. Even though these patterns fit the XRD analyses there remain unassigned peaks in the XRD analyses. This could perhaps be due to the XRD reference data not yet being determined at higher values of θ, or due to a more complicated XRD pattern formed because of both vanadium and titanium contained in the crystal structure, instead of just vanadium or titanium.

For the 90T14, 90T15 and 90T16480 samples none of the titanium oxide XRD patterns, or the vanadium oxide patterns fitted the XRD analyses, not even closely. The best fit was attained for the $V_2Ti_7O_{17}$ XRD pattern, but only filling some of the peaks in the XRD analyses data. Because the XRD patterns corresponding most favourably with the experimental data of the samples with $\geq$ 50 mass% TiO_2, initial sample composition, were those of the Magneli phases with the general formula of M_nO_{2n-1}, the phase diagram in Fig. 4.1. has the phase field between M_3O_5 and TiO_2 designated as Magneli phases. The existence of M_nO_{2n-1} with n=6,7,8,9,10 was found by Kosuge and Kachi[27] in the TiO_2-V_2O_3 pseudo-binary system

within the high TiO_2 compositional area, supporting the designation of phases within the high TiO_2 side of the TiO_2-V_2O_3 pseudo-binary diagram in Fig. 4.1 as Magneli phases.

Zador and Alcock[20] determined the partial oxygen pressure stability ranges for titanium containing Magneli phases at 1300°C, 1400°C and 1500°C. The data at 1400°C and 1500°C is summarised in Table 4.3. The partial oxygen pressures employed by Zador and Alcock[20] are more reducing than those employed in the present study, that is 3.02×10^{-10} atm at 1400°C and 2.99×10^{-9} atm at 1500°C. According to Zador and Alcock's data one would expect a pure TiO_2 sample reacted at these temperatures and partial oxygen pressures to have a rutile structure. This is confirmed by a sample reacted in the present study at 1500°C, under a partial oxygen pressure of 1.26×10^{-9} atm, for 18 hours. The XRD pattern for the sample is shown in Fig. 4.6 and it can be seen that the pattern for rutile fits. Therefore it appears that the Magneli phases in the high TiO_2 samples (≥ 50 mass% TiO_2 in initial sample) are stabilised by the vanadium additions.

In Table 4.4 the ionic radii for titanium and vanadium cations are compared. If the difference in ionic radii is in excess of 15%, substitutional solid solution formation is unlikely.[25] Therefore, with reference to Table 4.4., V^{5+}, V^{4+} and V^{3+} can substitute for Ti^{4+} and V^{2+} and V^{3+} can substitute for Ti^{3+}.

Table 4.3: Partial Oxygen Pressure Stability Ranges for Magneli Phases at 1400°C and 1500°C *(Zador and Alcock[20])*

Components	P_{O_2} (atm)	
	1400°C	1500°C
Ti_3O_5-Ti_4O_7	8.40×10^{-14}	2.24×10^{-12}
Ti_4O_7-Ti_5O_9	1.24×10^{-13}	----------
Ti_5O_9-Ti_6O_{11}	4.14×10^{-13}	6.09×10^{-12}
Ti_6O_{11}-Ti_7O_{13}	7.53×10^{-13}	1.01×10^{-11}
Ti_7O_{13}-Ti_8O_{15}	9.61×10^{-13}	----------
Ti_8O_{15}-Ti_9O_{17}	1.30×10^{-12}	1.64×10^{-11}
Ti_9O_{17}-$Ti_{10}O_{19}$	1.50×10^{-12}	1.99×10^{-11}
$Ti_{10}O_{19}$-$Ti_{20}O_{39}$	1.92×10^{-12}	2.80×10^{-11}
$Ti_{20}O_{39}$-TiO_2	4.71×10^{-12}	1.42×10^{-10}

Similarly, the binary system Cr_2O_3-TiO_2 contains a series of shear phases $Ti_{n-2}Cr_2O_{2n-1}$, n = 6 to 11, in which the oxygen-to-metal ratio is reduced by substitution of Cr^{3+} for Ti^{4+}.[27] Vanadium and chromium are both transition elements on the periodic table, and are situated next to each other on the periodic table, indicating that the chemical behaviour of these two

elements is similar. Therefore the behaviour of V in the TiO_2-V_2O_3 system should be similar to that of Cr in the TiO_2-Cr_2O_3 system. However, accordingly to Table 4.4 one expect V^{4+} to substitute for Ti^{4+}, and V^{3+} to substitute for Ti^{3+}.

According to Handfield and Charette[28] the structure of molten high TiO_2 slags should be similar to that of the corresponding solid slags since the electrical properties of these slags changed very little in passing from solid to the liquid state. Thus the solid solution formation of mixtures of TiO_2 and V_2O_3, in Magneli phase co-ordination, found in this work should prevail when these mixtures are melted.

According to Reznichenko et al.,[29,30] as discussed by Handfield and Charette,[28] high titania slags in the solid state consist of a solid solution based on the Ti_3O_5 type structure (orthorhombic), and a solid solution of the Ti_2O_3 type structure (rhombohedral) and glassy materials filling the spaces between the crystals. Depending on the slag composition any one of the solid solutions can form. The proposed general formula for the respective solid solutions are: for the Ti_3O_5 solid solution: m[(Ti, Mg, Mn, Fe)O.2TiO_2]•n[(Ti, Fe, Al, Cr, V)$_2O_3$.TiO_2]; for the Ti_2O_3 solid solution: a[(Ti, Mg, Mn, Fe)O.TiO_2]•b[(Ti, Fe, Al, Cr, V)$_2O_3$]. According to the above vanadium and chromium exist as V^{3+} and Cr^{3+}, and iron as Fe^{2+} and Fe^{3+} within these high TiO_2 solids and slags.

Table 4.4: Radii of Cations[24]

Cation	Radius (Å)	%Difference with respect to Ti^{4+} radius = 0.68 Å	%Difference with respect to Ti^{3+} radius = 0.76 Å
V^{5+}	0.59	13	22
V^{4+}	0.63	7	17
V^{3+}	0.74	8	2.6
V^{2+}	0.88	22	14

Fig. 4.4: XRD Patterns for TiO_2 - V_2O_5 Samples reacted at 1400°C

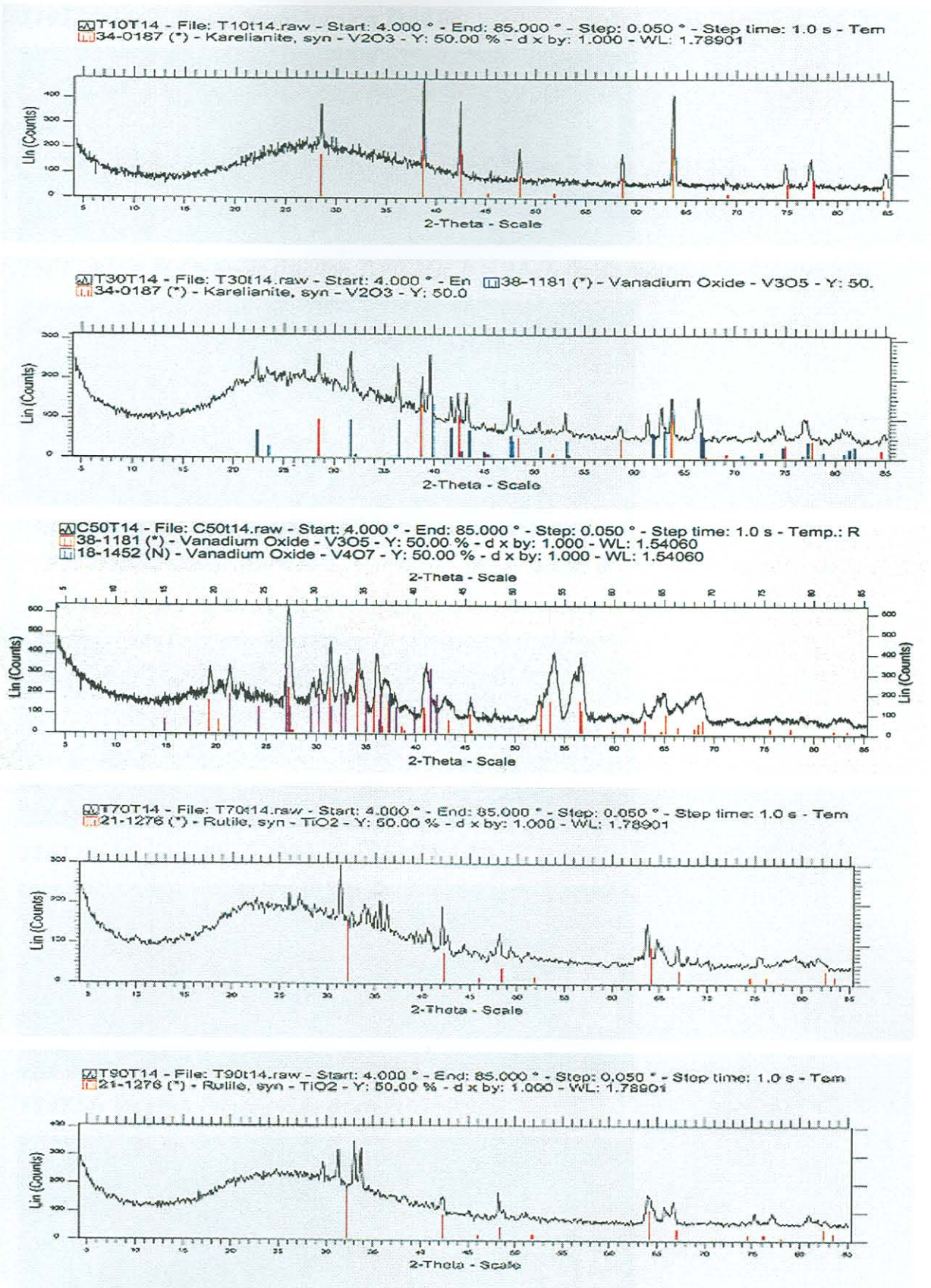

T10T14 = 10 mass% TiO_2 in initial sample; T30T14 = 30 mass% TiO_2 in initial sample;

T50T14 = 50 mass% TiO_2 in initial sample; T70T14 = 70 mass% TiO_2 in initial sample;

T90T14 = 90 mass% TiO_2 in initial sample

Fig. 4.5: Photomicrographs for TiO_2 - V_2O_5 Samples reacted at 1400°C

T10T14: *M_2O_3 Phase (mole fraction Ti=0.08)*

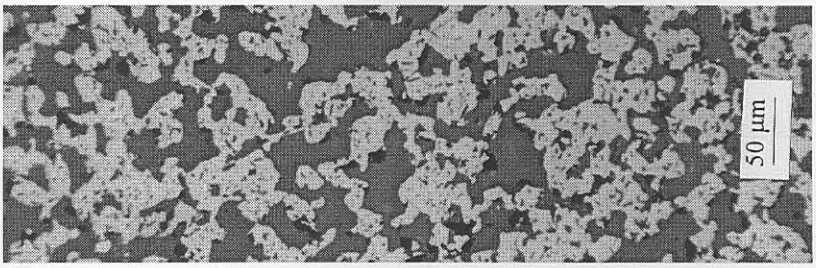

T30T14: *a = M_2O_3 (mole fraction Ti=0.21); b = M_3O_5 (mole fraction Ti=0.35);(x400)*

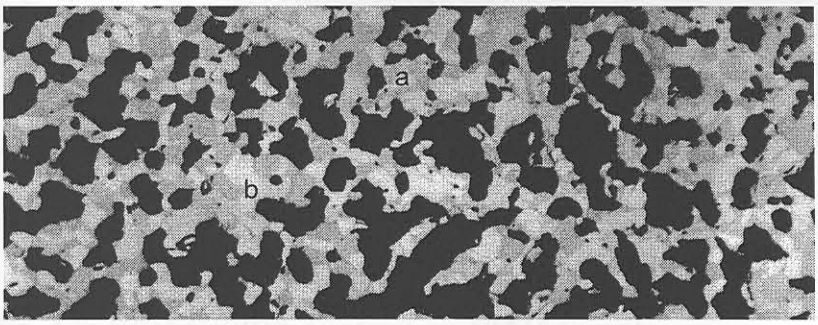

T50T14: *(M_3O_5(mole fraction Ti=0.64) and M_4O_7 according to XRD analysis, but only one phase seen under reflected light at magnifications employed)*

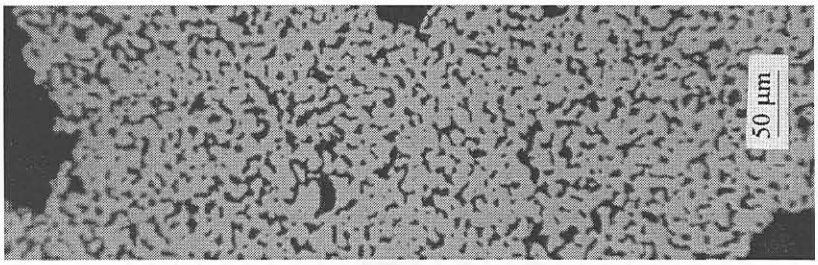

T70T14: *Magneli Phase (mole fraction Ti=0.72)*

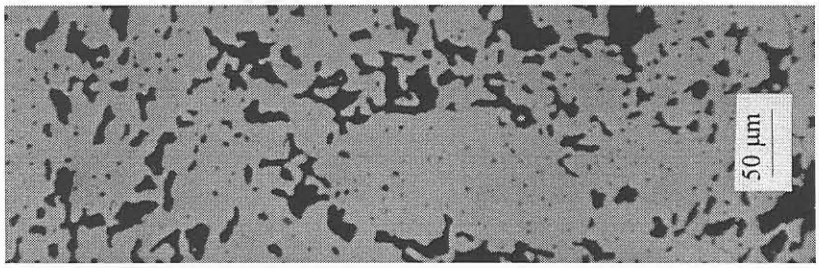

T90T14: *Magneli Phase (mole fraction Ti=0.91)*

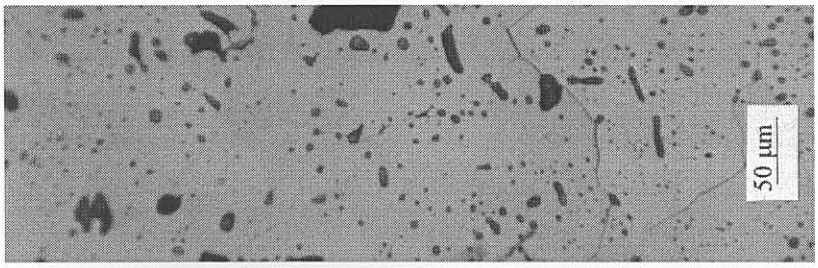

T10T14 = 10 mass% TiO_2 in initial sample; T30T14 = 30 mass% TiO_2 in initial sample;
T50T14 = 50 mass% TiO_2 in initial sample; T70T14 = 70 mass% TiO_2 in initial sample;
T90T14 = 90 mass% TiO_2 in initial sample

Fig. 4.6: XRD Pattern for 100% TiO_2 Sample Reacted for 18 hours at 1500°C and Partial Oxygen Pressure = 1.26 x 10^{-9} atm

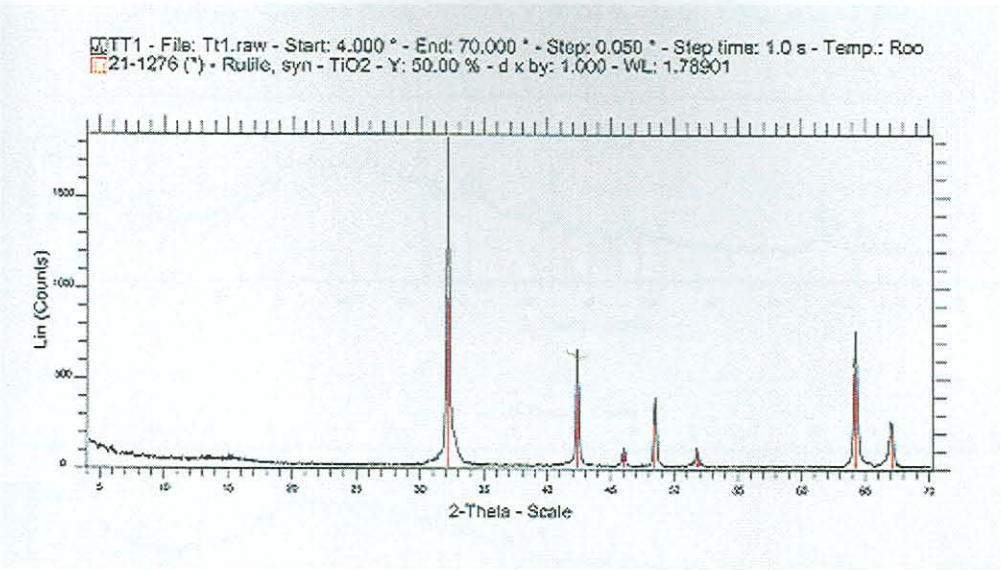

Fig. 4.7: EPMA(WDS) Analyses on 50T15 Sample

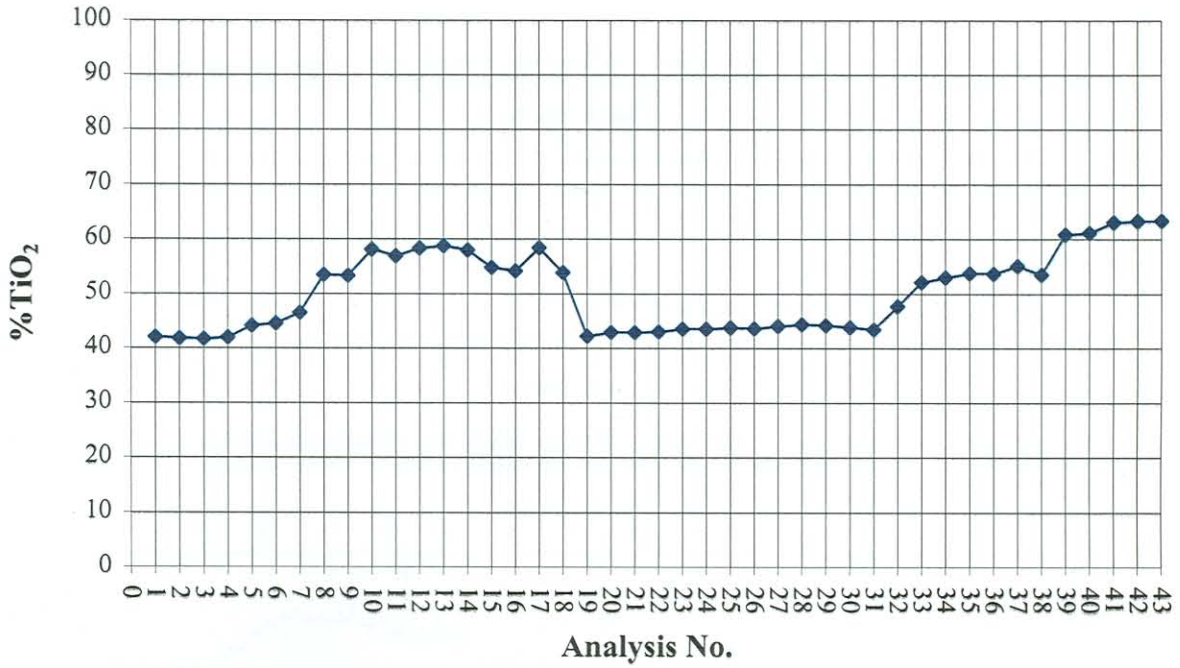

Fig. 4.8: XRD Analyses of 70 mass% TiO_2 Samples Compared with XRD Data for best fitting Magneli Phases

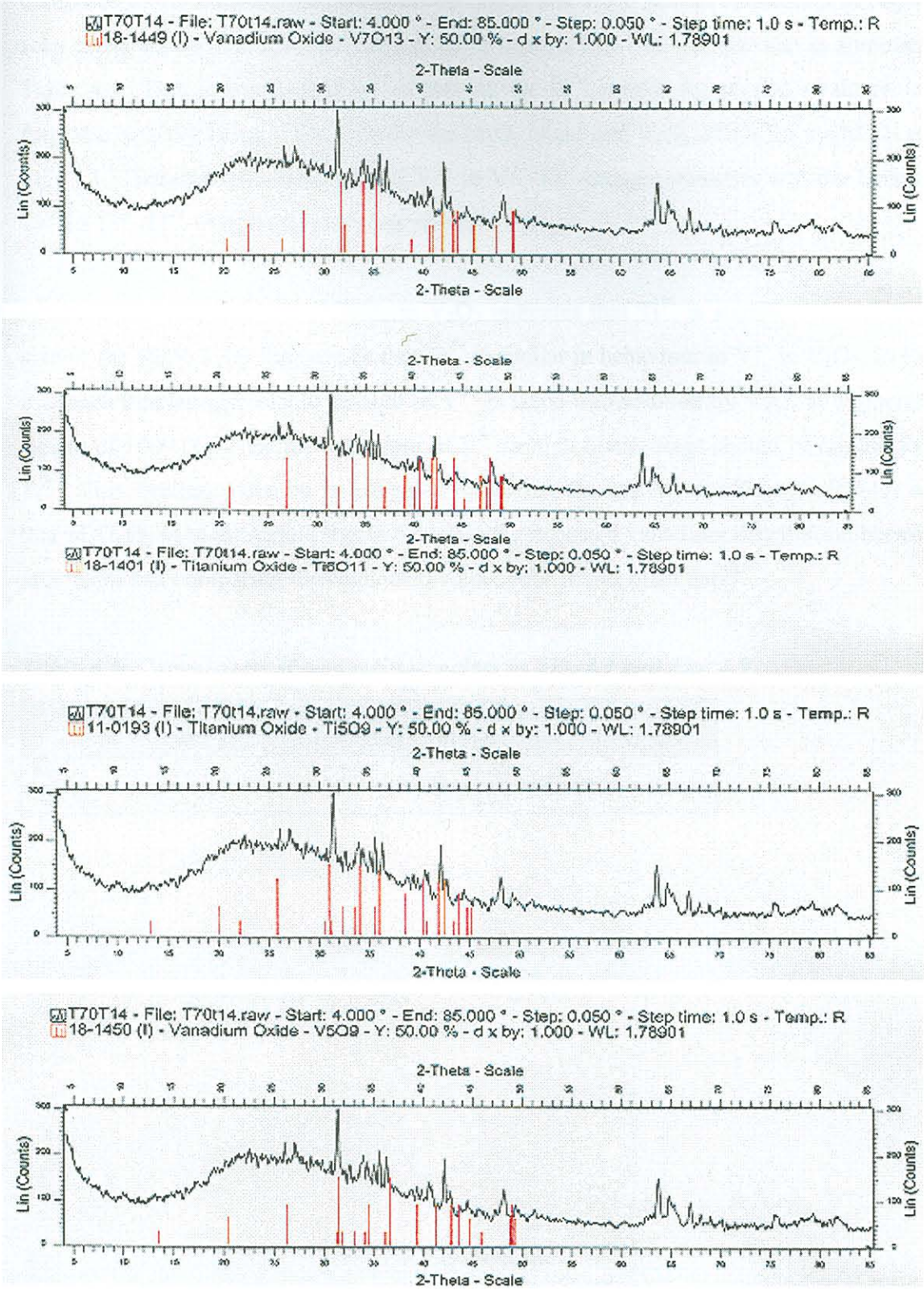

When the composition points for the M_3O_5 and M_4O_7 phases boundaries in Fig. 4.1 are compared to the composition points for the Ti_3O_5 and Ti_4O_7 phases boundaries in Fig. 4.9 it is seen these composition points correspond in magnitude. The comparison is summarised in Table 4.5. This indicates that V^{3+} substitute for Ti^{3+} within the crystal structure with the formulas actually being $V_2O_3.TiO_2$ for the M_3O_5 phase and $V_2O_3.2TiO_2$ for the M_4O_7 phase in Fig. 4.1. Therefore the behaviour of V^{3+} in V^{3+}-Ti^{4+}-oxygen mixtures and the behaviour of Ti^{3+} in Ti^{3+}-Ti^{4+}-oxygen mixtures are similar.

Furthermore the solubility of TiO_X in V_2O_3 indicates that Ti^{3+} is stabilised in the V_2O_3-rich side of the V_2O_3-TiO_2 diagram, or that Ti^{4+} is similar in behaviour to V^{4+} in V_2O_3. In Fig. 4.10 it is seen that an appreciable amount of V^{4+} is taken into solution by V_2O_3 at temperatures in excess of 1000 °C. Thus the behaviour of V^{3+} in high titania slags should be similar to that of Ti^{3+}. This similarity can be investigated by setting the activity coefficient of V_2O_3 equal to that of Ti_2O_3 in high titania slags to calculate the expected vanadium distribution between slag and metal and comparing the calculated values with actual plant data*.

Table 4.5: Comparison of composition points in Fig. 4.1 and Fig. 4.9

Phase Type	Mole Fraction Ti^{4+}: Fig. 4.9 (Ti_2O_3-TiO_2 system)	Mole Fraction Ti: Fig. 4.1 (V_2O_3-TiO_2 system)
M_3O_5	0.33	~ 0.40
M_4O_7	0.50	~ 0.55

*Private Communication: Dr. W.H. van Niekerk, Iscor Heavy Minerals

Fig. 4.9: Optimised Ti_2O_3-TiO_2 phase diagram: Eriksson and Pelton[12]

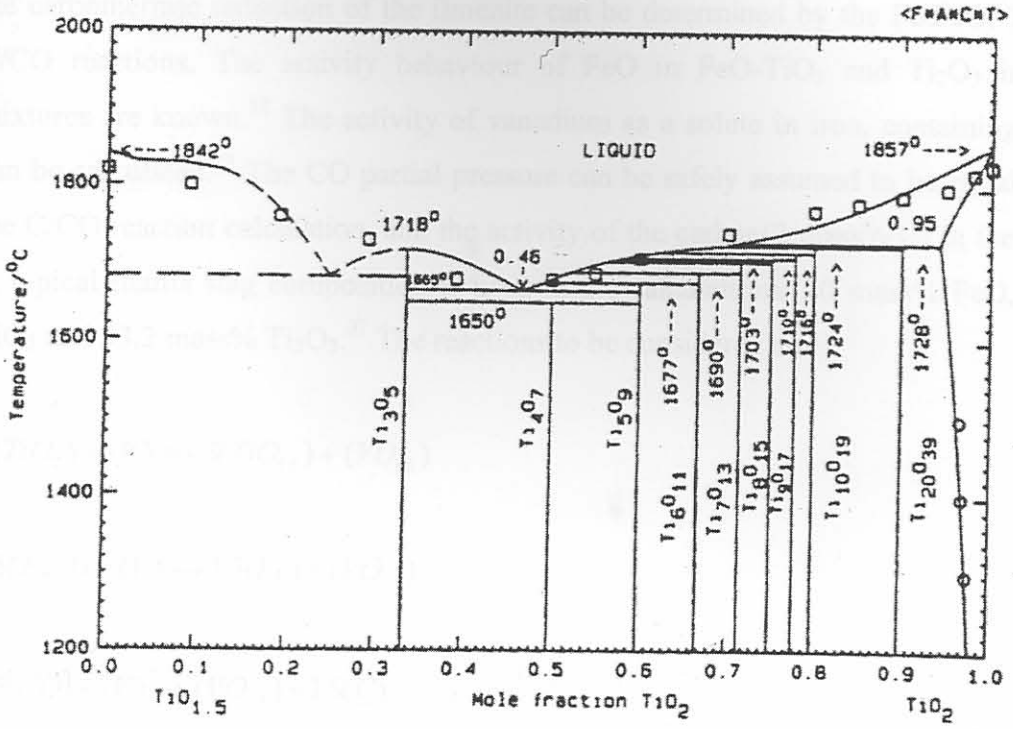

Fig. 4.10: V-O phase diagram: Wriedt[19]

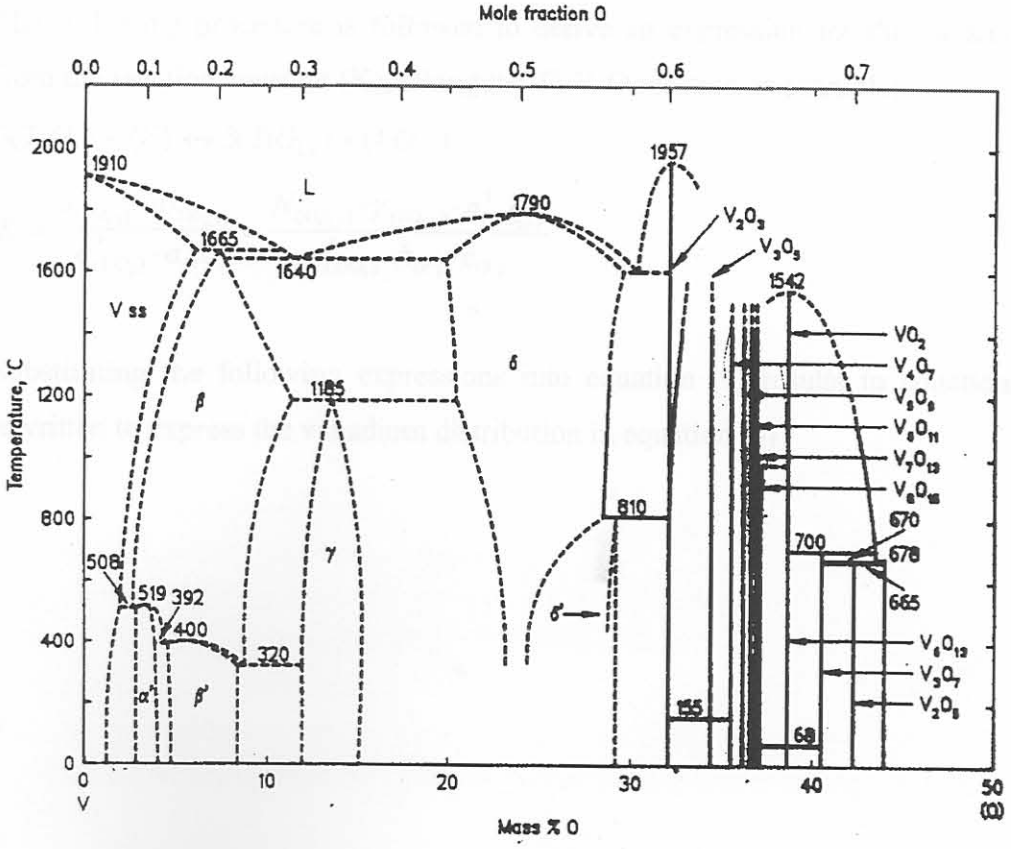

In calculating the vanadium distribution from thermodynamics the partial oxygen pressure in the carbothermic reduction of the ilmenite can be determined by the Fe/FeO, Ti_2O_3/TiO_2 or C/CO reactions. The activity behaviour of FeO in $FeO\text{-}TiO_2$ and Ti_2O_3 in $Ti_2O_3\text{-}TiO_2$ mixtures are known.[12] The activity of vanadium as a solute in iron, containing 2 mass% C, can be calculated.[33] The CO partial pressure can be safely assumed to be equal to 1 atm for the C/CO reaction calculation, and the activity of the carbon(2 mass% C) in the iron is 0.1.[39] A typical titania slag composition is used in the calculations: 10 mass% FeO, 51.8 mass% TiO_2 and 33.2 mass% Ti_2O_3.[37] The reactions to be considered are:

$$3(TiO_2) + \langle V \rangle \leftrightarrow 3(TiO_{1.5}) + (VO_{1.5}) \quad (1)$$

$$1.5(FeO) + \langle V \rangle \leftrightarrow 1.5(Fe) + (VO_{1.5}) \quad (2)$$

$$1.5[CO] + \langle V \rangle \leftrightarrow (VO_{1.5}) + 1.5(\underline{C}) \quad (3)$$

(X): Component X is in the liquid state

$\langle X \rangle$: Component X is in the solid state

$[X]$: Component X is in the gas phase

The following procedure is followed to derive an expression for the vanadium distribution from the reaction constant (K), taking the Ti-V-O reaction as example:

$$3(TiO_2) + \langle V \rangle \leftrightarrow 3(TiO_{1.5}) + (VO_{1.5}) \quad (1)$$

$$K = \frac{a_{(VO_{1.5})} \cdot a^3_{(TiO_{1.5})}}{a^3_{(TiO_2)} \cdot a_{\langle V \rangle}} = \frac{N_{(VO_{1.5})} \cdot \gamma_{(VO_{1.5})} \cdot a^3_{(TiO_{1.5})}}{a^3_{(TiO_2)} \cdot h_{\langle V \rangle} \cdot c_{\langle V \rangle}} \quad (4)$$

Substituting the following expressions into equation (4) results in equation (5), which is rewritten to express the vanadium distribution in equation (6).

$$h_{\langle V\rangle} = \langle \%V \rangle \cdot f_{\langle V\rangle}$$

$$\log(f_{\langle V\rangle}) = e_V^C \cdot (\%C)$$

$$c_{\langle V\rangle} = \frac{mm_{Fe} \cdot \gamma_V^\circ}{100 \cdot mm_V}$$

$$N_{(VO_{1.5})} = \frac{\%V_2O_3 \cdot mm_{slag}}{100 \cdot mm_{(VO_{1.5})}}$$

$$\%V_2O_5 = \frac{\%V_2O_3 \cdot mm_{V_2O_5}}{mm_{V_2O_3}} = 1.213(\%V_2O_3)$$

$mm_{slag} = 76.02 g/mol$ (average value)

$$K = \frac{0.836 \cdot (\%V_2O_5) \cdot \gamma_{(VO_{1.5})} \cdot a^3_{(TiO_{1.5})}}{100 \cdot a^3_{(TiO_2)} \cdot \langle \%V \rangle \cdot f_{\langle V\rangle} \cdot c_{\langle V\rangle}} \qquad (5)$$

$$\frac{(\%V_2O_5)}{\langle \%V \rangle} = L_V = \frac{100 \cdot K \cdot a^3_{(TiO_2)} \cdot f_{\langle V\rangle} \cdot c_{\langle V\rangle}}{0.824 \cdot \gamma_{(VO_{1.5})} \cdot a^3_{(TiO_{1.5})}} \qquad (6)$$

Similar expressions for the vanadium distribution can be developed for reactions (2) and (3) by following the same procedure as set out here for reaction (1).

---

a_i = activity of component i

N_i = mole fraction of component i

γ_i = Raoultian activity coefficient of component i

f_i = Henrian activity coefficient of component i with the 1 mass% solution as the reference state

e_V^C = first order interaction coefficient of C on V in liquid iron

mm_i = molar mass of component i

γ_V° = activity coefficient of vanadium at infinite dilution in liquid iron

h_i = Henrian activity coefficient of i with pure i as the reference state

The calculated vanadium distribution values and the vanadium distribution values obtained from plant data are shown in Fig. 4.11. It is seen that the plant vanadium distributions are independent of temperature and that the plant values are larger than that calculated from the C/CO and Fe/FeO reactions, but slightly below the values calculated for the Ti_2O_3/TiO_2, indicating that the reduction of vanadium from the slag into the metal, from a system oxygen partial pressure point of view, is likely to be controlled by an interaction between reaction (1) and reaction (2).

Fig. 4.11: Vanadium Distribution: Calculated vs. Actual

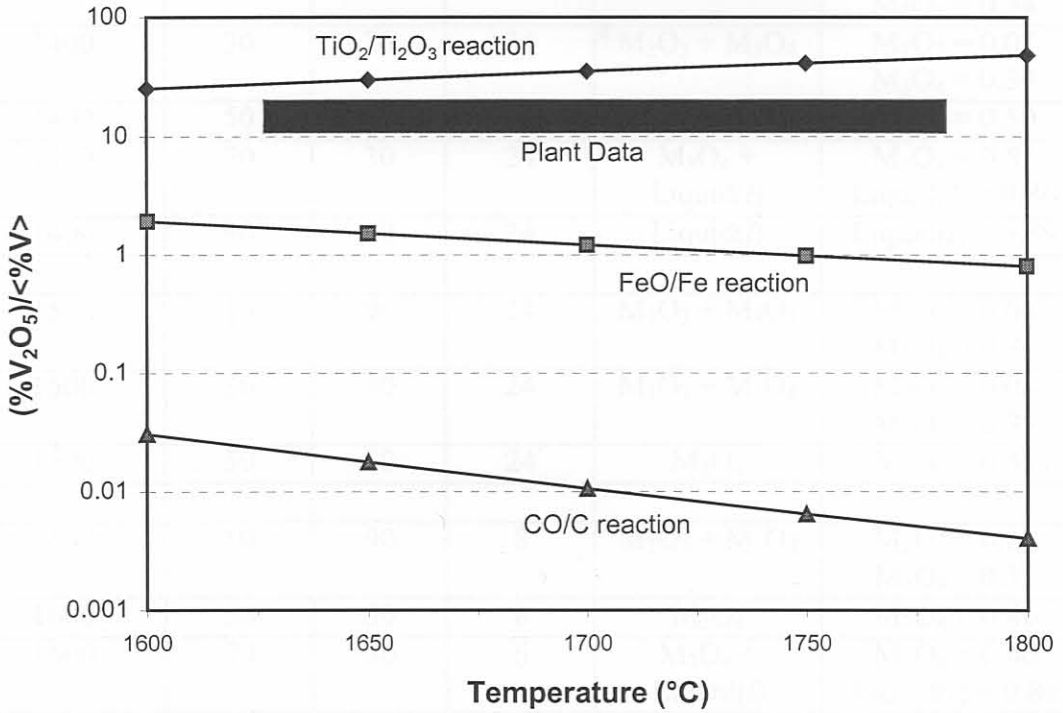

The conclusion made from the work discussed in this section is that vanadium and titanium cations, V^{3+} and Ti^{3+}, and V^{4+} and Ti^{4+} substitute for each other in oxide solid solutions under the conditions of partial oxygen pressure and temperature used in this work. Furthermore, the chemical behaviour of V_2O_3 in high titania slags is similar to that of Ti_2O_3 in these slags. This knowledge made the thermodynamic calculation of the vanadium distribution within these slags possible, indicating that the vanadium distribution is most likely controlled by an interaction between reaction (1), the TiO_2/Ti_2O_3 reaction, and reaction (2), the FeO/Fe reaction.

4.2. V_2O_3 - FeO System

Table 4.6 gives a summary of the sample compositions reacted, the reaction times used and phases identified in each sample. The reacted samples were subjected to XRD analysis, optical microscopy under reflected light and EPMA with an EDS facility.

Table 4.6: Summary of Experiments

Reaction Temperature (°C)	Initial Composition (Mass %)		Reaction Time (Hours)	Phases Identified	mol Fe/ (mol Fe +mol V) in Phase
	Fe_2O_3	V_2O_5			
1400	10	90	24	$M_2O_3 + M_3O_4$	$M_2O_3 = 0.07$ $M_3O_4 = 0.34$
1400	30	70	24	$M_2O_3 + M_3O_4$	$M_2O_3 = 0.07$ $M_3O_4 = 0.34$
1400	50	50	24	M_3O_4	$M_3O_4 = 0.50$
1400	70	30	24	M_3O_4 + Liquid(l)	$M_3O_4 = 0.57$ Liquid(l) = 0.86
1400	90	10	24	Liquid(l)	Liquid(l) = 0.89
1500	10	90	24	$M_2O_3 + M_3O_4$	$M_2O_3 = 0.08$ $M_3O_4 = 0.34$
1500	30	70	24	$M_2O_3 + M_3O_4$	$M_2O_3 = 0.08$ $M_3O_4 = 0.35$
1500	50	50	24	M_3O_4	$M_3O_4 = 0.45$
1600	10	90	8	$M_2O_3 + M_3O_4$	$M_2O_3 = 0.08$ $M_3O_4 = 0.35$
1600	50	50	8	M_3O_4	$M_3O_4 = 0.40$
1600	70	30	6	M_3O_4 + Liquid(l)	$M_3O_4 = 0.46$ Liquid(l) = 0.86

The phase diagram deduced from the information in Table 4.6 is shown in Fig. 4.12. The diagram consists of five phase fields in which three different phases, i.e. M_2O_3, M_3O_4 and liquid could be distinguished, where M indicates both vanadium and iron ions. The M_2O_3 and M_3O_4 phases were both solid at all of the experimental temperatures.

The XRD patterns for the series of samples reacted at 1400°C are shown in Fig. 4.13. The corresponding photomicrographs for the samples are shown in Fig. 4.14. A summary of the EPMA analyses is shown in Appendix 5.

The samples of 10 and 30 mass% Fe_2O_3 initial composition contained the two solid-solutions of M_2O_3 and M_3O_4. These phases appeared as a banded structure within each other as is shown in Fig. 4.14. The samples of 50 mass% Fe_2O_3 initial composition consist of the spinel

solid-solution(M_3O_4) only, and therefore have to lie within the spinel phase field. Because only one phase was present within these samples their chemical composition should be close to the initial composition, as is the case for the sample reacted at 1400°C. However, the samples for 1500°C and 1600°C shifted in composition from the 0.53 mole fraction Fe composition, to compositions containing less iron, as is shown in Table 4.7. A possible explanation for this is the absorption of iron into the platinum wire sample containers, with an increase in the quantity of iron diffusing into the Pt and Pr-Rh wire, with an increase in experimental temperature. This does not influence the position of the phase boundaries of the spinel solid-solution phase field because samples consisting of only one phase as is the case for the 50 mass% Fe_2O_3-50 mass% V_2O_5 initial sample compositions, is not used in plotting phase boundaries. The 70 mass% Fe_2O_3 sample reacted at 1400°C consisted of liquid and spinel solid-solution as shown in Fig. 4.14 and indicated the phase boundaries for liquid and the M_3O_4 phase at 1400°C. The presence of liquid in this sample is affirmed by the presence of quench crystals, which are fine dot-like crystals, that crystallised from the liquid on quenching the sample. The sample of 70 mass% Fe_2O_3 reacted at 1600°C was reacted for six hours instead of the required equilibrium time of eight hours. This shortened reaction period was used because with increasing temperatures, above 1400°C, more liquid formed. The liquid dripped from the Pt-Rh wire cone more easily, perforating the PVC layer which closed off the furnace tube, so rendering the experiment useless. The standard deviation in the EPMA analyses for the mol Fe, shown in Appendix 5, is 0.004 for the M_3O_4 phase and 0.052 for the liquid phase. This can be compared for the standard deviation, on the mol Fe, for the sample of 70 mass% Fe_2O_3 reacted for 24 hours at 1400°C: 0.006 for the M_3O_4 phase and 0.005 for the liquid phase. Because the standard deviations on the EPMA analyses are comparable for the samples reacted for 24 and 6 hours respectively, the data generated from the 6 hour sample is used to plot the phase diagram.

Table 4.7: Composition Differences for 50 mass% Fe_2O_3 - 50 mass% V_2O_5 Initial Sample Composition

Particular Sample	Mol V	mol Fe	Mole fraction Fe
Theoretical Input Into Sample	0.55	0.63	0.53
1400°C Sample	0.68	0.69	0.50
1500°C Sample	0.75	0.61	0.45
1600°C Sample	0.81	0.55	0.40

Fig. 4.12: V_2O_3 - FeO Phase Diagram

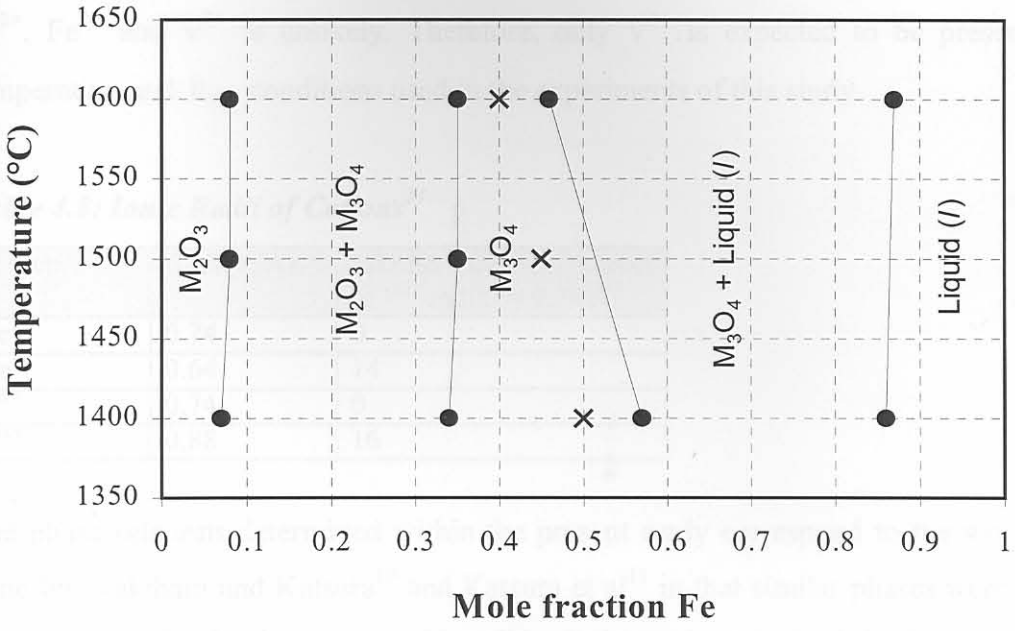

× : Composition points of samples consisting of one phase

• : Composition points of respective phases in two phase samples

The 90 mass% Fe_2O_3 sample reacted at 1400°C consisted of liquid only as indicated by the absence of any crystals in the photomicrograph shown in Fig. 4.14. The absence of crystals was also observed under the electron microscope at large magnifications. Another important indication that this sample was molten at the experimental temperature is that the sample formed individual droplets on quenching and the remainder of the liquid wetted the Pt-Rh wire container. The XRD pattern of this sample is shown in Fig. 4.13 and it indicates that the sample consisted of wüstite and a small quantity of magnetite, once the sample had solidified. The magnetite formed on quenching, when wüstite transformed to magnetite.[23] The transformation could however not be completed because of quenching of the sample, halting the transformation reaction at an early stage. The existence of 100% liquid in the 90 mass% Fe_2O_3 - 10 mass% V_2O_5 sample, at 1400°C, can be compared to the liquidus temperature of wüstite at $P_{O_2} = 1 \times 10^{-9.5}$ atm of 1377°C.[23]

From the co-ordination of cations to oxygen as indicated by the XRD analyses M^{2+} and M^{3+} cations are expected in the solid and liquid solutions formed in the FeO-V_2O_3 system. When the ionic radii of Fe^{2+}, Fe^{3+}, V^{2+} and V^{3+} are compared, see Table 4.8, it is seen that substitutional solid solution formation between Fe^{2+}, Fe^{3+} and V^{3+} is likely to occur because

the ionic radii of these cations differs by less than 15%. The ionic radius of V^{2+} differs from those of Fe^{2+} and Fe^{3+} by more than 15%, indicating that solid-solution formation between Fe^{2+}, Fe^{3+} and V^{2+} is unlikely. Therefore, only V^{3+} is expected to be present under the temperature and P_{O_2} conditions used in the experiments of this study.

Table 4.8: Ionic Radii of Cations[24]

Cation	Radius (Å)	%Difference with respect to V^{3+} radius = 0.74 Å
Fe^{2+}	0.74	0
Fe^{3+}	0.64	14
V^{3+}	0.74	0
V^{2+}	0.88	16

The phase relations determined within the present study correspond to the work previously done by Wakihara and Katsura[10] and Katsura et al[11] in that similar phases were identified in the present study, that is a sesquioxide solid solution and a spinel solid solution.

Fig. 4.13: XRD Patterns for Fe_2O_3 - V_2O_5 Samples reacted at 1400°C

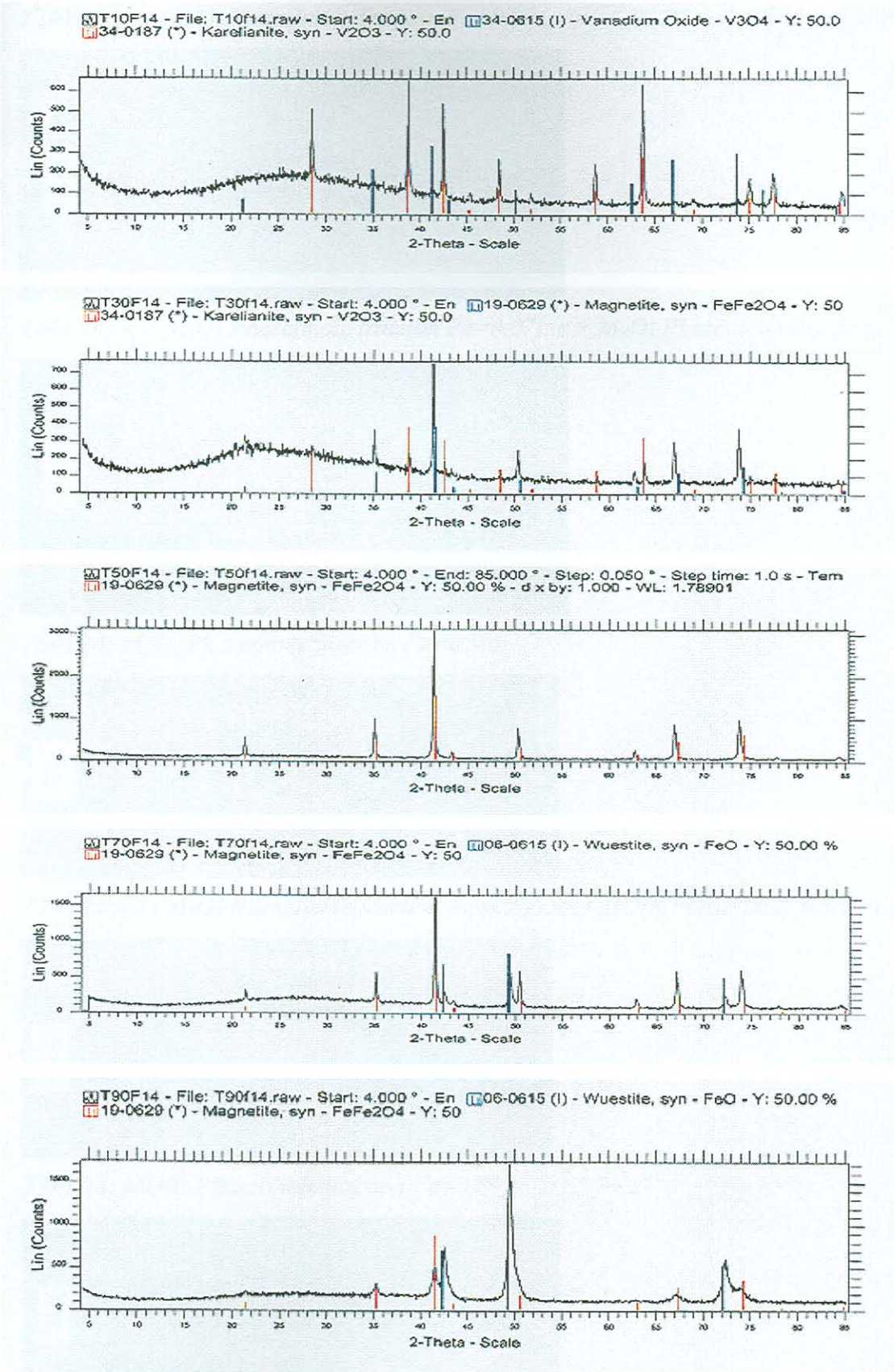

T10F14 = 10 mass% Fe_2O_3 in initial sample; T30F14 = 30 mass% Fe_2O_3 in initial sample;

T50F14 = 50 mass% Fe_2O_3 in initial sample; T70F14 = 70 mass% Fe_2O_3 in initial sample;

T90F14 = 90 mass% Fe_2O_3 in initial sample

Fig. 4.14: Photomicrographs for Fe_2O_3 - V_2O_5 Samples reacted at 1400°C

T10F14: *a = M_2O_3 Phase(mole fraction Fe=0.07), e = M_3O_4 Phase(mole fraction Fe=0.34)*

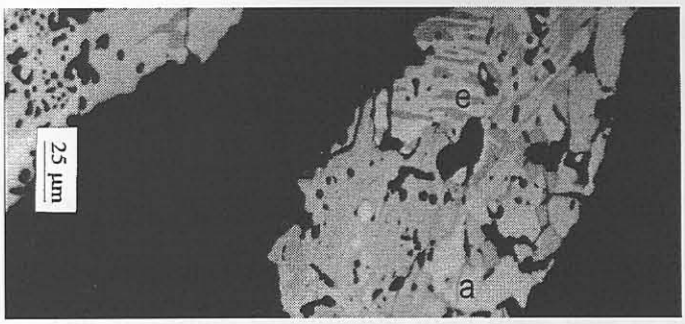

T30F14: *a = M_2O_3 Phase(mole fraction Fe=0.07), e = M_3O_4 Phase(mole fraction Fe=0.34)*

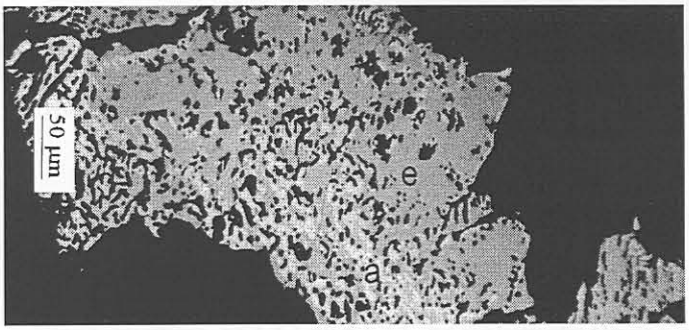

T50F14: *M_3O_4 Phase(mole fraction Fe=0.50)*

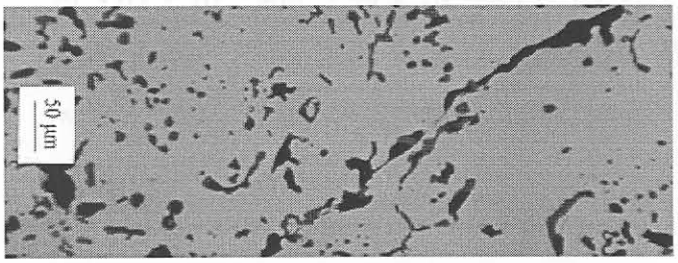

T70F14: *a = M_3O_4 Phase(mole fraction Fe=0.57), c = MO(l) Phase(mole fraction Fe=0.86)*

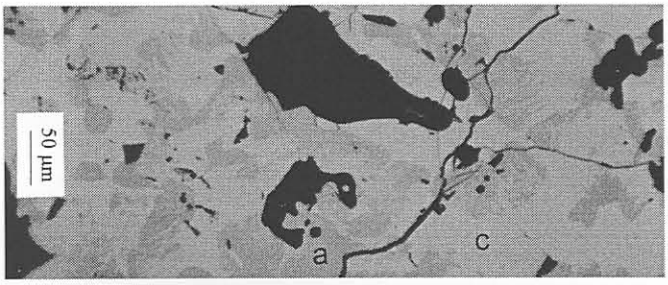

T90F14: *MO(l) Phase(mole fraction Fe=0.89)*

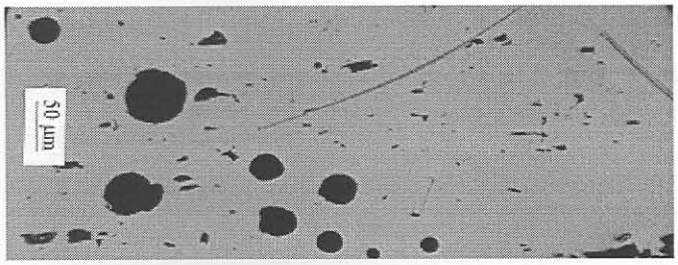

T10F14 = 10 mass% Fe_2O_3 in initial sample; T30F14 = 30 mass% Fe_2O_3 in initial sample;

T50F14 = 50 mass% Fe_2O_3 in initial sample; T70F14 = 70 mass% Fe_2O_3 in initial sample;

T90F14 = 90 mass% Fe_2O_3 in initial sample

5. CONCLUSIONS

- The V_2O_3-TiO_2 pseudo-binary phase diagram consists of the solid solution phases M_2O_3, M_3O_5 and higher Magneli phases, M=(V, Ti), in equilibrium with a gas mixture of CO and CO_2 of volumetric ratio of 3 representing partial oxygen pressures of 3.02×10^{-10} atm, 2.99×10^{-9} atm and 2.31×10^{-8} atm at 1400°C, 1500°C and 1600°C respectively. In the Ti-V oxide solid solutions V^{3+} and Ti^{3+} substitute for each other, and V^{4+} and Ti^{4+} substitute for each other. Furthermore, the chemical behaviour of V_2O_3 in TiO_2 is similar to that of Ti_2O_3. The vanadium distribution from plant data is situated between the calculated vanadium distributions for the Fe/FeO reaction and the Ti_2O_3/TiO_2 reaction, indicating that the vanadium distribution is likely to be controlled, in terms of partial oxygen pressure, by interaction between these two reactions.

- The V_2O_3-FeO pseudo-binary phase diagram consists of the phases M_2O_3, M_3O_4 and liquid, M=(V, Fe), in the temperature range of 1400°C-1600°C and in equilibrium with a gas mixture of CO and CO_2 of volumetric ratio of 3 representing partial oxygen pressures of 3.02×10^{-10} atm, 2.99×10^{-9} atm and 2.31×10^{-8} atm at 1400°C, 1500°C and 1600°C respectively. From ionic radius calculations V^{3+}, Fe^{3+} and Fe^{2+} substitute for each other within the M_2O_3 and M_3O_4 solid solution phases

- The experimental technique used in this study is suitable for phase relation determinations within the pseudo-binary systems FeO-V_2O_3 and TiO_2-V_2O_3 in the temperature range of 1400°C-1600°C and at partial oxygen pressures of 3.02×10^{-10} atm. to 2.31×10^{-8} atm., and should be suitable for phase relation studies in the pseudo-ternary system TiO_2-V_2O_3-FeO under the same conditions of temperature and partial oxygen pressure.

- The data gathered in this study provides a starting point from which phase relations in the pseudo-ternary system TiO_2-V_2O_3-FeO can be determined. Furthermore, this data confirms that high melting components exist within the TiO_2-rich region of the system so that future investigations into phase relations within this region of the system should be conducted at temperatures above 1600°C.

6. RECOMMENDATIONS FOR FUTURE WORK

- Phase relations in the pseudo-ternary system TiO_2-FeO-V_2O_3 should be determined at temperatures of at least 1600°C in order to identify the liquid phase field within the system.

- Subsequently, activity-composition relations of iron oxides and vanadium oxides in the TiO_2-rich liquid phase area of the TiO_2-FeO-V_2O_3 pseudo-ternary should be determined.

- The experimental procedure used in the present study can serve as the basis of the approach to be followed in doing the proposed future work.

7. REFERENCES

1. Mackey, T.S., *JOM*, April 59 (1994)
2. Kahn, J.A., *JOM*, July 33 (1984)
3. *Kirk-Othmer Encyclopedia of Chemical Technology. (Third Edition)*, **23** 143-163, John Wiley and Sons, 1983, U.S.A.
4. Communication: *SCM Chemicals*, Baltimore, Maryland, U.S.A.
5. MacChesney, J.B. and Muan, A., *Amer. Mineral.*, **46** 572 (1961)
6. Grieve, J. and White, J., *J. Roy. Tech. Coll. (Glasgow)*, **4** 444 (1939)
7. Smith, I.C. and Bell, H.B., *Trans. Inst. Min. Metall. C*, **79** C253 (1970)
8. Grau, A.E., *Can. Metall. Q.*, **18** 313 (1979)
9. Lindsley, D.H., *Year Book*, Carnergie Institution, **64** 144 (1965)
10. Wakihara, M. and Katsura, T., *Bull. Chem. Soc. Japan*, **44** [11] 3043 (1971)
11. Katsura, T., Wakihara, M., Hara, S.I. and Sugihara, T., *J. Solid State Chem.*, **13** 107 (1975)
12. Eriksson, G. and Pelton, A.D., *Metall. Trans. B.*, **24B** Oct. 795 (1993)
13. Personal Communication: L. Dearlove and C. Visser, Geologists, *Iscor Research and Development. Pretoria, R.S.A.*
14. Schmahl, N.G. and Dillenburg, H., *Z. Physikal. Chem. (Frankfurt)*, **65** 119 (1969)
15. Roth, R.S., Dennis, J.R. and McMurdie, H.F., *Phase Diagrams for Ceramists Vol. VI*, 191 (1987)
16. Fotiev, A.A., Surat, L.L. and Tre' yakov, A.I., *Russ. J. Inorg. Chem.*, **26** [5] 739 (1981)
17. Deines, P., Nafziger, R.H., Ulmer, G.C. and Woermann, E., *Bulletin of the Earth and Mineral Sciences Experiment Station*, Pennsylvania State University, University Park, Pennsylvania, [88] (1974)
18. Nafziger, R.H., Ulmer, G.C. and Woermann, E., *Research Techniques for High Pressure and High Temperature,* Ulmer, G.C. (Ed.), Springer-Verlag, New-York, 34 (1971)
19. Wriedt, H.A., *Bull. Alloy. Phase Diagrams,* **10** [3] 271 (1989)
20. Zador, S., Alcock, B., *High Temp. Sci.,* **16** 187 (1983)
21. Murray, J.L. and Wriedt, H.A., *Bull. Alloy. Phase Diagrams,* **8** [2] 148 (1987)
22. Wakihara, M. and Katsura, T., *Metall. Trans. B.,* **1** Feb. 363 (1970)
23. Schürmann, E. and Janhsen, U., *Steel Research,* **64** [6] 279 (1993)
24. Weast, R.C., Astle, M.J., *Handbook of Chemistry and Physics, 62nd Edition, 1981-1982,* CRC Press, Inc., Boca Raton, Florida

25. Thornton, P.A., Colangelo, V.J., *Fundamentals of Engineering Materials,* Prentice-Hall, Inc., 147 (1985)

26. Young, H.D., *Statistical Treatment of Experimental Data,* McGraw-Hill Book Company, Inc., 78 (1962)

27. Kosuge, K. and Kachi, S., *Chemica Scripta,* [8] 70 (1975)

28. Handfield, G. and Charette, G.G., *Canadian Metallurgical Quarterly,* **10** [3] 235 (1971)

29. Reznichenko, V.A. et al, The metallurgy of titanium: investigation of electric melting of titanium slags. English Translation, U.S. Depeartment of Commerce (1963)

30. Reznichenko, V.A., *Izv. Akad. Nauk. S.S.S.R. Metally.*, [5] 43 (1967)

31. Brauer, G. and Littke, W., *J. Inorg. Nucl. Chem.,* **16** 67 [1960]

32. Turkdogan, E.T., *Physical Chemistry of High Temperature Technology,* Academic Press, Inc., (London) Ltd., 5 (1980)

33. Sigworth, G.K. and Elliot, J.F., *Metal Science*, **8** 298 (1974)

34. F*A*C*T Thermochemical Database - Home Page: http://www.crct.polymtl.ca/fact/fact.htm

35. Eriksson, G., Pelton, A.D., Woermann, E., Ender, A., *Ber. Bunsenges. Phys. Chem.,* **100** 11 1839 (1996)

36. Du Plooy, H., M.Eng Thesis: *Melting Point Determinations on TiO_2-Rich Slags,* University of Pretoria, R.S.A., 1997

37. Bessinger, D., Du Plooy, H., Pistorius, P.C., Visser, C., *Heavy Minerals 1997,* Robinson, R.E. (Ed.), The South African Institute of Mining and Metallurgy, Johannesburg, 151 (1997)

38. Powder diffraction file ACDD PDF-2 Database, Sets 1-45, 1995, Dataware Technologies, Inc., 1985-1995

39. Chipman, J., *Metall. Trans. B.,* **1** Aug. 2163 (1970)

8. APPENDICES

Appendix 1: Temperature Variation vs. Position in Furnace at 1500°C

Fig. 1: Temperature vs. Depth into Furnace Tube in the Furnace Hot Zone
(Depth measured from the top of the rubber plug, at the top of the furnace)

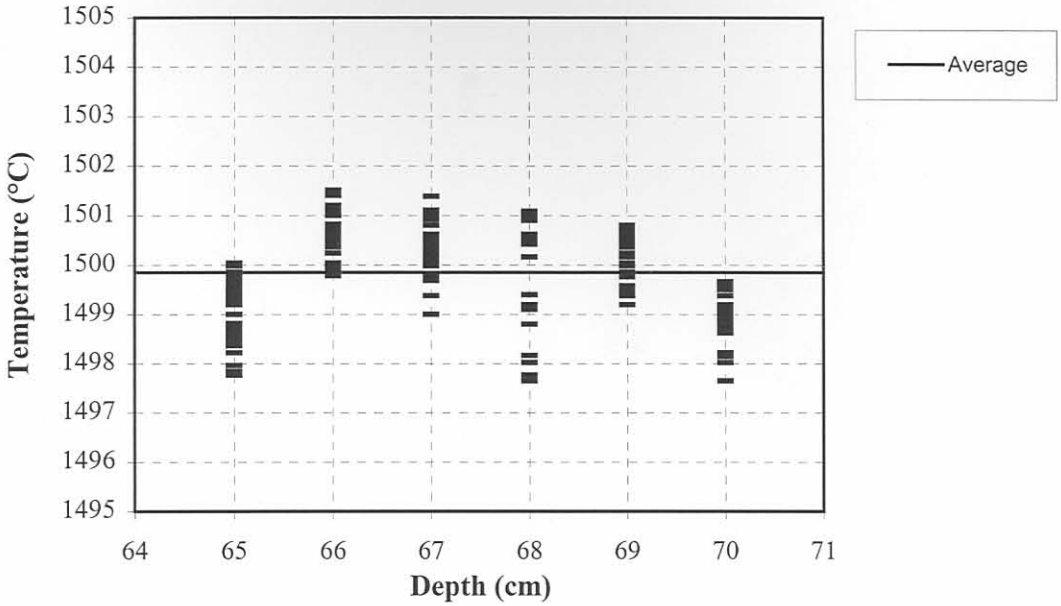

Appendix 2: Recorder Chart for Temperature Measurements at 1500°C

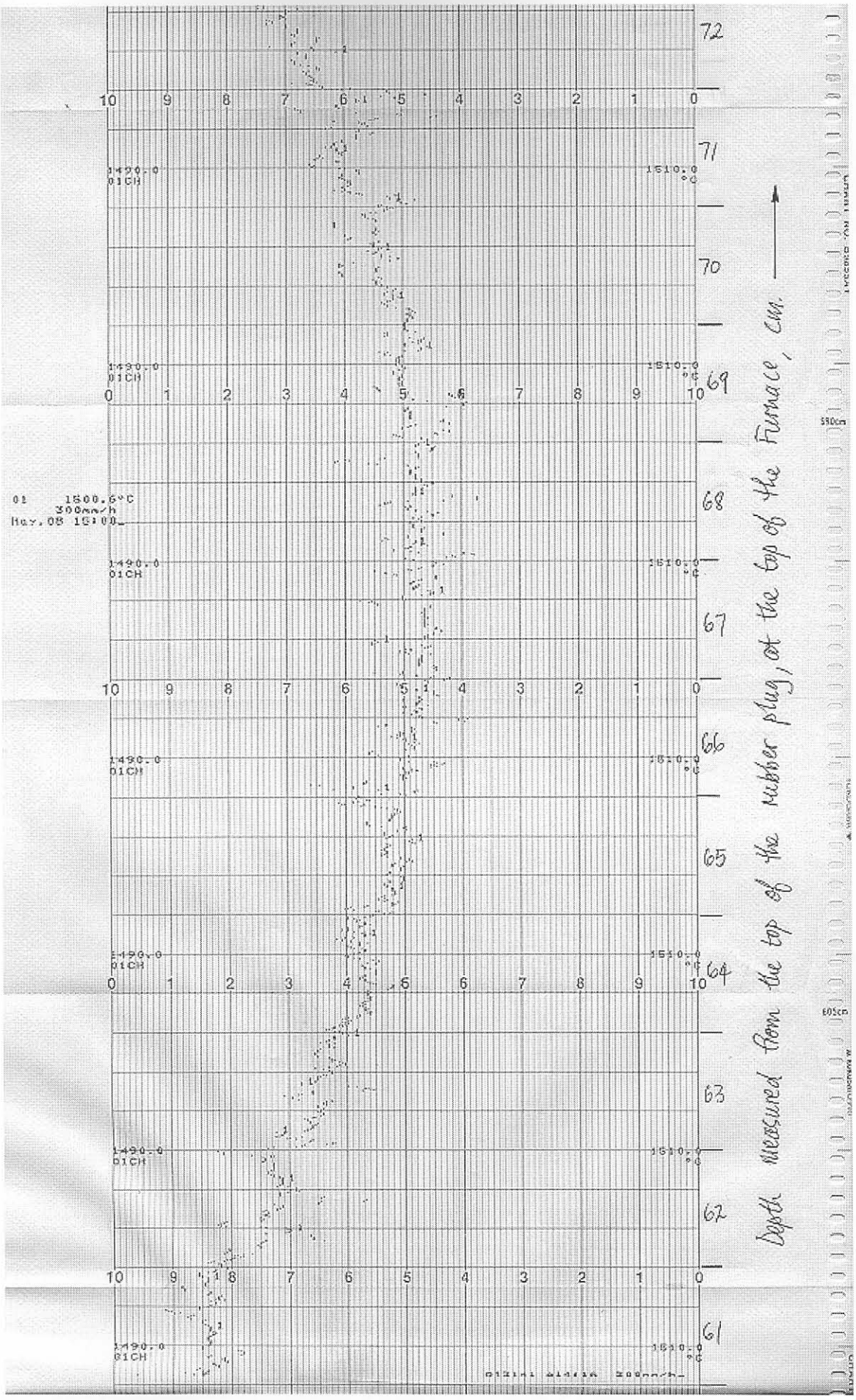
Depth measured from the top of the rubber plug, at the top of the Furnace, cm.
01 1500.6°C
300mm/h
Nov.08 15:00
1490.0
01CH
1510.0
°C

Appendix 3: EPMA(WDS) Analyses for V_2O_3 - TiO_2 System

Sample: 10T14; Initial Sample Composition = 10 mass% TiO_2 - 90 mass% V_2O_5; Reaction Temperature = 1400°C; Phases Identified = M_2O_3

Analysis No.	Mass % V2O3	Mass% TiO2	Total	mol V	mol Ti	Mole fraction Ti
1	91.10	7.06	98.16	1.22	0.09	0.07
2	93.30	6.34	99.64	1.24	0.08	0.06
3	93.34	7.21	100.55	1.25	0.09	0.07
4	91.22	6.92	98.13	1.22	0.09	0.07
5	92.97	7.82	100.80	1.24	0.10	0.07
6	92.59	7.78	100.37	1.24	0.10	0.07
7	92.40	8.45	100.85	1.23	0.11	0.08
8	91.75	8.31	100.05	1.22	0.10	0.08
9	94.63	5.77	100.39	1.26	0.07	0.05
10	94.77	5.75	100.51	1.26	0.07	0.05
11	94.61	5.68	100.30	1.26	0.07	0.05
12	88.97	8.21	97.18	1.19	0.10	0.08
13	92.22	8.87	101.08	1.23	0.11	0.08
14	91.65	8.19	99.84	1.22	0.10	0.08
15	91.66	8.07	99.73	1.22	0.10	0.08
16	92.85	8.07	100.91	1.24	0.10	0.08
17	90.71	7.76	98.47	1.21	0.10	0.07
18	92.27	7.79	100.06	1.23	0.10	0.07
19	90.40	8.39	98.79	1.21	0.11	0.08
20	90.65	8.44	99.10	1.21	0.11	0.08
21	91.57	8.93	100.50	1.22	0.11	0.08
22	91.55	8.52	100.07	1.22	0.11	0.08
23	92.31	8.51	100.82	1.23	0.11	0.08
24	91.25	9.31	100.56	1.22	0.12	0.09
25	90.83	9.63	100.46	1.21	0.12	0.09
26	91.02	9.52	100.54	1.21	0.12	0.09
27	92.28	8.29	100.57	1.23	0.10	0.08
28	92.08	8.96	101.03	1.23	0.11	0.08
29	91.63	8.97	100.60	1.22	0.11	0.08
30	90.88	9.33	100.21	1.21	0.12	0.09
31	91.53	9.60	101.13	1.22	0.12	0.09
32	90.96	9.86	100.82	1.21	0.12	0.09
33	88.33	10.30	98.63	1.18	0.13	0.10
34	90.19	11.00	101.19	1.20	0.14	0.10
35	89.08	12.66	101.74	1.19	0.16	0.12
36	86.60	12.23	98.83	1.16	0.15	0.12
37	88.78	12.68	101.47	1.18	0.16	0.12
38	88.61	12.69	101.30	1.18	0.16	0.12
39	87.13	12.17	99.31	1.16	0.15	0.12
Average	**91.30**	**8.82**	**100.12**	**1.22**	**0.11**	**0.08**

Sandard Deviation	**1.86**	**1.84**	**1.04**	**0.02**	**0.02**	**0.02**
95% Confidence Limit	**0.58**	**0.58**	**0.33**	**0.01**	**0.01**	**0.01**

Sample: 30T14; Initial Sample Composition = 30 mass% TiO_2 - 70 mass% V_2O_5; Reaction Temperature = 1400°C; Phases Identified = M_2O_3 and M_3O_5

M_2O_3-Phase

Analysis No.	Mass% V2O3	Mass% TiO2	Total	mol V	mol Ti	Mole fraction Ti
1	75.01	24.86	99.86	1.00	0.31	0.24
2	76.61	25.45	102.05	1.02	0.32	0.24
3	76.36	23.60	99.96	1.02	0.30	0.22
4	79.83	21.57	101.40	1.07	0.27	0.20
5	79.91	20.38	100.29	1.07	0.26	0.19
6	76.77	24.45	101.23	1.02	0.31	0.23
7	79.49	20.47	99.96	1.06	0.26	0.19
8	79.87	21.82	101.69	1.07	0.27	0.20
9	74.19	25.01	99.20	0.99	0.31	0.24
10	78.91	21.86	100.77	1.05	0.27	0.21
11	74.35	25.61	99.96	0.99	0.32	0.24
12	*79.9*	*20.1*	*100*	*1.07*	*0.25*	*0.19*
13	*80*	*20*	*100*	*1.07*	*0.25*	*0.19*
14	*80.3*	*19.8*	*100*	*1.07*	*0.25*	*0.19*
15	*80.31*	*19.69*	*100*	*1.07*	*0.25*	*0.19*
Average	**78.12**	**22.31**	**100.42**	**1.04**	**0.28**	**0.21**
Standard Deviation	**2.31**	**2.27**	**0.81**	**0.03**	**0.03**	**0.02**
95% Confidence Limit	**1.17**	**1.15**	**0.41**	**0.02**	**0.01**	**0.01**

Italic = SEM-EDS Analyses

M_3O_5-Phase

Analysis No.	Mass% V2O3	Mass% TiO2	Total	mol V	mol Ti	Mole fraction Ti
1	61.22	38.95	100.17	0.82	0.49	0.37
2	63.18	36.41	99.58	0.84	0.46	0.35
3	66.40	35.93	102.33	0.89	0.45	0.34
4	63.98	37.58	101.56	0.85	0.47	0.36
5	62.56	39.29	101.85	0.83	0.49	0.37
6	60.40	39.82	100.21	0.81	0.50	0.38
7	66.12	35.66	101.78	0.88	0.45	0.34
8	60.16	37.74	97.90	0.80	0.47	0.37
9	61.33	39.99	101.32	0.82	0.50	0.38
10	60.75	39.92	100.67	0.81	0.50	0.38
11	61.90	39.70	101.60	0.83	0.50	0.38
12	61.11	40.28	101.38	0.82	0.50	0.38
13	61.02	40.41	101.43	0.81	0.51	0.38
14	62.72	37.79	100.51	0.84	0.47	0.36

15	61.41	38.09	99.50	0.82	0.48	0.37
16	62.06	38.85	100.92	0.83	0.49	0.37
17	68.03	32.76	100.79	0.91	0.41	0.31
18	70.47	29.32	99.79	0.94	0.37	0.28
19	70.67	31.28	101.95	0.94	0.39	0.29
20	67.96	33.47	101.42	0.91	0.42	0.32
21	65.32	33.76	99.08	0.87	0.42	0.33
22	68.32	33.18	101.50	0.91	0.42	0.31
23	69.92	31.89	101.81	0.93	0.40	0.30
24	69.29	31.45	100.73	0.92	0.39	0.30
25	71.26	30.47	101.73	0.95	0.38	0.29
26	72.46	28.10	100.56	0.97	0.35	0.27
27	*61.13*	*38.87*	*100.00*	*0.82*	*0.49*	*0.37*
28	*61.18*	*38.82*	*100.00*	*0.82*	*0.49*	*0.37*
29	*61.37*	*38.63*	*100.00*	*0.82*	*0.48*	*0.37*
30	*60.97*	*39.03*	*100.00*	*0.81*	*0.49*	*0.38*
Average	**64.49**	**36.25**	**100.74**	**0.86**	**0.45**	**0.35**
Standard Deviation	**3.94**	**3.70**	**1.01**	**0.05**	**0.05**	**0.04**
95% Confidence Limit	**1.41**	**1.32**	**0.36**	**0.02**	**0.02**	**0.01**

Italic = SEM-EDS Analyses

Sample: 50T14; Initial Sample Composition = 50 mass% TiO_2 - 50 mass% V_2O_5; Reaction Temperature = 1400°C; Phases Identified = M_3O_5 and M_4O_7

M_4O_7-Phase

Analysis No.	Mass% V2O3	Mass% TiO2	Total	mol V	mol Ti	Mole fraction Ti
1	31.35	69.40	100.75	0.42	0.87	0.67
2	32.08	69.63	101.70	0.43	0.87	0.67
3	32.32	68.52	100.84	0.43	0.86	0.67
4	32.01	69.19	101.20	0.43	0.87	0.67
5	33.09	66.41	99.50	0.44	0.83	0.65
6	32.23	68.70	100.93	0.43	0.86	0.67
7	39.02	62.57	101.59	0.52	0.78	0.60
8	31.96	69.23	101.19	0.43	0.87	0.67
9	31.66	69.47	101.13	0.42	0.87	0.67
10	31.74	69.10	100.84	0.42	0.86	0.67
11	35.48	65.70	101.18	0.47	0.82	0.63
12	35.31	65.59	100.91	0.47	0.82	0.64
13	34.62	65.04	99.66	0.46	0.81	0.64
14	32.93	67.92	100.86	0.44	0.85	0.66
15	33.70	67.54	101.24	0.45	0.85	0.65
16	32.14	68.95	101.09	0.43	0.86	0.67
17	32.17	69.14	101.31	0.43	0.87	0.67
18	31.67	69.02	100.69	0.42	0.86	0.67
19	33.37	67.94	101.31	0.45	0.85	0.66
20	39.14	62.65	101.79	0.52	0.78	0.60
21	38.69	62.64	101.33	0.52	0.78	0.60
22	31.86	68.39	100.25	0.43	0.86	0.67
23	38.86	62.61	101.47	0.52	0.78	0.60
24	38.77	62.79	101.55	0.52	0.79	0.60
25	34.78	66.32	101.10	0.46	0.83	0.64
26	36.98	61.85	98.83	0.49	0.77	0.61
27	38.94	62.51	101.45	0.52	0.78	0.60
28	34.33	66.65	100.97	0.46	0.83	0.65
29	32.35	68.71	101.06	0.43	0.86	0.67
30	38.51	62.82	101.33	0.51	0.79	0.60
31	39.21	62.37	101.58	0.52	0.78	0.60
32	33.61	67.48	101.09	0.45	0.84	0.65
33	35.22	63.56	98.78	0.47	0.80	0.63
34	34.04	67.36	101.40	0.45	0.84	0.65
35	38.21	63.54	101.75	0.51	0.80	0.61
36	37.63	63.66	101.29	0.50	0.80	0.61
37	36.20	65.15	101.35	0.48	0.82	0.63
38	31.89	68.94	100.83	0.43	0.86	0.67
39	35.02	66.23	101.25	0.47	0.83	0.64

40	37.29	64.76	102.06	0.50	0.81	0.62
41	35.02	64.42	99.45	0.47	0.81	0.63
42	34.41	66.61	101.01	0.46	0.83	0.64
43	35.78	65.32	101.10	0.48	0.82	0.63
44	38.58	63.08	101.65	0.51	0.79	0.61
45	33.59	67.62	101.21	0.45	0.85	0.65
46	38.18	62.98	101.15	0.51	0.79	0.61
47	38.91	62.52	101.42	0.52	0.78	0.60
48	36.42	64.72	101.14	0.49	0.81	0.63
49	38.71	62.25	100.96	0.52	0.78	0.60
50	34.47	66.47	100.94	0.46	0.83	0.64
51	32.00	69.28	101.28	0.43	0.87	0.67
52	31.08	68.56	99.64	0.41	0.86	0.67
53	31.58	69.72	101.30	0.42	0.87	0.67
54	37.32	64.12	101.44	0.50	0.80	0.62
55	36.66	64.74	101.40	0.49	0.81	0.62
56	31.43	69.59	101.02	0.42	0.87	0.67
57	37.05	63.49	100.54	0.49	0.79	0.62
Average	**34.94**	**66.06**	**101.00**	**0.47**	**0.83**	**0.64**
Standard Deviation	**2.72**	**2.61**	**0.67**	**0.04**	**0.03**	**0.03**
95% Confidence Limit	**0.71**	**0.68**	**0.18**	**0.01**	**0.01**	**0.01**

Sample: 70T14; Initial Sample Composition = 70 mass% TiO_2 - 30 mass% V_2O_5; Reaction Temperature = 1400°C; Phases Identified = Magneli Phase

Analysis No.	Mass% V2O3	Mass% TiO2	Total	mol V	mol Ti	Mole fraction Ti
1	25.28	72.87	98.14	0.34	0.91	0.73
2	30.15	69.64	99.79	0.40	0.87	0.68
3	30.37	68.99	99.36	0.41	0.86	0.68
4	25.65	73.13	98.77	0.34	0.92	0.73
5	26.90	72.02	98.91	0.36	0.90	0.72
6	29.99	69.04	99.02	0.40	0.86	0.68
7	25.70	73.26	98.96	0.34	0.92	0.73
8	30.40	69.84	100.24	0.41	0.87	0.68
9	30.24	69.74	99.99	0.40	0.87	0.68
10	24.88	75.79	100.67	0.33	0.95	0.74
11	24.63	75.72	100.35	0.33	0.95	0.74
12	24.83	75.73	100.56	0.33	0.95	0.74
13	25.33	75.27	100.60	0.34	0.94	0.74
14	24.84	74.01	98.85	0.33	0.93	0.74
15	25.29	75.38	100.66	0.34	0.94	0.74
16	25.70	74.65	100.34	0.34	0.93	0.73
17	30.80	70.63	101.42	0.41	0.88	0.68
18	30.46	70.63	101.08	0.41	0.88	0.69
19	26.31	74.16	100.47	0.35	0.93	0.73
20	26.00	74.25	100.25	0.35	0.93	0.73
21	29.62	71.12	100.74	0.40	0.89	0.69
22	25.90	75.23	101.13	0.35	0.94	0.73
23	25.79	74.75	100.54	0.34	0.94	0.73
24	26.01	74.92	100.93	0.35	0.94	0.73
25	25.59	74.74	100.33	0.34	0.94	0.73
26	25.77	75.07	100.84	0.34	0.94	0.73
27	25.72	75.09	100.81	0.34	0.94	0.73
28	25.72	74.83	100.55	0.34	0.94	0.73
29	25.77	74.98	100.75	0.34	0.94	0.73
30	25.75	75.60	101.35	0.34	0.95	0.73
31	26.10	75.26	101.36	0.35	0.94	0.73
32	25.73	75.44	101.16	0.34	0.94	0.73
33	25.74	75.59	101.33	0.34	0.95	0.73
34	25.62	75.37	100.99	0.34	0.94	0.73
35	25.77	75.29	101.06	0.34	0.94	0.73
36	25.76	75.21	100.97	0.34	0.94	0.73
37	25.44	74.92	100.35	0.34	0.94	0.73
38	25.85	75.41	101.26	0.34	0.94	0.73
39	25.91	74.99	100.89	0.35	0.94	0.73
40	30.21	71.35	101.55	0.40	0.89	0.69

41	25.77	75.24	101.01	0.34	0.94	0.73
42	25.70	75.19	100.90	0.34	0.94	0.73
43	30.03	71.03	101.06	0.40	0.89	0.69
44	25.84	75.07	100.91	0.34	0.94	0.73
45	26.09	75.09	101.17	0.35	0.94	0.73
46	25.88	75.15	101.03	0.35	0.94	0.73
47	30.60	70.50	101.10	0.41	0.88	0.68
48	29.97	70.12	100.09	0.40	0.88	0.69
49	29.61	70.00	99.61	0.40	0.88	0.69
50	30.20	69.75	99.94	0.40	0.87	0.68
51	30.28	69.48	99.76	0.40	0.87	0.68
52	27.97	71.72	99.68	0.37	0.90	0.71
53	25.59	74.01	99.60	0.34	0.93	0.73
54	26.22	73.54	99.76	0.35	0.92	0.72
55	26.08	73.41	99.49	0.35	0.92	0.73
56	25.72	73.81	99.52	0.34	0.92	0.73
57	25.47	74.18	99.64	0.34	0.93	0.73
58	30.28	69.60	99.87	0.40	0.87	0.68
59	30.44	69.75	100.19	0.41	0.87	0.68
60	30.02	70.04	100.06	0.40	0.88	0.69
61	30.34	69.76	100.10	0.40	0.87	0.68
62	25.63	74.50	100.13	0.34	0.93	0.73
63	25.45	74.03	99.48	0.34	0.93	0.73
64	25.44	74.43	99.88	0.34	0.93	0.73
65	25.73	74.63	100.36	0.34	0.93	0.73
66	27.08	72.77	99.84	0.36	0.91	0.72
67	25.66	74.23	99.89	0.34	0.93	0.73
68	25.66	74.37	100.03	0.34	0.93	0.73
69	25.57	74.48	100.05	0.34	0.93	0.73
70	25.64	74.92	100.56	0.34	0.94	0.73
71	25.39	75.29	100.68	0.34	0.94	0.74
72	26.23	74.88	101.11	0.35	0.94	0.73
73	25.83	75.41	101.24	0.34	0.94	0.73
74	25.72	75.40	101.12	0.34	0.94	0.73
75	25.71	75.22	100.93	0.34	0.94	0.73
76	25.83	75.21	101.04	0.34	0.94	0.73
77	25.65	75.54	101.19	0.34	0.95	0.73
78	25.88	74.96	100.85	0.35	0.94	0.73
79	25.72	75.10	100.82	0.34	0.94	0.73
80	25.76	75.14	100.90	0.34	0.94	0.73
81	29.23	71.52	100.75	0.39	0.90	0.70
82	25.88	75.16	101.03	0.35	0.94	0.73
83	25.69	75.65	101.34	0.34	0.95	0.73
84	25.98	75.81	101.79	0.35	0.95	0.73

85	25.79	75.62	101.40	0.34	0.95	0.73
Average	**26.80**	**73.65**	**100.45**	**0.36**	**0.92**	**0.72**
Sandard Deviation	**1.93**	**2.14**	**0.74**	**0.03**	**0.03**	**0.02**
95% Confidence Limit	**0.41**	**0.46**	**0.16**	**0.01**	**0.01**	**0.004**

Sample: 90T14; Initial Sample Composition = 90 mass% TiO_2 - 10 mass% V_2O_5; Reaction Temperature = 1400°C; Phases Identified = Magneli Phase

Analysis No.	Mass% V2O3	Mass% TiO2	Total	mol V	mol Ti	Mole fraction Ti
1	8.63	90.97	99.60	0.12	1.14	0.91
2	8.55	91.68	100.23	0.11	1.15	0.91
3	7.89	92.19	100.08	0.11	1.15	0.92
4	7.84	92.53	100.37	0.10	1.16	0.92
5	7.94	92.57	100.51	0.11	1.16	0.92
6	8.76	90.32	99.07	0.12	1.13	0.91
7	8.86	91.35	100.21	0.12	1.14	0.91
8	8.48	91.89	100.37	0.11	1.15	0.91
9	8.68	90.74	99.41	0.12	1.14	0.91
10	8.64	91.73	100.37	0.12	1.15	0.91
11	8.37	91.83	100.20	0.11	1.15	0.91
12	8.39	91.95	100.34	0.11	1.15	0.91
13	8.31	91.07	99.37	0.11	1.14	0.91
14	8.20	90.38	98.57	0.11	1.13	0.91
15	8.17	90.92	99.09	0.11	1.14	0.91
16	8.42	92.19	100.61	0.11	1.15	0.91
17	8.64	92.46	101.09	0.12	1.16	0.91
18	8.20	93.08	101.28	0.11	1.16	0.91
19	8.26	93.00	101.26	0.11	1.16	0.91
20	8.35	92.26	100.61	0.11	1.15	0.91
21	8.22	92.38	100.61	0.11	1.16	0.91
22	8.50	91.18	99.67	0.11	1.14	0.91
23	8.53	92.14	100.67	0.11	1.15	0.91
24	8.68	90.59	99.26	0.12	1.13	0.91
25	8.74	91.26	99.99	0.12	1.14	0.91
26	8.74	91.69	100.43	0.12	1.15	0.91
27	8.78	91.82	100.60	0.12	1.15	0.91
Average	**8.43**	**91.71**	**100.14**	**0.11**	**1.15**	**0.91**
Standard Deviation	**0.28**	**0.76**	**0.68**	**0.004**	**0.010**	**0.003**
95% Confidence Limit	**0.11**	**0.29**	**0.26**	**0.001**	**0.004**	**0.001**

Sample: 10T15; Initial Sample Composition = 10 mass% TiO_2 - 90 mass% V_2O_5; Reaction Temperature = 1500°C; Phases Identified = M_2O_3

Analysis No.	Mass% V2O3	Mass% TiO2	Total	mol V	mol Ti	Mole fraction Ti
1	87.92	12.26	100.18	1.17	0.15	0.12
2	88.31	12.50	100.81	1.18	0.16	0.12
3	87.60	12.32	99.92	1.17	0.15	0.12
4	88.07	12.77	100.84	1.18	0.16	0.12
5	87.78	12.55	100.33	1.17	0.16	0.12
6	87.73	12.68	100.41	1.17	0.16	0.12
7	87.53	13.54	101.07	1.17	0.17	0.13
8	87.98	13.82	101.80	1.17	0.17	0.13
9	86.83	13.74	100.56	1.16	0.17	0.13
10	87.68	13.68	101.36	1.17	0.17	0.13
11	86.55	13.69	100.23	1.15	0.17	0.13
12	87.11	14.26	101.37	1.16	0.18	0.13
13	86.89	14.57	101.46	1.16	0.18	0.14
14	86.50	14.42	100.92	1.15	0.18	0.14
15	86.42	14.65	101.08	1.15	0.18	0.14
16	87.15	14.47	101.62	1.16	0.18	0.13
17	86.73	14.18	100.90	1.16	0.18	0.13
18	86.37	14.40	100.77	1.15	0.18	0.14
19	86.16	14.74	100.90	1.15	0.18	0.14
20	86.43	14.71	101.13	1.15	0.18	0.14
21	85.95	15.24	101.19	1.15	0.19	0.14
22	85.95	15.21	101.15	1.15	0.19	0.14
23	85.85	15.76	101.61	1.15	0.20	0.15
24	85.51	15.56	101.07	1.14	0.19	0.15
25	85.64	15.73	101.37	1.14	0.20	0.15
26	84.05	15.65	99.70	1.12	0.20	0.15
27	85.72	15.96	101.68	1.14	0.20	0.15
28	85.06	16.11	101.17	1.14	0.20	0.15
29	85.61	16.23	101.84	1.14	0.20	0.15
30	84.93	16.21	101.14	1.13	0.20	0.15
31	84.56	16.04	100.60	1.13	0.20	0.15
32	84.63	16.12	100.76	1.13	0.20	0.15
33	84.52	16.64	101.16	1.13	0.21	0.16
34	83.87	16.38	100.26	1.12	0.21	0.15
35	82.49	16.41	98.90	1.10	0.21	0.16
36	84.57	16.97	101.54	1.13	0.21	0.16
37	84.06	17.02	101.09	1.12	0.21	0.16
38	83.97	17.26	101.23	1.12	0.22	0.16
39	84.24	16.99	101.23	1.12	0.21	0.16
40	84.06	17.41	101.47	1.12	0.22	0.16

41	83.31	17.28	100.60	1.11	0.22	0.16
42	83.92	17.52	101.45	1.12	0.22	0.16
43	82.89	17.55	100.44	1.11	0.22	0.17
44	81.79	17.30	99.09	1.09	0.22	0.17
45	83.76	17.69	101.45	1.12	0.22	0.17
46	83.69	17.70	101.39	1.12	0.22	0.17
47	83.60	17.78	101.38	1.12	0.22	0.17
48	83.57	17.87	101.44	1.12	0.22	0.17
49	83.45	18.01	101.46	1.11	0.23	0.17
50	81.56	16.78	98.34	1.09	0.21	0.16
51	83.31	17.40	100.71	1.11	0.22	0.16
52	83.83	17.59	101.42	1.12	0.22	0.16
53	83.81	17.65	101.45	1.12	0.22	0.16
54	82.94	17.23	100.17	1.11	0.22	0.16
Average	**85.27**	**15.63**	**100.90**	**1.14**	**0.20**	**0.15**
Standard Deviation	**1.78**	**1.72**	**0.72**	**0.02**	**0.02**	**0.02**
95% Confidence Limit	**0.47**	**0.46**	**0.19**	**0.01**	**0.01**	**0.004**

Sample: 30T15; Initial Sample Composition = 30 mass% TiO_2 - 70 mass% V_2O_5; Reaction Temperature = 1500°C; Phases Identified = M_2O_3 and M_3O_5

M_3O_5-Phase

Analysis No.	Mass% V2O3	Mass% TiO2	Total	mol V	mol Ti	Mole fraction Ti
1	70.08	31.02	101.10	0.94	0.39	0.29
2	65.12	35.53	100.65	0.87	0.44	0.34
3	70.49	30.79	101.27	0.94	0.39	0.29
4	64.89	35.83	100.73	0.87	0.45	0.34
5	62.71	37.70	100.40	0.84	0.47	0.36
6	60.81	39.63	100.44	0.81	0.50	0.38
7	61.39	39.12	100.50	0.82	0.49	0.37
8	60.94	39.95	100.88	0.81	0.50	0.38
9	60.19	39.91	100.09	0.80	0.50	0.38
10	61.20	39.80	101.00	0.82	0.50	0.38
11	61.07	39.79	100.86	0.81	0.50	0.38
12	60.64	39.65	100.28	0.81	0.50	0.38
13	63.18	37.53	100.70	0.84	0.47	0.36
14	60.62	40.33	100.95	0.81	0.50	0.38
15	59.58	39.43	99.00	0.79	0.49	0.38
16	60.17	40.07	100.24	0.80	0.50	0.38
17	59.93	40.59	100.53	0.80	0.51	0.39
18	58.87	41.46	100.34	0.79	0.52	0.40
19	56.67	40.55	97.22	0.76	0.51	0.40
20	58.08	42.73	100.81	0.78	0.53	0.41
21	57.54	42.22	99.76	0.77	0.53	0.41
22	57.50	43.09	100.59	0.77	0.54	0.41
23	57.27	43.65	100.92	0.76	0.55	0.42
24	57.10	43.56	100.66	0.76	0.55	0.42
25	58.10	43.43	101.54	0.78	0.54	0.41
26	57.25	43.99	101.24	0.76	0.55	0.42
27	57.18	44.16	101.34	0.76	0.55	0.42
28	55.57	42.78	98.35	0.74	0.54	0.42
29	55.21	43.63	98.84	0.74	0.55	0.43
30	55.31	45.10	100.41	0.74	0.56	0.43
31	56.62	43.64	100.26	0.76	0.55	0.42
32	56.35	44.38	100.73	0.75	0.56	0.42
33	56.80	44.23	101.03	0.76	0.55	0.42
34	55.46	45.45	100.91	0.74	0.57	0.43
35	56.35	45.19	101.54	0.75	0.57	0.43
36	57.01	44.10	101.11	0.76	0.55	0.42
37	56.43	44.74	101.17	0.75	0.56	0.43
38	57.06	43.87	100.93	0.76	0.55	0.42
39	55.83	43.28	99.11	0.74	0.54	0.42

40	57.01	43.23	100.25	0.76	0.54	0.42
41	57.44	43.64	101.08	0.77	0.55	0.42
42	56.80	43.55	100.34	0.76	0.55	0.42
43	58.04	43.20	101.23	0.77	0.54	0.41
44	58.32	43.18	101.49	0.78	0.54	0.41
45	58.58	42.65	101.23	0.78	0.53	0.41
46	59.62	42.12	101.74	0.80	0.53	0.40
47	59.55	41.66	101.20	0.79	0.52	0.40
48	59.76	41.16	100.92	0.80	0.52	0.39
49	59.61	41.10	100.71	0.80	0.51	0.39
50	58.99	41.97	100.96	0.79	0.53	0.40
51	59.06	42.12	101.18	0.79	0.53	0.40
52	55.19	42.84	98.03	0.74	0.54	0.42
53	56.81	44.08	100.89	0.76	0.55	0.42
54	50.66	39.66	90.32	0.68	0.50	0.42
55	57.16	44.17	101.33	0.76	0.55	0.42
56	56.93	44.15	101.08	0.76	0.55	0.42
57	50.20	51.05	101.26	0.67	0.64	0.49
58	51.83	48.57	100.40	0.69	0.61	0.47
59	51.23	49.77	101.00	0.68	0.62	0.48
60	56.56	43.62	100.18	0.75	0.55	0.42
61	57.56	43.93	101.49	0.77	0.55	0.42
62	58.03	43.11	101.14	0.77	0.54	0.41
63	58.27	43.04	101.31	0.78	0.54	0.41
64	56.14	44.01	100.15	0.75	0.55	0.42
65	53.52	46.96	100.48	0.71	0.59	0.45
66	53.40	47.57	100.98	0.71	0.60	0.46
67	57.33	44.34	101.67	0.77	0.55	0.42
68	57.66	43.94	101.60	0.77	0.55	0.42
69	57.37	43.74	101.11	0.77	0.55	0.42
70	57.23	43.91	101.14	0.76	0.55	0.42
71	57.05	43.84	100.88	0.76	0.55	0.42
72	60.68	39.29	99.97	0.81	0.49	0.38
73	61.00	39.88	100.89	0.81	0.50	0.38
74	67.50	33.76	101.27	0.90	0.42	0.32
75	70.03	30.75	100.78	0.93	0.38	0.29
76	67.13	33.55	100.67	0.90	0.42	0.32
77	57.35	42.58	99.93	0.77	0.53	0.41
78	57.21	42.99	100.20	0.76	0.54	0.41
79	57.55	43.12	100.67	0.77	0.54	0.41
80	57.84	42.40	100.23	0.77	0.53	0.41
81	*61.64*	*38.36*	*100.00*	*0.82*	*0.48*	*0.37*
82	*63.54*	*36.46*	*100.00*	*0.85*	*0.46*	*0.35*
Average	**58.62**	**41.89**	**100.51**	**0.78**	**0.52**	**0.40**

Standard Deviation	**3.85**	**3.74**	**1.39**	**0.05**	**0.05**	**0.04**
95% Confidence Limit	**0.83**	**0.81**	**0.30**	**0.01**	**0.01**	**0.01**

Italic = SEM-EDS Analyses

M_2O_3-Phase

Analysis No.	Mass% V2O3	Mass% TiO2	Total	mol V	mol Ti	Mole fraction Ti
1	*82.53*	*17.47*	*101.10*	*1.10*	*0.22*	*0.17*
2	*82.02*	*17.98*	*100.65*	*1.09*	*0.23*	*0.17*
3	*82.14*	*17.86*	*101.27*	*1.10*	*0.22*	*0.17*
Average	**82.23**	**17.77**	**100.00**	**1.10**	**0.22**	**0.17**
Standard Deviation	**0.27**	**0.27**		**0.004**	**0.003**	**0.003**
95% Confidence Limit	**0.30**	**0.33**		**0.004**	**0.004**	**0.003**

Italic = SEM-EDS Analyses

Sample: 50T15; Initial Sample Composition = 50 mass% TiO_2 - 50 mass% V_2O_5; Reaction Temperature = 1500°C; Phases Identified = M_3O_5 and M_4O_7

M_3O_5-Phase:

Analysis No.	Mass% V2O3	Mass% TiO2	Total	mol V	mol Ti	Mole fraction Ti
1	58.99	42.01	101.00	0.79	0.53	0.40
2	59.55	41.74	101.29	0.79	0.52	0.40
3	58.71	41.63	100.34	0.78	0.52	0.40
4	58.54	41.91	100.45	0.78	0.52	0.40
5	56.57	44.11	100.67	0.75	0.55	0.42
6	56.38	44.54	100.92	0.75	0.56	0.43
7	54.40	46.47	100.87	0.73	0.58	0.44
8	58.29	42.16	100.45	0.78	0.53	0.40
9	58.14	42.87	101.00	0.78	0.54	0.41
10	57.54	42.87	100.41	0.77	0.54	0.41
11	57.44	43.01	100.45	0.77	0.54	0.41
12	56.97	43.51	100.48	0.76	0.54	0.42
13	56.97	43.49	100.46	0.76	0.54	0.42
14	56.82	43.78	100.60	0.76	0.55	0.42
15	56.81	43.58	100.39	0.76	0.55	0.42
16	56.71	44.07	100.78	0.76	0.55	0.42
17	56.58	44.32	100.90	0.76	0.55	0.42
18	57.13	44.19	101.33	0.76	0.55	0.42
19	55.98	43.81	99.79	0.75	0.55	0.42
20	54.36	43.39	97.75	0.73	0.54	0.43
Average	**57.14**	**43.37**	**100.52**	**0.76**	**0.54**	**0.42**
Standard Deviation	**1.35**	**1.17**	**0.74**	**0.02**	**0.01**	**0.01**
95% Confidence Limit	**0.59**	**0.51**	**0.33**	**0.01**	**0.01**	**0.01**

M_4O_7-Phase:

Analysis No.	Mass% V2O3	Mass% TiO2	Total	mol V	mol Ti	Mole fraction Ti
1	47.49	53.43	100.93	0.63	0.67	0.51
2	47.44	53.24	100.68	0.63	0.67	0.51
3	41.98	58.08	100.07	0.56	0.73	0.56
4	43.56	56.88	100.44	0.58	0.71	0.55
5	42.26	58.27	100.54	0.56	0.73	0.56
6	41.61	58.71	100.32	0.56	0.73	0.57
7	41.18	57.93	99.10	0.55	0.73	0.57
8	44.43	54.79	99.22	0.59	0.69	0.54
9	46.80	54.11	100.91	0.62	0.68	0.52
10	42.07	58.38	100.45	0.56	0.73	0.57
11	46.66	53.84	100.50	0.62	0.67	0.52

12	48.33	52.07	100.40	0.64	0.65	0.50
13	47.93	52.95	100.88	0.64	0.66	0.51
14	47.38	53.73	101.11	0.63	0.67	0.52
15	47.02	53.68	100.70	0.63	0.67	0.52
16	45.45	55.10	100.54	0.61	0.69	0.53
17	47.79	53.49	101.28	0.64	0.67	0.51
18	40.06	60.83	100.89	0.53	0.76	0.59
19	40.07	61.12	101.19	0.53	0.76	0.59
20	37.82	63.08	100.90	0.50	0.79	0.61
21	37.94	63.29	101.23	0.51	0.79	0.61
22	37.81	63.37	101.17	0.50	0.79	0.61
Average	**43.78**	**56.83**	**100.61**	**0.58**	**0.71**	**0.55**
Standard Deviation	**3.64**	**3.68**	**0.57**	**0.05**	**0.05**	**0.04**
95% Confidence Limit	**1.52**	**1.54**	**0.24**	**0.02**	**0.02**	**0.02**

Sample: 70T15; Initial Sample Composition = 70 mass% TiO_2 - 30 mass% V_2O_5; Reaction Temperature = 1500°C; Phases Identified = Magneli Phase

Analysis No.	Mass% V2O3	Mass% TiO2	Total	mol V	mol Ti	Mole fraction Ti
1	23.96	77.56	101.52	0.32	0.97	0.75
2	23.78	77.22	101.00	0.32	0.97	0.75
3	23.93	77.05	100.98	0.32	0.96	0.75
4	23.92	77.35	101.27	0.32	0.97	0.75
5	23.81	76.70	100.51	0.32	0.96	0.75
6	23.95	77.31	101.26	0.32	0.97	0.75
7	20.00	80.42	100.41	0.27	1.01	0.79
8	23.86	76.88	100.74	0.32	0.96	0.75
9	23.33	76.61	99.93	0.31	0.96	0.75
10	23.86	77.28	101.15	0.32	0.97	0.75
11	23.78	77.36	101.14	0.32	0.97	0.75
12	24.15	76.98	101.13	0.32	0.96	0.75
13	24.68	76.23	100.90	0.33	0.95	0.74
14	29.58	71.63	101.21	0.39	0.90	0.69
15	24.90	75.84	100.73	0.33	0.95	0.74
16	26.87	74.57	101.43	0.36	0.93	0.72
17	29.60	71.89	101.49	0.40	0.90	0.69
18	29.38	71.59	100.97	0.39	0.90	0.70
19	29.14	71.86	101.01	0.39	0.90	0.70
20	26.03	74.18	100.20	0.35	0.93	0.73
21	29.39	71.58	100.98	0.39	0.90	0.70
22	29.47	71.77	101.24	0.39	0.90	0.70
23	25.13	75.58	100.70	0.34	0.95	0.74
24	29.34	71.12	100.46	0.39	0.89	0.69
25	29.19	71.67	100.86	0.39	0.90	0.70
26	29.24	69.81	99.05	0.39	0.87	0.69
27	29.30	70.02	99.32	0.39	0.88	0.69
28	29.61	69.22	98.83	0.40	0.87	0.69
29	24.67	76.16	100.83	0.33	0.95	0.74
30	24.64	76.19	100.83	0.33	0.95	0.74
31	24.32	76.14	100.46	0.32	0.95	0.75
32	24.35	75.82	100.17	0.32	0.95	0.74
33	24.50	75.87	100.37	0.33	0.95	0.74
34	24.52	76.31	100.84	0.33	0.96	0.74
35	24.25	76.21	100.46	0.32	0.95	0.75
36	24.36	76.24	100.60	0.33	0.95	0.75
37	24.44	76.19	100.63	0.33	0.95	0.75
38	24.44	76.18	100.62	0.33	0.95	0.75
39	23.28	74.87	98.15	0.31	0.94	0.75
40	23.59	75.32	98.92	0.31	0.94	0.75

41	24.18	76.73	100.92	0.32	0.96	0.75
42	24.03	76.73	100.76	0.32	0.96	0.75
43	24.08	77.03	101.11	0.32	0.96	0.75
44	23.93	76.86	100.79	0.32	0.96	0.75
45	24.39	76.49	100.87	0.33	0.96	0.75
46	25.56	75.11	100.67	0.34	0.94	0.73
Average	**25.45**	**75.17**	**100.62**	**0.34**	**0.94**	**0.73**
Standard Deviation	**2.40**	**2.52**	**0.72**	**0.03**	**0.03**	**0.02**
95% Confidence Limit	**0.69**	**0.73**	**0.21**	**0.01**	**0.01**	**0.01**

Sample: 90T15; Initial Sample Composition = 90 mass% TiO_2 - 10 mass% V_2O_5; Reaction Temperature = 1500°C; Phases Identified = Magneli Phase

Analysis No.	Mass% V2O3	Mass% TiO2	Total	mol V	mol Ti	Mole fraction Ti
1	8.57	91.86	100.44	0.11	1.15	0.91
2	8.51	90.97	99.48	0.11	1.14	0.91
3	8.62	91.14	99.76	0.12	1.14	0.91
4	8.46	91.80	100.26	0.11	1.15	0.91
5	8.49	91.86	100.35	0.11	1.15	0.91
6	8.52	91.88	100.40	0.11	1.15	0.91
7	8.49	91.70	100.19	0.11	1.15	0.91
8	8.48	91.69	100.18	0.11	1.15	0.91
9	8.42	91.25	99.67	0.11	1.14	0.91
10	8.50	91.67	100.16	0.11	1.15	0.91
11	8.44	91.77	100.20	0.11	1.15	0.91
12	8.43	91.35	99.77	0.11	1.14	0.91
13	8.46	91.90	100.36	0.11	1.15	0.91
14	8.44	91.24	99.68	0.11	1.14	0.91
15	8.29	91.21	99.49	0.11	1.14	0.91
16	8.30	91.63	99.93	0.11	1.15	0.91
17	8.40	91.41	99.81	0.11	1.14	0.91
18	8.37	92.28	100.65	0.11	1.15	0.91
19	8.24	91.93	100.17	0.11	1.15	0.91
20	8.36	91.62	99.98	0.11	1.15	0.91
21	8.41	91.59	100.00	0.11	1.15	0.91
22	8.49	91.70	100.19	0.11	1.15	0.91
23	8.26	92.31	100.57	0.11	1.16	0.91
24	8.34	91.47	99.80	0.11	1.14	0.91
25	8.38	92.02	100.41	0.11	1.15	0.91
26	8.23	91.79	100.02	0.11	1.15	0.91
27	8.31	91.82	100.13	0.11	1.15	0.91
28	8.33	92.00	100.33	0.11	1.15	0.91
29	8.28	92.17	100.46	0.11	1.15	0.91
30	8.29	92.04	100.33	0.11	1.15	0.91
31	8.40	91.76	100.16	0.11	1.15	0.91
32	8.32	92.13	100.45	0.11	1.15	0.91
33	8.22	91.49	99.72	0.11	1.15	0.91
34	8.39	92.00	100.39	0.11	1.15	0.91
35	8.27	92.09	100.37	0.11	1.15	0.91
36	8.29	91.72	100.01	0.11	1.15	0.91
37	8.33	91.83	100.16	0.11	1.15	0.91
38	8.21	91.01	99.22	0.11	1.14	0.91
39	8.30	91.92	100.22	0.11	1.15	0.91
40	8.24	92.26	100.50	0.11	1.15	0.91

41	8.30	92.27	100.57	0.11	1.15	0.91
42	8.22	92.34	100.55	0.11	1.16	0.91
43	8.33	92.09	100.42	0.11	1.15	0.91
44	8.11	92.27	100.38	0.11	1.15	0.91
45	8.01	89.10	97.11	0.11	1.12	0.91
46	8.25	92.27	100.52	0.11	1.15	0.91
47	8.37	91.93	100.30	0.11	1.15	0.91
48	8.25	91.60	99.86	0.11	1.15	0.91
49	8.39	91.95	100.35	0.11	1.15	0.91
Average	**8.35**	**91.74**	**100.09**	**0.11**	**1.15**	**0.91**
Standard Deviation	**0.12**	**0.52**	**0.54**	**0.0016**	**0.0065**	**0.0012**
95% Confidence Limit	**0.03**	**0.15**	**0.15**	**0.0004**	**0.0018**	**0.0003**

Sample: 90T16480; Initial Sample Composition = 90 mass% TiO_2 - 10 mass% V_2O_5; Reaction Temperature = 1600°C; Phases Identified = Magneli Phase

Analysis No.	Mass% V2O3	Mass% TiO2	Total	mol V	mol Ti	Mole fraction Ti
1	8.58	91.89	100.46	0.11	1.15	0.91
2	8.58	92.16	100.74	0.11	1.15	0.91
3	8.56	92.23	100.79	0.11	1.15	0.91
4	8.75	91.35	100.10	0.12	1.14	0.91
5	8.60	91.38	99.98	0.11	1.14	0.91
6	8.54	91.38	99.93	0.11	1.14	0.91
7	8.53	90.78	99.32	0.11	1.14	0.91
8	8.56	91.56	100.12	0.11	1.15	0.91
9	8.59	91.61	100.21	0.11	1.15	0.91
10	8.59	91.55	100.14	0.11	1.15	0.91
11	8.59	91.76	100.35	0.11	1.15	0.91
12	8.59	91.98	100.57	0.11	1.15	0.91
13	8.48	91.89	100.37	0.11	1.15	0.91
14	8.69	91.42	100.11	0.12	1.14	0.91
15	8.55	91.32	99.87	0.11	1.14	0.91
16	8.51	91.15	99.66	0.11	1.14	0.91
17	8.63	91.66	100.29	0.12	1.15	0.91
18	8.56	91.26	99.82	0.11	1.14	0.91
19	8.66	91.42	100.08	0.12	1.14	0.91
20	8.67	91.51	100.18	0.12	1.15	0.91
21	8.30	91.43	99.72	0.11	1.14	0.91
22	8.14	89.51	97.65	0.11	1.12	0.91
23	8.22	91.54	99.76	0.11	1.15	0.91
24	8.26	92.45	100.71	0.11	1.16	0.91
25	8.39	92.46	100.86	0.11	1.16	0.91
26	8.34	91.36	99.70	0.11	1.14	0.91
27	8.27	91.25	99.51	0.11	1.14	0.91
28	8.23	91.45	99.68	0.11	1.14	0.91
29	8.26	91.48	99.74	0.11	1.14	0.91
30	8.24	91.29	99.53	0.11	1.14	0.91
31	8.22	92.31	100.54	0.11	1.16	0.91
32	8.16	91.99	100.15	0.11	1.15	0.91
33	8.10	90.88	98.98	0.11	1.14	0.91
34	8.29	91.56	99.84	0.11	1.15	0.91
35	8.32	91.84	100.16	0.11	1.15	0.91
36	8.32	92.13	100.45	0.11	1.15	0.91
37	8.56	91.83	100.39	0.11	1.15	0.91
38	8.52	91.71	100.22	0.11	1.15	0.91
39	8.51	91.60	100.11	0.11	1.15	0.91
40	8.57	91.54	100.11	0.11	1.15	0.91

41	8.75	91.21	99.95	0.12	1.14	0.91
Average	**8.46**	**91.56**	**100.02**	**0.11**	**1.15**	**0.91**
Standard Deviation	**0.18**	**0.50**	**0.55**	**0.002**	**0.006**	**0.002**
95% Confidence Limit	**0.06**	**0.15**	**0.17**	**0.001**	**0.002**	**0.001**

Appendix 4: EPMA(EDS) Analyses for V_2O_3 - TiO_2 System

EPMA(EDS) Analyses for V_2O_3 - TiO_2 System

Initial Composition Mass%		Tempe-rature	Phase Identified	Final Composition Mass%																Average Mass%		Standard Deviation Mass%
TiO_2	V_2O_5	°C		TiO_2	V_2O_3	TiO_2	V_2O_3	TiO_2	V_2O_3	TiO_2	V_2O_3	TiO_2	V_2O_3	TiO_2	V_2O_3	TiO_2	V_2O_3	TiO_2	V_2O_3	TiO_2	V_2O_3	TiO_2
10	90	1400	M_2O_3	10.70	89.30	10.17	89.83	5.98	94.02	8.08	91.92									8.73	91.27	2.16
30	70	1400	M_3O_5	38.87	61.13	38.82	61.18	38.63	61.37	39.03	60.97									38.84	61.16	0.16
30	70	1400	M_2O_3	20.09	79.91	20.01	79.99	19.75	80.25	19.69	80.31									19.89	80.12	0.19
50	50	1400	Magneli	61.61	38.39	60.88	39.12	68.78	31.22											63.76	36.24	4.37
70	30	1400	Magneli	77.65	22.35	73.29	26.71	72.08	27.92											74.34	25.66	2.93
90	10	1400	Magneli	90.61	9.39	90.39	9.61	90.13	9.87											90.38	9.62	0.24
10	90	1500	M_2O_3	10.47	89.53	11.76	88.24	17.55	82.45	19.71	80.29									14.87	85.13	4.46
30	70	1500	M_3O_5	38.36	61.64	36.46	63.54													37.41	62.59	1.34
30	70	1500	M_2O_3	17.47	82.53	17.98	82.02	17.86	82.14											17.77	82.23	0.27
50	50	1500	Magneli	55.72	44.28	63.49	36.51	58.76	41.24											59.32	40.68	3.92
70	30	1500	Magneli	79.01	20.99	78.80	21.20	75.17	24.83	75.64	24.36	75.40	24.60	78.54	21.46	75.45	24.55	71.48	28.52	76.19	23.81	2.54
90	10	1500	Magneli	90.74	9.26	90.59	9.41	90.21	9.79											90.51	9.49	0.27
90	10	1600	Magneli	90.46	9.54	90.74	9.26	90.86	9.14											90.69	9.31	0.20

Appendix 5: EPMA(EDS) Analyses for V_2O_3 - FeO System

EPMA Analyses: V_2O_3 - FeO System at 1400, 1500 and 1600 °C

Initial Composition Mass%		Temperature °C	Phase Identified	Final Composition Mol										Average Mol		Standard Deviation Mol	95% Confidence Interval
Fe_2O_3	V_2O_5			Fe	V	Fe	V	Fe	V	Fe	V	Fe	V	Fe	V	Fe	Fe
10	90	1400	M_3O_4	0.472	0.882	0.459	0.894	0.463	0.890					0.465	0.889	0.006	± 0.007
10	90	1400	M_2O_3	0.088	1.250	0.089	1.249	0.095	1.245	0.090	1.248			0.090	1.248	0.003	±0.003
30	70	1400	M_3O_4	0.466	0.887	0.461	0.893	0.469	0.885	0.463	0.890	0.472	0.883	0.466	0.888	0.004	± 0.004
30	70	1400	M_2O_3	0.096	1.242	0.093	1.245	0.099	1.240					0.096	1.242	0.003	± 0.003
50	50	1400	M_3O_4	0.692	0.673	0.689	0.674	0.675	0.687					0.685	0.678	0.009	± 0.010
70	30	1400	M_3O_4	0.768	0.598	0.772	0.594	0.779	0.587					0.773	0.593	0.006	± 0.006
70	30	1400	Liquid	1.194	0.191	1.186	0.197	1.184	0.199					1.188	0.196	0.005	± 0.006
90	10	1400	Liquid	1.236	0.151	1.235	0.151	1.232	0.153					1.234	0.152	0.002	± 0.002
10	90	1500	M_3O_4	0.472	0.882	0.468	0.886	0.462	0.891	0.451	0.902			0.463	0.890	0.009	± 0.008
10	90	1500	M_2O_3	0.103	1.236	0.103	1.236	0.104	1.234	0.102	1.237			0.103	1.236	0.001	± 0.001
30	70	1500	M_3O_4	0.477	0.878	0.477	0.878	0.468	0.886	0.480	0.874			0.476	0.879	0.005	± 0.005
30	70	1500	M_2O_3	0.110	1.229	0.109	1.230	0.104	1.234					0.108	1.231	0.003	± 0.003
50	50	1500	M_3O_4	0.603	0.757	0.628	0.733	0.608	0.751	0.599	0.761			0.609	0.750	0.013	± 0.013
10	90	1600	M_3O_4	0.477	0.877	0.480	0.874	0.476	0.878					0.478	0.876	0.003	± 0.003
10	90	1600	M_2O_3	0.116	1.224	0.072	1.265	0.120	1.220	0.117	1.222	0.120	1.220	0.109	1.230	0.020	± 0.018
50	50	1600	M_3O_4	0.580	0.778	0.560	0.798	0.521	0.835	0.533	0.823			0.548	0.809	0.027	± 0.026
70	30	1600	M_3O_4	0.633	0.727	0.629	0.731	0.635	0.726					0.632	0.728	0.004	± 0.004
70	30	1600	Liquid	1.235	0.151	1.141	0.240	1.215	0.169					1.197	0.187	0.052	± 0.059